A COMPUTATIONAL INVESTIGATION OF POTENTIAL DECOMPOSITION PATHWAYS TO PRODUCE SHORT-LIVED KETENES

PITAMBAR POUDEL

SUPERVISOR:

ASSOCIATE PROFESSOR SARAH MASTERS

Submitted in fulfilment of the requirements for

Master of Science in Chemistry

March, 2021

School of Physical and Chemical Sciences

University of Canterbury

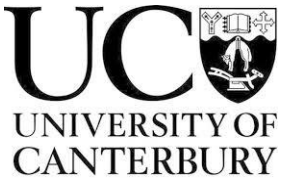

Acknowledgements

Firstly, I would like to thank my supervisors Associate Professor Sarah Masters and Dr Matthew Polson. To Sarah, thanks for your valuable guidance, support, encouraging words throughout this research work, and many hours proofreading this thesis. Your help is appreciated to obtain an international student welfare fund when I was affected financially and mentally due to loss of family business at the time of COVID-19 lockdown. To Matt, thanks for valuable discussion on guiding me about the synthetic apparatus.

I would like to thank my father, Matrika Prasad Poudel and mother, Indira Devi Poudel for their financial help to complete my study abroad plan. Hopefully I will assist you both after study. My study is catalytically encouraged by my lovely wife, Nirmala Ghimire. For most of the last two months during the weekend my four year old son Priyansh was with me at University and he was letting me do my work whilst playing quietly.

I also would like to thank Dr Aliyu Ja'o for helping me get started with the computational work. I am thankful to the research groups of Professor Rudi Marquez and Dr Daniel Foley, and Daniel himself for valuable discussion about the mechanism of organic reactions.

Abstract

Reactive intermediates are useful in organic synthesis, industrial chemistry and many biological processes. Knowledge of their structure and energetic behaviour enables the mechanisms of reactions to be further understood. The initial aim of this project was to determine the gaseous molecular structures of various short-lived ketenes using a new combined gas electron diffraction / mass spectrometry (GED/MS) apparatus, as well as a full analysis using computational methods. The proof-of-concept was to be focussed on ketene (ethenone) which can be generated cleanly from pyrolysis of diketene (4-methylideneoxetan-2-one). Due to the COVID-19 pandemic we were unable to get the required apparatus delivered to the University of Canterbury, therefore the project was refocused to a fully computational investigation of ketene and substituted ketenes.

Computational modelling of the structures and reaction pathways for the generation of ketene and substituted ketenes has been undertaken using the Gaussian 09 and NWChem suite of programs, utilizing the New Zealand e-Science Infrastructure (NeSI). The parent diketene can break down to give either ketene, or allene and CO_2. Both of these pathways have been studied in detail and this work demonstrates that the reaction pathway for the formation of ketene has a lower activation barrier than the alternative pathway (formation of allene and CO_2) using CBS-QB3 calculations. The predicted entropy, enthalpy and free energy of pyrolysis dissociation of diketene at the CCSD(T)/CBS level however indicates that the ketene formation pathway is spontaneous only at elevated reaction temperature.

The second reactive species discussed is methyleneketene. Pyrolysis of diazotetranoic acid [3-diazofuran-2, 4(3H, 5H)-dione] could give either methyleneketene and CO_2 or carbon sub-oxide and formaldehyde with liberation of nitrogen gas in both cases. Both pathways have been studied computationally. The methyleneketene and CO_2 formation pathway was found to be exergonic with a lower energy barrier than the carbon sub-oxide and formaldehyde formation pathway by CBS-QB3 level of theory. The thermochemical parameters have also been studied using CCSD(T)/CBS calculations.

Finally a series of substituted ketenes obtained from the decomposition of derivatives of Meldrum's acid (MA) are discussed. Methyleneketene, methyl-ketene, and dimethyl-ketene can all be obtained from the pyrolysis of Meldrum's acid (MA) derivatives, and all decomposition pathways have been studied theoretically using CBS-QB3 calculations. All were found to be thermodynamically feasible at 298.15 K with the exception of methylene-Meldrum's acid (MeMA). All reactions are endothermic, requiring energies in the range of 190 to 250 kJ/mol to cross the energy barrier towards the formation of substituted ketene.

Abbreviations and acronyms

B97M	Grimme semi-empirical generalised gradient approximation
CCD	Charge-Coupled Device
COVID-19	COrona VIrus Disease 2019
DFT	Density Functional Theory
DMMA	Di-Methyl-Meldrum's Acid
DYNAMITE	DYNAMic Interaction of Theory and Experiment
FC	Frozen Core
FTIR	Fourier Transform Infrared Spectroscopy
FVP	Flash Vacuum Pyrolysis
FVP-GED	Flash Vacuum Pyrolysis coupled with Gas Electron Diffraction
GED	Gas Electron Diffraction
GED-MS	Gas Electron Diffraction coupled with Mass Spectrometry
GGA	Generalised Gradient Approximation
HF	Hartree-Fock theory
IR	Infra-Red spectroscopy
IRC	Intrinsic Reaction Coordinate
LCNMR	Liquid-Crystal Nuclear Magnetic Resonance
LDA	Localised Density Approximation
M06-2X	Minnesota hybrid meta exchange-correlation functional
MA	Meldrum's Acid
MeMA	Methylene-Meldrum's Acid
MIC	Molecular Intensity Curve
MMMA	Mono-Methyl-Meldrum's Acid
MP2	Second-order Møller-Plesset perturbation series

MS	Mass Spectrometry
MW	Microwave spectroscopy
m/z	Mass-to-Charge ratio
NeSI	New Zealand e-Science Infrastructure
NMR	Nuclear Magnetic Resonance
PE	Photo-Electron
PES	Potential Energy Surface
P(*r*)	Probability of finding an inter-nuclear distance in the molecule under the radial distribution curve
r	Interatomic distance
r_a	Average interatomic distance (definition depends on method)
r_e	Equilibrium distance
r_{h1}	Interatomic distance corrected with curvilinear distance corrections
r_o	Maximum radius of rotating sector
R	Goodness of fit
R_D	*R*-factor assuming there is no correlation in the data
R_G	*R*-factor taking into account correlation between adjacent observations in the immediately off-diagonal position of the weight matrix
RDC	Radial Distribution Curve
RMS	Root-Mean-Square
SARACEN	Structural Analysis Restrained by *ab initio* Calculations for Electron diffractioN
SEMTEX	Structural Enhancement Methodology for Theory and

	Experiment
SHRINK	Program used to determine curvilinear corrections
TS	Transition State
UV	Ultra-Violet
VHT	Very-High-Temperature
VHT-GED-MS	Very-High-Temperature Gas Electron Diffraction coupled with Mass spectrometry

Table of Contents

1. Introduction

1.1. Reactive intermediates

Reactive intermediates are molecules that are generally high in energy, short-lived, and highly reactive in nature. These species, by their very nature, are hard to isolate and store. Knowledge of their structure and energetic behaviour can help to explain how chemical reactions take place[1] and allow the mechanisms of reactions to be further understood. The molecular structure of the intermediate is the key part to make use of its functionality. Such a structure is obtained computationally from an optimized geometry, and a frequency calculation is used to verify that the optimized structure is a minimum on the potential energy surface (PES). The experimental structures of such molecules can realistically be obtained from gas-phase techniques such as gas electron diffraction (GED).

1.2. Ketene and its preparation by using pyrolysis of diketene

Ketenes are the reactive class of organic oxo compounds that are useful in synthesis and industrial chemistry. Various applications are shown in Figure 1 below.

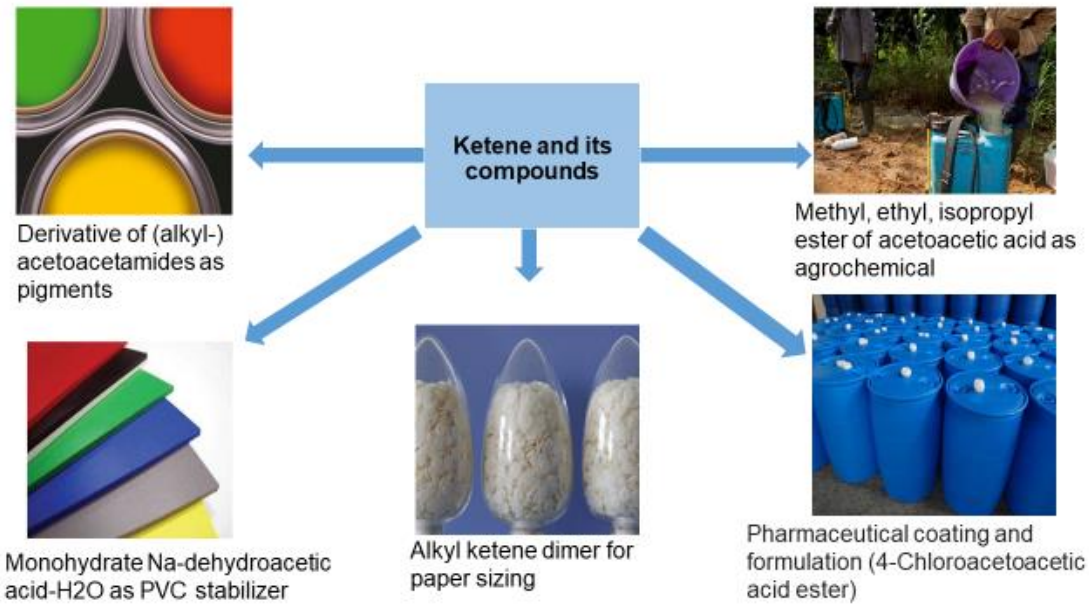

Figure 1: Uses of ketene and its derivatives

Ketene was first made by Hermann Staudinger[2] in 1905 with the reaction of α-chlorodiphenylacetyl chloride with zinc at a temperature of 452-453 K. He was seeking to obtain the radical $Ph_2\dot{C}COCl$,

inspired by Moses Gomberg[3] who prepared a stable triphenylmethyl radical, but the result was the unforeseen discovery of ketene. This new class of compounds were found to be strongly unsaturated, unstable, and to polymerize quickly after formation. The parent ketene, $H_2C=C=O$, was prepared from the pyrolysis of acetic anhydride using hot platinum wire[4] and a modified method where the platinum wire was held below the liquid surface. The ketenes were correctly represented in two tautomeric forms as $H_2C=C=O$ and $HC\equiv COH$. Ketenes are chosen in my thesis work due to their small size and short-lived nature (they dimerize rapidly at room temperature).[5] Both gaseous and liquid ketene polymerize to form a brown liquid with a pungent smell.

Diketene (4-methylene-2-oxatanone) is a reactive compound that is very useful in synthetic and structural chemistry.[6] Chick and Wilsmore made the first known diketene, as 'acetylketene', in 1908.[7] On standing the liquid or gaseous ketene at room temperature the new substance was formed as a pungent smelling brown liquid with possible formula $CH_3COCHCO$. Five different molecular structures were proposed[8] (one acyclic and four cyclic conformers as in Figure 2).

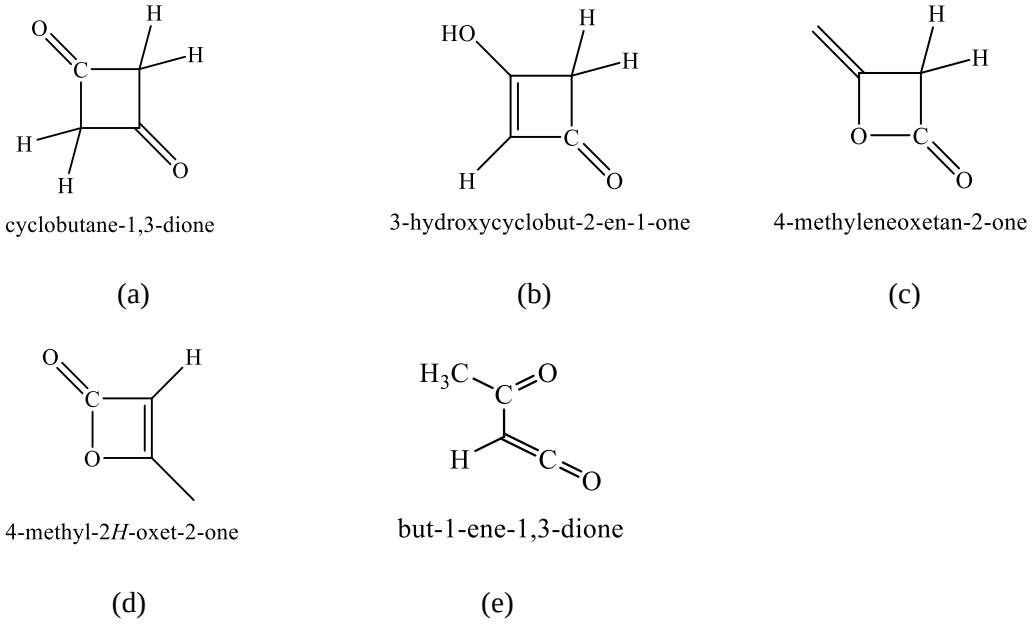

Figure 2: Structure of diketene (c) and its other cyclic (a, b and d) and acyclic (e) isomers

The gas-phase structure of diketene was investigated using GED by Bregmen and Bauer[9] after the X-ray crystallographic structure of diketene was revealed by Lipscomb and Kart.[10] Confirmation of the structure of diketene was provided by a series of experiments including X-ray crystallography,[10, 11] proton nuclear magnetic resonance (^{1}H NMR) spectroscopy,[12] and Infra-Red (IR) spectroscopy.[13, 14] Boese

carried out pyrolysis using two different methods, firstly refluxing the diketene over hot metal such as platinum or resistant metal and secondly passing the vapour of diketene through a hot tube at 823-873 K. The pyrolysis chamber was fitted with a reflux condenser extended to the ice bath region for the collection of ketenes so that unchanged diketene was noticed.[8] The process was about 50% efficient. In 1965 Andreades and Carlson[15] synthesised ketene by the pyrolysis of diketene with a flow of nitrogen, which yielded 46-55% ketene. Ketene was prepared from pyrolysis of diluted diketene with ultra-pure argon by thermally decomposition at a temperature of 510-603 K and a constant pressure of 800 Torr.[16] The impurities, such as unpyrolysed diketene and carbon dioxide, were observed in the products by Fourier Transform Infrared spectroscopy (FTIR) investigation but the quantity was not measured. Ketene was generated from pyrolysis of three sources: acetic anhydride, Meldrum's acid (MA), and acetone and studied previously using flash vacuum pyrolysis coupled with gas electron diffraction (FVP-GED).[17] The formation of diketene at room temperature during the experiment was not noticed by Noble-Eddy in the Masters research group.[17, 18] A more efficient method (about 95% yield) considered is to prepare ketene first, as shown in Figure 3, using the improved apparatus of Williams and Hurd.[19] Ketene will spontaneously convert to diketene at standard temperature during collection. Diketene then can be reconverted to ketene for use in the GED experiment.

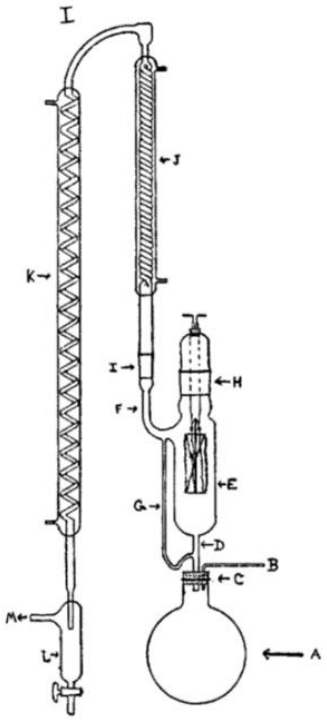

Figure 3: An improved apparatus[19] for laboratory preparation of ketene from pyrolysis decomposition of diketene, where A – round bottom flask, B – glass tube, C – rubber stopper, D – connecting tube, E – heating chamber, F – side arm of chamber, G – reflux return tube, H – ground glass joint, I – joint, J and K –condensers, M – outlet tube and L – liquid trap.

Two alternative pyrolytic decomposition pathways of diketene are proposed, shown in Figure 4. Pathway 1 leads to the formation of 2 equivalent ketenes, whereas pathway 2 yields allene and carbon dioxide. Neither pathway has been studied in detail previously.

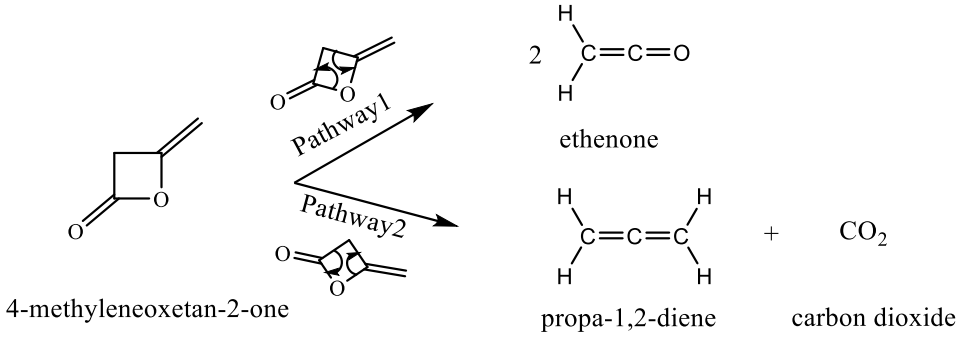

Figure 4: Pyrolytic decomposition of diketene: pathway 1 – formation of ketene, and pathway 2 – formation of allene and CO_2.

1.3. Methyleneketene and its preparation from decomposition of diazotetranoic acid

Methyleneketene, also known as propa-1,2-diene-1-one, is a reactive compound that was first detected in 1976[20] with debate over its geometry and its electronic structure. Conventionally, the molecular structure was believed to be a linear with C_{2v} symmetry.[21] Then, a microwave (MW) spectroscopy study[22] indicated a bent geometry with the aid of calculations performed at the Hartree-Fock level. The IR spectroscopy study of the pyrolytic decomposition of diazotetranoic acid was inconclusive regarding the molecular structure of methyleneketene.[23] Chapman *et al.* found that the pyrolysis of diazotetranoic acid, 3-diazofuran-2,4(3*H*,5*H*)-dione, at 953 K gives clean methyleneketene.[23] The pyrolytic decompositions of diazotetranoic acid can take two pathways shown in Figure 5. Pathway 1 forms methyleneketene and carbon dioxide and Pathway 2 forms carbon sub-oxide and formaldehyde. These are proposed pathways and have not been studied in detail before. The intermediate, 3-oxo-methylideneoxetan-2-one is a common transition state (TS) for both pathways.

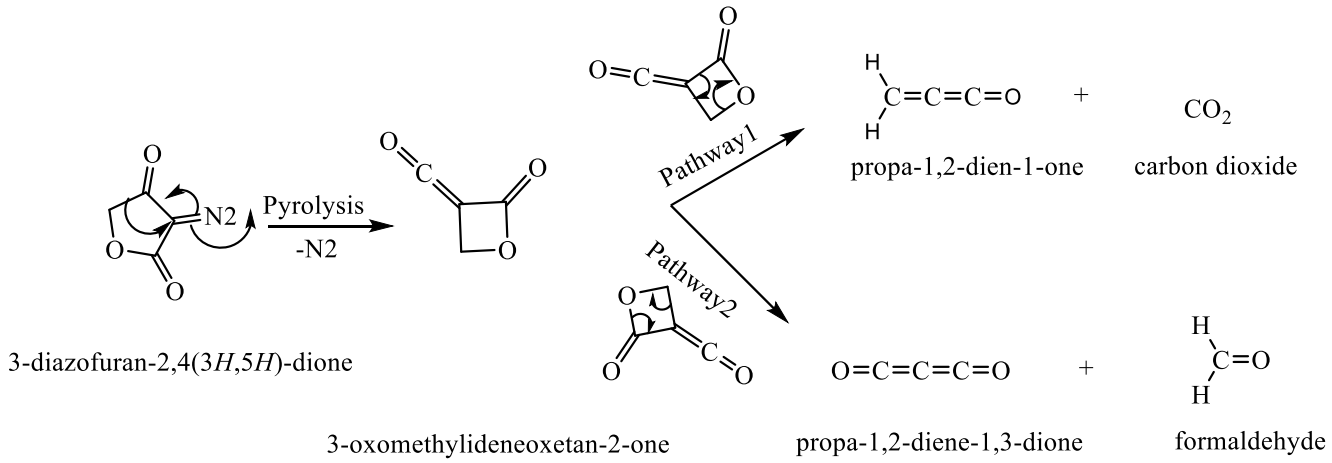

Figure 5: Pyrolytic decomposition of diazotetranoic acid: Pathway 1 – formation of methyleneketene and carbon dioxide, and Pathway 2 – formation of carbon sub-oxide and formaldehyde.

1.4. Substituted ketenes and their preparation by pyrolysis of Meldrum's Acid derivatives

Meldrum's Acid (MA), also known as 2,2-dimethyl-1,3-dioxane-4,6-dione, was first made by Andrew Norman Meldrum in 1908 using a condensation reaction of malonic acid and acetone in acetic anhydride containing a small amount of sulfuric acid.[24] The compound was initially misidentified, due to its unusually high pKa value, as a β-lactone. After 40 years, the correct structure was found by Davidson and Bernhard.[25] An early theoretical study by Koberl and Schuster[26] and ^{1}H NMR study of Abramovitch *et al.*[27] considered the compound possessed the chair conformation. However X-ray diffraction structural

investigation by Pfluger and Boyle,[28] as well as a theoretical study by Lee *et al.*,[29] predicted the boat conformer as the most favourable for MA to balance the strain created by the planarity of the lactone ring. It was also found that the experimental dipole from electron density analysis[30] in MA is 1.42 Debye units higher than that of dioxin.[26] A combined gas electron diffraction (GED) and *ab initio* calculation study undertaken by the Masters group confirmed MA had a boat conformer with C_s symmetry.[17, 31] MA and its derivatives have extensive applications in organic synthesis such as in Figures 6a and 6b.[32, 33, 34]

At temperatures above 473 K,[32] MA decomposes into acetone, carbon dioxide and ketene.[35] Two possible mechanisms can be considered. In the first one, the transition state of the MA decomposition reaction has a cyclic geometry with a single step process, and the reaction is therefore a pericyclic reaction.[36] The next proposed mechanism is initial breaking of the two ring C-O bonds[34] in MA to form acetone. The first step is the formation of acetone and unstable malonic anhydride or similar compounds and then the malonic anhydride decomposes[37] to the respective ketenes and carbon dioxide in the second step. MA derivatives can also be used as precursors to form substituted ketenes. The pyrolysis decomposition of MA and its derivatives[32, 33, 34, 38] results in different ketene derivatives along with carbon dioxide and acetone as shown reactions in Figure 6a and 6b. In this research project, the thermochemical and kinetic feasibility of decomposition of MA and its derivatives such as mono-methyl-Meldrum's acid (MMMA), di-methyl-Meldrum's acid (DMMA) and methylene-Meldrum's acid (MeMA) were studied in detail.

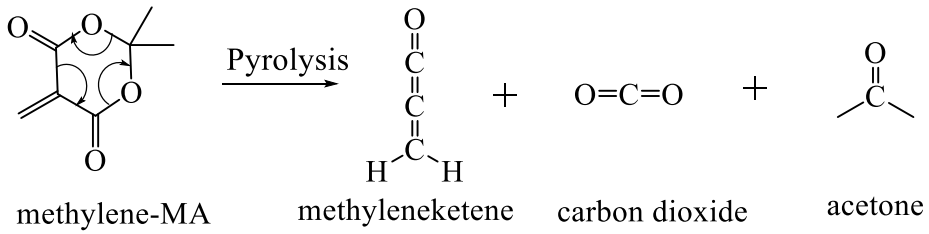

Figure 6a: Pyrolytic decomposition scheme of methylene-MA (MeMA) into methyleneketene, carbon dioxide and acetone.

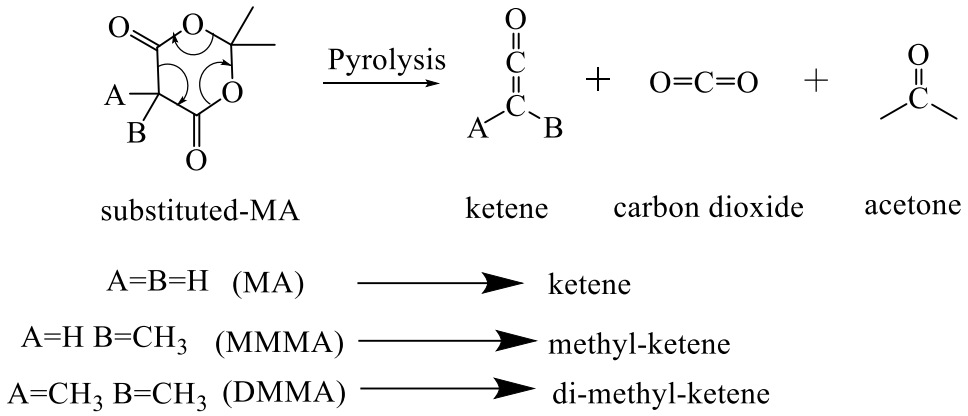

Figure 6b: General pyrolytic decomposition scheme of various MA derivatives into ketene substitutes, carbon dioxide and acetone.

1.5. Spectroscopic techniques used for short-lived species

The study of short-lived species is difficult using techniques such as NMR methods, as limited information can be deduced. For example, the ^{1}H NMR chemical shift of ketenes is a high field shift of C_{β} with a value of δ = 2.43-2.46, noticeably higher field than the olefinic proton,[39] but it is not an ideal diagnostic tool for ketene structure identification, as other factors like substituent effects can change the chemical shift of $C\alpha$, which was not studied in detail by the authors. Only a little information about the structure was revealed from the ^{13}C NMR spectroscopic analysis and for more detailed information about ketene in the solid-state along with linear and pseudolinear molecules, *ab initio* calculations coupled with the Hartree-Fock method were used.[40] The method of rapid injection NMR may work for some species but is limited by spin requirement as well as challenges associated with overlapping of multiple peaks. Ultraviolet (UV) spectroscopy showed two $\pi \rightarrow \pi$ and one $n \rightarrow \pi$ transitions in the double bond of ketene[41] but the effect of changes in substituents on the UV spectrum has not been studied systematically.

Photoelectron (PE) spectral data of ketenes provided the experimental photoelectron ionization potentials and compared well with theoretical values.[42] IR spectroscopy can be used to investigate reactive intermediates in conjunction with pyrolysis. For example, the result of delocalization and hybridization of the benzyl radical was successfully studied by this method. Rotational constants of ketenes and their IR frequencies[17] from both experimental and computational results revealed the resonance structures as well as the dipole moment of the bond. This facilitated the early understanding of the electronic structure of ketenes.

Rotational or MW spectroscopy is a technique that can be used to determine the gas-phase structure of small molecules. For larger molecules, the experiments quickly get complicated as there is a requirement to use multiple isotopic substitutions to elucidate molecular structure. That said, individual species may be detected from the mixture.

By their very nature, reactive intermediates are short-lived but they may be trapped in a matrix to enable their study. However, the nature of the matrix needs to be accounted for and development for separation methods is still in its infancy.[17]

1.6. Flash vacuum pyrolysis

Flash vacuum pyrolysis (FVP) or flash vacuum thermolysis (FVT) can be used to prepare reactive species like ketenes that can be stabilized at very low temperatures enabling the study of thermal parameters in the reactions. In this technique, the substrate is volatilized under vacuum and passed into a hot pyrolytic zone. The product of pyrolysis then passes out of the hot zone and condenses in a cold trap.[43] The problem with this condensed phase is that the precursor or solvent or products can generate unwanted secondary reactions and sometimes the product itself decomposes thermally during the generation of short-lived species. The reaction can be controlled to generate reactive intermediates under unimolecular conditions in the gas phase and low-pressure flow conditions can be used to ensure individual molecules spend a very short time (of the order of milliseconds) in the reaction zone enabling the thermally unstable product to be quenched without decomposition. Reactive intermediates in the cold trap can be trapped by a suitable reagent for subsequent analysis.[44]

1.7. Diffraction techniques

Solid, liquid and gas are the three common states in which a molecule can exist. The structure of the molecule is affected in solid and solution or liquid form by considering intermolecular forces such as hydrogen bonding, van der Waals forces and London interactions. Solid- or liquid-state structures are correct for the phase; however they can be different from that in the gas phase. A molecule in the gaseous phase is usually free of such constraints and the structure of the molecule can be studied and compared with that from the respective solid or liquid or solution phases. There are different techniques to determine the structure of solid and liquid phase molecules, such as X-ray crystallography and Liquid Crystal Nuclear Magnetic Resonance (LCNMR). The chance of structure distortion is highest in the solid

phase and less likely in the liquid and gaseous phases. The accurate structural determination of larger molecules is an intense challenge without any gas-phase techniques and high-level computational benchmarking.[45] For instance, early X-ray diffraction analysis of biphenyl indicated the molecule possesses a coplanar ring but GED study put forward the correct inter-planar ring with a twist angle of 44.4°.[46]

GED is a technique that can be used to study the molecular structure in the gas phase. In GED, the electron beam is passed through the gaseous beam of molecules and the interference pattern recorded. The pattern is used to deduce inter-nuclear distances from which the complete three-dimensional structure can be determined. A cooled sample of ketene and its derivatives such as diketene, methyldiketene, bis(trimethylgermyl)ketene, dichloroketene, and bis(trifluoromethylthio)diketene have been studied by using GED. [9, 47, 48, 49, 50, 51] In the GED study of ketene and its dimer, the results were interpreted based on visual inspection of the photographic plates. Even so, the result was comparatively better than IR and MW studies. This is despite the bond distances and angles being assumed in both acetylene and methane. The complication arose that the GED method may have generated different unwanted byproducts, for instance ketene dimers and acetone pyrolysis decomposition products. The experiment can be modified to incorporate FVP into the GED apparatus (FVP-GED) to enable direct analysis of products of pyrolysis *in situ* rather than trapping them and subsequently analyzing them.

2. This work

This thesis aims to determine the thermochemistry and kinetics for the generation of ketene from diketene and establish whether these pathways are favourable in comparison to alternative reaction pathways such as formation of allene and carbon dioxide. The thesis then examines the reaction pathways for the formation of various substituted ketenes. This is a theoretical study using computational methods. The first part of this thesis concentrates on the computational findings relating to short-lived molecules such as ketene and methyleneketene, and the feasibility of their preparatory decomposition pathway reactions. The second part predicts the thermochemistry and kinetics for the formation of substituted ketenes generated from decomposition of MA derivatives. Finally the parent compounds were studied using computational methods to predict the dissociation pathways that generated the desired intermediate or short-lived species.

This work is the basis for the future experimental work with *in situ* gas electron diffraction coupled with mass spectrometry (MS-GED). Due to COVID-19 the MS was unable to be delivered in time to the University of Canterbury and therefore the proposed *in situ* structural studies of species generated using flash vacuum pyrolysis methods in conjunction with mass spectrometry to evaluate the composition of the gases was not undertaken.[51]

3. Methods

3.1. Gas Electron Diffraction

3.1.1. Theory

The theory behind the GED technique is the wave-particle duality of a microscopic object, such as an electron given by Louis de Broglie.[53]

$$p = h / \lambda \qquad \text{or } \lambda = h / mv \qquad (1)$$

Where the momentum of the electron, p, is related to Planck's constant h and wavelength, λ. p is equal to the product of the speed of the electron (v) and the mass of the electron (m). This equation explains the duality of matter in terms of wave property and particle nature for an electron, and the particle or waveform can be interconverted by the application of equation 1. The wave nature was epitomized by Young's double slits experiments[54] that the electron, on passing through the multiple slits, can form maxima and minima (as shown in Figure 7) due to diffraction and interference phenomena. It was noted that when a beam of electrons is incident on a molecule, the gap between atoms in the molecule functions as a slit to result in the diffraction of electrons. This phenomenon of electron diffraction was first noted by German and Davisson[55] and then confirmed by Thomson.[56] The first gas-phase X-ray diffraction experiment was undertaken by Debye[57] and then about a year later Mark and Wierl[58] carried out the first GED experiment.

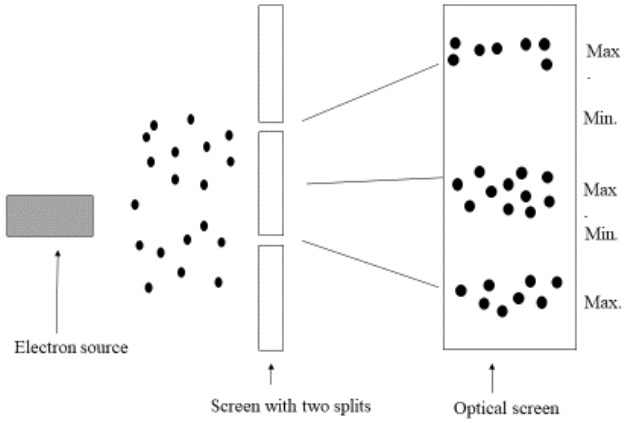

(a)

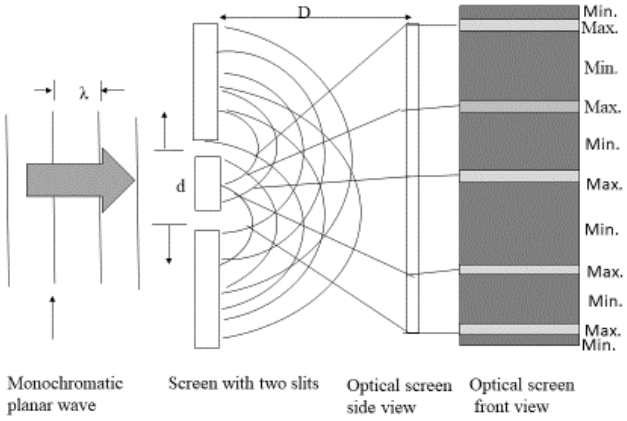

(b)

Figure 7: Obtained maxima and minima from diffraction in the double-slit experiment (a) a particle model (b) wave model (Max. = Maxima resulted from two converging waves, constructive interference, Min. = minima resulted from two diverging waves, destructive interference, λ = wave length, d = distance between two slits, D = distance between slits screen and optical screen side view).

3.1.2. GED apparatus

The schematic diagram of a typical GED apparatus is presented in Figure 8. They are not available commercially. The underlying principle is the same in all apparatus although settings and details vary.

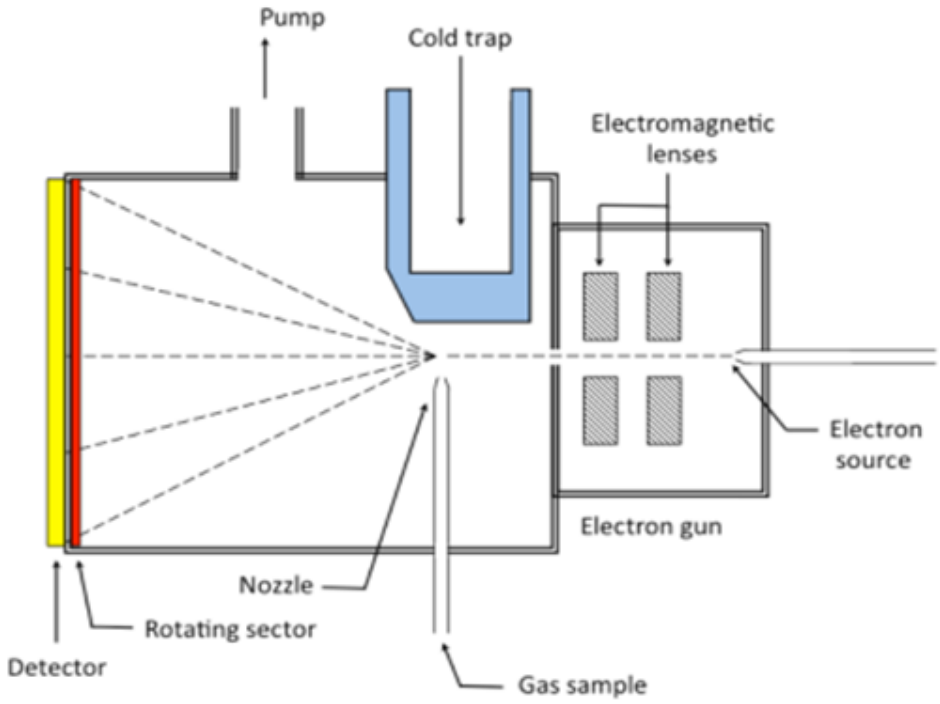

Figure 8: Schematic of the Canterbury GED apparatus taken from the Masters Research group.[18]

The gas sample is introduced from the nozzle into the path of the electron beam intersecting at right angles. A vacuum pump is used to minimize the scattering of the electron beam by unwanted sources. The source of the electron beam for the UC apparatus is tungsten wire of an electron gun, with an accelerating voltage (*ca*.) of 40 keV. This is focussed through a series of magnetic lenses and apertures to produce a wavelength comparable to the interatomic spacing in a molecule. The vapour pressure of the sample should be balanced by its flow rate from the nozzle. For a heated sample, the nozzle is also made hot to prevent the condensation of the sample. When the electron beam is incident on the sample gas, it produces an interference pattern on the screen which is then recorded.

3.1.3. Canterbury VHT Nozzle

A new very high temperature (VHT) inlet nozzle, as shown in Figures 9 (a) and (b), was made for the GED apparatus to enable *in situ* FVP-GED study of reactive and short-lived species. The nozzle was

tested for molecular structure determination of antimony (III) oxide.[59] The nozzle is configured to study involatile samples by allowing access to a higher range of temperatures.

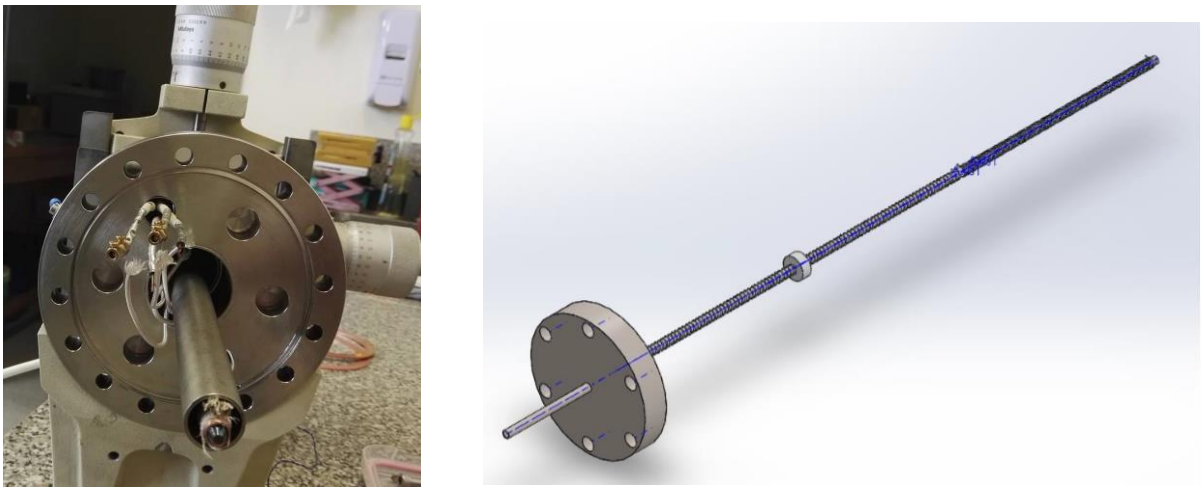

(a) (b)

Figure 9: (a) VHT nozzle inlet for Canterbury GED, (b) solidworks design of VHT inlet

The setup consists of an external inlet which passes the sample through the hot tube and out of an effusive nozzle into diffraction zone in the GED apparatus. The nozzle is designed in a way to make changing the sample easy to permit benzene calibration (of the nozzle to camera distance) to be obtained without changing the nozzle or breaking the vacuum.

When the electron beam is incident on the sample, it will be scattered and scattered electrons are recorded by a detector. The detector used by the Masters Research Group uses photographic film whereas image plates or a charge-coupled device (CCD) can also be used, although these do not have such a good dynamic range. The distance between the nozzle and detector is important as demonstrated by Young's Double slit experiment, this distance is calibrated using benzene, whose gas-phase structure is known accurately.

3.1.4. Data collection

Due to the random orientation of the gaseous molecules (one of the postulates of Kinetic Theory of Gases) with respect to the electron beam, interference pattern is obtained in the form of concentric rings which are the consequences of maxima and minima formed by the wave-front interferences (Figure 10a).

The intensity of scattered electrons falls off as r^4, where r is the radius of the diffraction pattern, thus the dynamic range of the intensity is too large to measure at high and low r at the same time. To overcome this problem, a rotating sector (a heart-shaped one is used by the Masters Research Group as shown in Figure 10b) is used which acts as a filter and normalises the exposure of the photographic film. One of the characteristic features of this sector is its curved edge (similar to the fourth power with an opening angle 'α'). On decreasing the scattering intensity to $1/4^{th}$ power, 'α' increases as the function of r^4 to the distance 'r_o', the maximum radius of the rotating sector. A beam stop is also used to prevent the backscattering of the non-diffracted electron beam.

(a) (b)

Figure 10: Illustration of a diffraction pattern (a)[60] obtained from the Canterbury GED apparatus with the use of the rotating sector (b).

A flatbed scanner is used to read the intensities over the whole plate and scan the diffraction pattern on the detector film, allowing digitization to extract the data.

The optical data (obtained by the above process) is first converted to total electron scattering intensity (I_{total}) as shown in equation 2:

$$I_{total} = I_{atomic} + I_{molecular} + I_{background} \qquad (2)$$

The atomic scattering and background scattering must be subtracted. Only molecular scattering contains the interference information from all pairs of atoms in the molecule and this is used to obtain the structural

information. Atomic scattering intensity results from scattering by a single-atom so does not produce an interference pattern. Total atomic scattering is the sum of the diffraction contribution of each atom in the molecule with atomic scattering factors, $F_i(s)$, obtained from published tables.

The total atomic scattering intensity can be expressed, as the function of the scattering angle, θ, and the scattering variable[61] (S), is given by equations 3 and 4.

$$S = 4\pi \sin(\theta / 2)/ \lambda \quad (3)$$

$$I_{\text{atomic}}(S) = \Sigma_i F_i (S)^2 / S^4 \quad (4)$$

Atomic scattering will not vary between molecules and can be subtracted from total electron scattering intensity. Background scattering consists of scattering from many sources such as incoherent inelastic scattering and extraneous scattering. This is removed by fitting a cubic spline function to the intensity curve. The molecular intensity curve (MIC) can be expressed into frequency components by Fourier transformation. The obtained Radial Distribution Curve (RDC) provides information about the probability of finding the inter-nuclear distance in the molecule, P(r). This probability distribution consists of Gaussian curves for each distance, superimposed to give the overall probability of an interatomic distance occurring at a particular distance. The conversion of a MIC to a RDC is shown in Figure 11.

The wide of the Gaussian curves in the RDC is determined by the mean vibrational amplitudes, with the area under each peak given by:

$$Area \propto (n_{ij} Z_i Z_j) / r_{ij} \quad (5)$$

Where n_{ij} is the multiplicity of r_{ij}, Z_i and Z_j are the atomic numbers of i and j atoms respectively. One of the problems of using this equation, similar interatomic distances, will give a composite peak that need to be deconvoluted. Due to the poor scattering power of hydrogen atoms, just like X-ray diffraction, GED cannot define their positions precisely. From the complete analysis of the diffraction patterns, the wavelength of the electrons and the distances between atoms a molecular structure can be elucidated.

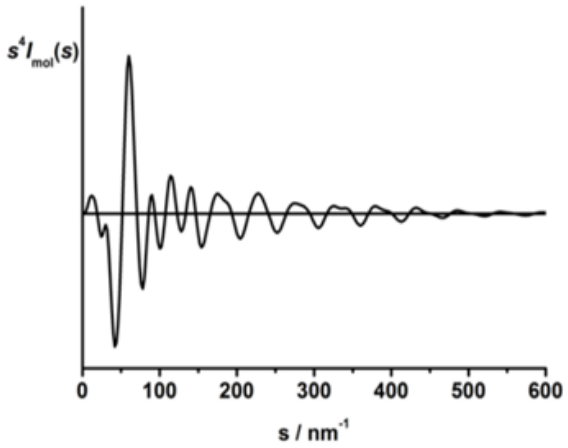

(a)

↕ **Fourier transform**

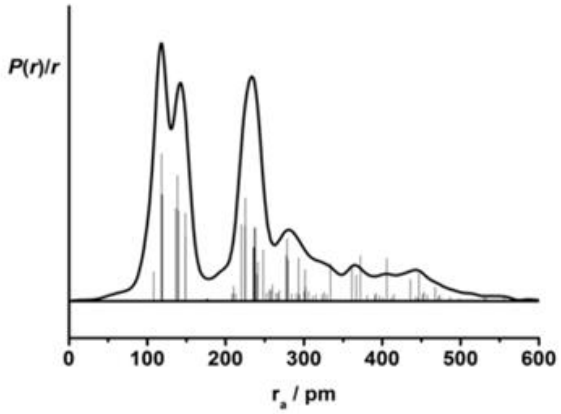

(b)

Figure 11: Conversion of (a) MIC to (b) RDC for the GED experimental data of the Canterbury apparatus, using $s^4I_{mol}(s)$.

3.1.5. Least-squares refinement

Experimental data is analyzed by comparison of the experimental MIC to that produced from a parameterized model of the molecule. A molecular model is made using the FORTRAN program using

the minimal number of parameters like bond lengths, bond angles, dihedral angles to complete the geometry of the molecule, using average and differences of structural parameters where appropriate. Starting values of the parameterized model are taken from the quantum chemical calculations such as *ab initio* or density functional theory (DFT) calculations, which provide the starting geometry for the refinement. The MIC of the model is prepared from the scattering equations.

In the least square refinement process, parameters in the model are adjusted to minimize the difference between the model and experimental data. This requires the molecular content of the analyzed gas vapour to be known. Fitting of the refined parameters can be checked throughout the experiment and agreement is made based on the goodness-of-fit factor, *R*-factor. A low *R*-factor means a better fit and there are two different ones quoted in GED papers, the first is R_D which represents the goodness of fit ignoring any correlation in the experimental data whereas R_G denotes the correlation of adjacent observations in the immediately off-diagonal position of the weight matrix.[62, 63]

The ratio of multiple isomers in the GED data can be determined using the Boltzmann factor. It is defined by relation as:

$$N_2 / N_1 = exp\ (-(E_2 - E_1)) / kT \qquad (6)$$

Where N_1 and N_2 are the number of molecules in state 1 and state 2 with respective energy in each state E_1 and E_2, k is the Boltzmann's constant (1.381×10^{23} JK^{-1}), and T is the absolute temperature in Kelvin scale.

3.1.6. Limitations

GED analysis on its own is usually limited to small and/or highly symmetric molecules. It does not elucidate enough information for a complex molecule or those with more than one conformer. The difficulty is in the similar internuclear distances in the molecule and hence overlapping peaks in the RDC. To solve this problem, several techniques such as combined analysis and Structural Analysis Restrained by *ab initio* Calculations for Electron diffractioN (SARACEN)[64, 65, 66] methods were developed. The combined analysis methods include GED, MW spectroscopy and/or LCNMR in the analysis. In the SARACEN method, the most probable structure is determined by combining experimental data with *ab initio* or DFT information. The DYNAMic Interaction of Theory and Experiment (DYNAMITE)[63] method, developed by Masters Research Group, works by dynamically linking theoretical data to the

experimental data within least-square refinement in the SARACEN method.[64, 65, 66] This method is further modified by introducing the Structural Enhancement Methodology for Theory and Experiment (SEMTEX),[67] which allows information from higher-level theoretical calculations to be incorporated into the refinement process.

The intermolecular vibration effect is another problem in GED. Molecules are vibrating, and the observed MIC in the GED refinement is an average of all vibrational states. For instance, the linear molecule CO_2 tends to be observed as bent rather than linear if left uncorrected from GED experiments, although the C=O bond length remains largely unchanged during the vibration. This effect is termed the shrinkage effect and the correction is made by using SHRINK software[68, 69] which applies a vibrational correction to each pair of atoms in the refinement process. For pairs of atoms with large amplitude motions, a molecular dynamics approach is better than using SHRINK corrections[70] as these are often not well defined using harmonic motions.

It is possible to use all the above information to generate theoretical RDCs for molecules and combinations of molecules. This was undertaken in this project to evaluate the feasibility of deconvoluting the RDCs to determine the structures of individual molecules.

3.2. Computational chemistry

As mentioned above, computational methods can be used to augment the observations from GED experiments, as well as calculate various other parameters of interest in molecules. Given the restrictions on the experimental research in this project, computational methods became the main tool for investigation of structural, thermodynamic and kinetic parameters for the systems being studied.

3.2.1. *Ab initio* methods

Ab initio methods of calculation employ quantum mechanical principles to find the solution of the time-independent Schrödinger equation.

$$\hat{H}\Psi = E\Psi \qquad (7)$$

Where, $\hat{H}$ is Hamiltonian operator (kinetic and potential energy term for both nucleus and electrons), Ψ is the molecular wave function, and E is the total energy of the system. The solution of this equation is used to find the energy of a specific molecular arrangement. The Schrödinger equation can only be solved exactly for one-electron systems. For multi-electron systems, certain simplifications are required to components of equation 7. Initially, $\hat{H}$ is simplified by the Born Oppenheimer (BO) Approximation, according to which the mass of hydrogen nucleus, equivalent to one proton, is about 1837 times of mass of electron so they should be treated separately. $\hat{H}$ is then reduced into the kinetic and potential energies of electrons, and nuclear-nuclear repulsion term becomes constant. There is difficulty in calculating electron-electron repulsion since the moving field of one electron affects the interaction with other electrons if present. Therefore the Schrödinger equation cannot be solved for the systems with more than one electron.

The Hartree-Fock (HF) potential is used to replace the electron repulsion to solve the one-electron Schrödinger equation. It is not precise to use the mean-field approximation, an assumption considering all electrons are static and an individual electron has average electron density to the other electrons in the molecule. This only defines about 99% of the energy of a system. When electrons come too close then energy of the system rises and there may be a change in structural parameters such as bond distances, angles and dihedral angles. To solve this problem, Møller–Plesset perturbation theory (MP)[71] adds electron correlation through a perturbation to the Hamiltonian utilizing Rayleigh–Schrödinger perturbation theory as in equation 8.

$$\hat{H} = \hat{H}_0 + \lambda V \qquad (8)$$

Where $\hat{H}_0$ is the unperturbed Hamiltonian operator, V is the small perturbation added and λ is an arbitrary real parameter that controls the size of the perturbation at usually to second (MP2), third (MP3) or fourth (MP4) order. MP2 is used in this thesis to generate the force fields required by Shrink during the preparation of input files for generation of the theoretical RDCs. It is less computationally expensive than other *ab initio* methods, such as coupled cluster, in terms of including electron correlation. DFT methods are also used and are a computationally faster way to evaluate vibrational frequencies.

3.2.2. Density Functional Theory (DFT) methods

Density Functional Theory encompasses mapping between electron density and energy of the condensed system or a single molecule, originating from the theoretical footing of Kohn and Hohenberg.[72] The mapping is explained by approximations such as the Local-Density Approximation (LDA) and Generalised Gradient Approximation (GGA).[73] In the former the exchange-correlation functional, the energy functional in Kohn-Sham theory[74] which are written using molecular orbitals to express the non-interacting kinetic energy, is approximated and in the latter, the first derivative of electron density is used. Hybrid DFT methods combine DFT exchange-correlation with that resulted from HF methods. DFT is a less accurate method than post-HF methods but is suitable for large systems. In my work, DFT methods like B97M[75] and a hybrid meta exchange-correlation functional (M06-2X)[76] are used for geometry optimizations as well as intrinsic reaction coordinate (IRC)[77] calculations.

3.2.3. Configuration Interaction (CI) and Coupled Cluster (CC) methods

The most commonly used and accurate methods to account for electron correlation are the Configurational Interaction (CI)[78] and Couple Cluster (CC)[79, 80] methods, which are more computationally expensive than other methods due to the long CPU time and large amount of memory required. These are called post-HF methods with the mixed ground and excited state, and linear variational method for solving the non-relativistic Schrödinger equation within the Born–Oppenheimer approximation for a quantum chemical multi-electron system. Some commonly used examples are CIS (S denotes single excitation), CCSD (D related to double excitation), and CCSD(T) with ‘T’ triple excitation. For the thermochemical calculations in this thesis the latter method is used.

3.2.4. Complete Basis Set (CBS) methods

George Petersson and coworkers developed a family of composite methods called complete basis set methods. These methods extrapolate several single-point energies to an exact energy. In Gaussian 09 CBS-4M, CBS-QB3, and CBS-APNO are available (in increasing order of accuracy) and these methods offer errors of 10.5, 4.6, and 2.9 kJ/mol on the G2 test set. To determine the transition state structures and energy profile diagrams, the CBS-QB3[81, 82] energy calculations are used in my work representing a compromise between accuracy and resource requirement to run the calculations.

3.2.5. Basis sets

A set of mathematical functions that are used to signify the electronic wave function in an orbital within the molecules are called basic sets. These are used with DFT or HF[83] methods to change the partial differential equation of the model, a program with a set of mathematical functions, into algebraic equations for easy and workable implementation on a computer. The Schrödinger equation can calculate the simplified basis sets. It is not possible to use the basis sets of infinite size but larger truncated basis sets are used to define the location of an electron around the nucleus.

Basis sets may be classified as minimal (calculation by single basic function for each orbital on each atom of the molecule, for example STO-nG type), split-valance (having more basis functions per atom), and polarized (consists of orbitals with higher angular momentum than is needed to describe the basic orbitals; this allows molecular orbitals to change shape). 3-21G[84, 85] and 6-31G[76, 86] are examples of split valance (double-zeta) basis sets with two sizes basic function for each valance orbitals. Larger-sized of s and p functions are added to basis sets by introducing diffuse functions, such as 6-311++G (d,p)[87, 88] where two polarized functions, p function to hydrogen and d function to heavy atoms, and two diffuse functions, one on a heavy atom and another on the hydrogen, are added. Pople-type split valence basis sets[76,84, 85, 86, 87, 88] and Dunning's correlation consistent basis sets[89,90] are used in this thesis.

4. Experimental

4.1. Theoretical methods

The initial computational investigation for all molecules used both DFT and MP2 perturbation theory and was undertaken using both the Gaussian 09[91] and NWChem programs.[92] NWChem calculations were carried out by using the resources of New Zealand e-Science Infrastructure (NeSI). All MP2[93] methods were frozen core [MP2(FC)]. Geometric optimizations of molecules in this work were at the HF level with a 6-31G* basis set and at the MP2[93] and M06-2X[94] levels using the 6-31G*, 6-311G*, 6-311+G*, 6-311++G**[76, 95, 96, 97] and aug-cc-pVTZ[98] basis sets. Frequency calculations were conducted at MP2/6-311++G**. The thermodynamic parameters and transition state structures with reaction pathways were calculated using the synchronous transit-guided quasi-Newton (STQN) method.[99] The thermodynamic parameters were calculated using CCSD(T)/CBS with composite CBS-QB3[81] method as described by Curtiss et al.[60, 100] This method predicts thermochemical parameters with chemical accuracy in the range of mean absolute deviation less than 5.27 kJ/mol.[101] For the CCSD(T)/CBS method, the method is based on extrapolation of the energy to complete basis limit (CBS) using the power function extrapolation scheme suggested by Helgaker *et al.*[102] with the augmented correlation consistent basis sets, aug-cc-pVnZ basis sets of Dunning,[89] where n = D, T, and Q have been used.

$$E(x) = E_{\infty} + B X^{-\alpha} \qquad (9)$$

Where x is two for double-zeta basis sets, three for triple-zeta basis sets, etc. E_{∞} is energy at the basis set limit, and *'B'* and 'α*'* are fitting parameters.

Transition-state (TS) structures for the compounds along with the pyrolytic decomposition of all reaction pathways have been obtained using the synchronous transit-guided quasi-Newton (STQN) method.[99] The energy profile diagram was generated from the optimizations at the CBS-QB3[81] level. The input coordinates of this level were taken from the optimized TS at the B97D[75]/6-31++G(d,p) level. To ascertain the identity of the relevant transition structures, intrinsic reaction coordinate[77] (IRC) calculations were undertaken at the B97D[75]/6-31++G(d,p) level.

5. Results

5.1. Ketene and its preparation from diketene

5.1.1. Quantum chemical calculations

The *ab initio* ground state structure of diketene has C_s symmetry and its decomposition products ketene, carbon dioxide and allene have C_{2v}, $D_{\infty h}$, and D_{2d} symmetry respectively. The complete basis set and electron correlation calculation was introduced at the MP2[93] and M06-2X[94] level of theory, using the Pople-type basis sets augmented with diffuse and polarization functions, and Dunning's correlation consistent basis sets.[89] The structural parameters are given in Table 1 and Figure 12 below and can be used to provide initial parameters for the structural refinement of the GED experimental data.

Table 1: Optimized structural parameters for diketene, ketene, carbon dioxide and allene at different levels of theory and basis set. The atom numbering is shown in Figure 12 and calculated coordinates are given in Appendix Tables A9.2.1. to A9.2.5.

Parameters	MP2/ 6-31+G*	MP2/ 6-311G*	MP2/ 6-311+G*	MP2/ 6-311++G**	M06-2X/ aug-cc-pVTZ
Diketene					
rC(1)=O(10)	120.1	118.8	119.0	118.9	117.8
rC(5)=C(6)	132.9	132.8	132.9	133.0	131.3
rC-O(9)av	141.4	140.4	140.6	140.6	139.3
rC-O(9) diff	1.7	0.8	1.2	1.0	1.9
rC-C(2)av	151.5	151.7	151.7	151.8	151.4
rC-C(2) diff	2.0	2.3	2.2	2.2	1.9
rC-H av	108.8	108.7	108.7	108.7	108.3
∠C=C-H(8)	121.0	120.7	120.9	120.8	120.8
∠C=C-H(7)	119.9	120.0	119.8	119.5	119.7
∠O-C=C(6)	126.1	126.7	126.4	126.5	126.9

∠O-C=O(10)	127.6	127.5	127.5	127.5	127.6
∠C(1)-O(9)-C(5)	90.5	90.7	90.8	90.8	91.4
∠O=C-C(2)	139.3	139.4	139.4	139.4	139.4
∠C-C(2)-H	114.1	114.2	114.1	114.0	114.2
ϕH(3)-C-C=O(10)	64.0	64.3	64.2	64.4	64.5
Ketene					
rC(11)=O(15)	118.2	116.9	116.9	116.8	115.5
rC(11)=C(12)	132.3	132.0	132.1	132.2	130.7
rC(12)-H av	108.1	108.0	108.0	108.0	107.7
∠H-C=C(11)	119.6	119.5	119.5	119.1	119.1
Carbon dioxide					
rC(16)=O	118.1	116.9	117.0	117.0	115.5
Allene					
rC(22)=C	131.6	131.3	131.4	131.4	129.9
rC-H	108.6	108.6	108.6	108.6	108.2
∠H-C=C(22)	121.2	121.1	121.1	120.9	120.9

[All bond distances (r) in pm, and bond angles (∠) and dihedral angles (ϕ) are in degree (°)]

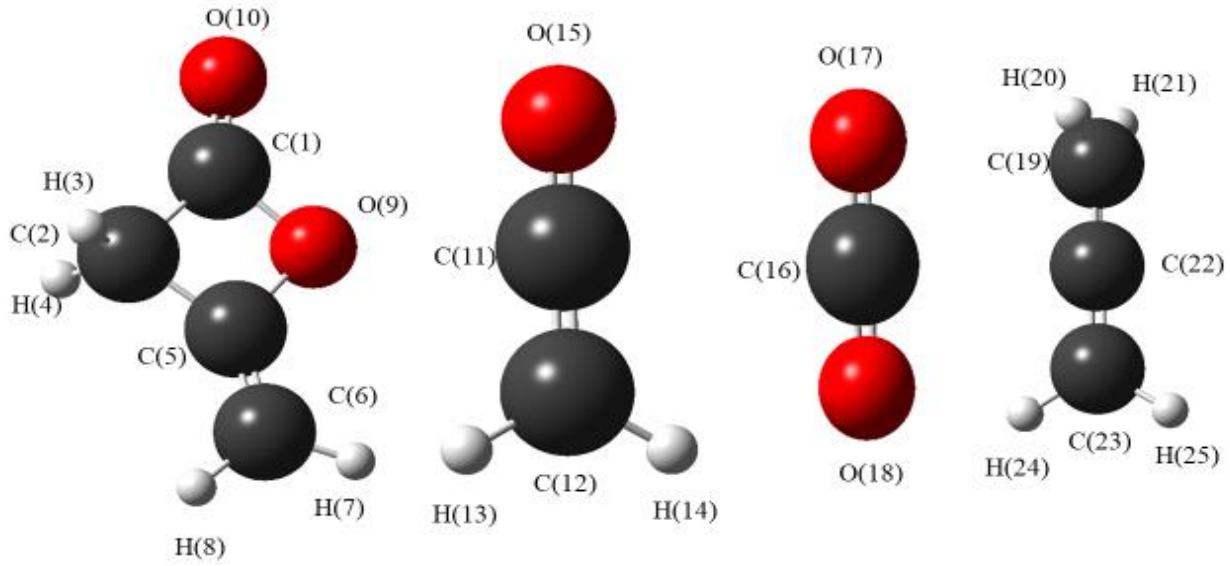

Figure 12: Lowest energy ground state structure of diketene, ketene, carbon dioxide and allene (left to right)

5.1.2. Thermochemical calculations

Thermochemical values have been computed at the CCSD(T)/CBS and CBS-QB3[81] levels of theory. The method is based on extrapolation of the energy to CBS using power function extrapolation scheme,[102] and the augmented correlation consistent basis sets (aug-cc-pVnZ of Dunning,[89] n = 2, 3 & 4) level. Two alternative pyrolysis decomposition pathways of diketene were studied, Pathway 1 leading to ketene formation and Pathway 2 leading to the formation of both allene and carbon dioxide. The pathways are shown above in Figure 4 (Section 1.2). The reaction to form allene and carbon dioxide (Pathway 2), parameters shown in Table 2, was found to be exothermic and spontaneous compared to the ketene formation (Pathway 1) reaction at standard temperature. This is an unexpected observation, however the temperature of the pyrolysis reaction of diketene is usually in the range of 653 to 823 K. The calculated energies and thermochemical parameters are given in Appendix Table A9.2.7.

Table 2: Calculated thermochemical parameters of Pathway 1 and Pathway 2 calculated from CCSD(T)/CBS (Energy) and MP2/cc-pVTZ (*H*corr. and *G*corr.) and CBS-QB3 level for decomposition of diketene.

	Reaction Pathway 1		Reaction Pathway 2	
Thermochemical parameters	CCSSD(T)/CBS	CBS-QB3	CCSSD(T)/CBS	CBS-QB3
ΔH	92.6	78.1	-21.5	-23.0
ΔG	38.6	25.1	-68.8	-68.3
ΔS	181.0	178.0	158.5	151.9

[Pathway 1 = ketene formation and Pathway 2 = allene and CO_2 formation as shown in Figure 4, all the values are in kJ/mol except ΔS, whose values are in J/mol]

Given the unusual results for the room temperature calculations, thermochemical parameters were also predicted at elevated temperatures. The calculations gave different thermochemical correction parameters, such as *H*corr and *G*corr, which were then used to obtain the thermochemistry of the two reaction pathways of diketene decomposition at that particular temperature. The same energies from the CCSD(T)/CBS calculations, as in Table 2 above, were used. It was found that the change of temperature affects the thermochemical parameters of both reactions quite dramatically as shown in Table 3. The calculations were performed at three different temperatures, the lowest possible decomposition temperature was taken as 653 K and the highest possible temperature was assumed to be 823 K along with standard room temperature 298.15 K. It was predicted that Pathway 1, forming ketene, was more favoured than Pathway 2 forming allene and carbon dioxide at elevated temperatures. The ketene formation of Pathway 1 reaction is predicted to be spontaneous under the regime of the pyrolysis reaction temperatures (negative free energy values).

Table 3: Predicted thermochemical properties at different temperatures (298.15 K, 653 K, and 823 K) of diketene decomposition pathways taken from CCSD(T)/CBS (energy) extrapolation and MP2/cc-pVTZ (*H*corr. and *G*corr.).

	Reaction Pathway 1			Reaction Pathway 2		
Properties	298.15 K	653 K	823 K	298.15 K	653 K	823 K
ΔH	92.6	94.5	93.3	-21.5	-21.4	25.6
ΔG	38.6	-27.3	-58.8	-68.8	55.6	125.8
ΔS	181	186.5	184.9	158.5	-118	121.7

[Pathway 1 = ketene formation and Pathway 2 = allene and carbon dioxide formation as shown in Figure 3, all the values are in kJ/mol except ΔS, whose values are in J/mol]

5.1.3. Kinetic calculations

The kinetics of decomposition of the diketene was calculated at CBS-QB3[81] level. The input coordinates for this level were taken from the B97D[75]/6-31++G(d, p) level optimized TS structure. Ketene forming intermediate state (TS1) and allene and carbon dioxide forming intermediate state (TS2) were confirmed from the IRC[77] calculations at the same level. The progress of the reactions was plotted based on the relative energies of reactants, TS and products, in Figures 13 and 14 with the structures of TS1 and TS2 shown in Figure 15. Of the two pathways, ketene formation (Pathway 1) is kinetically favoured with a lower relative activation energy (E_a) than allene and carbon dioxide formation (Pathway 2) by about 30 kJ/mol at standard temperature (298.15 K).

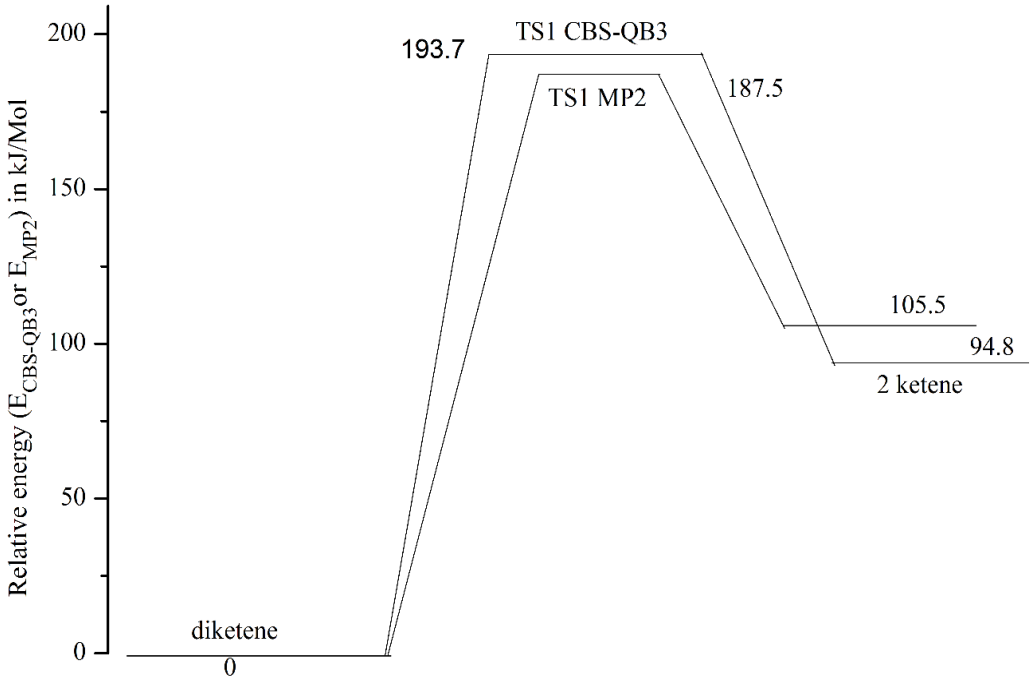

Figure 13: Energy profile diagram for Pathway 1 (TS1) at 298.15 K with CBS-QB3 and MP2 level of theory. Relative energies are in kJ/mol.

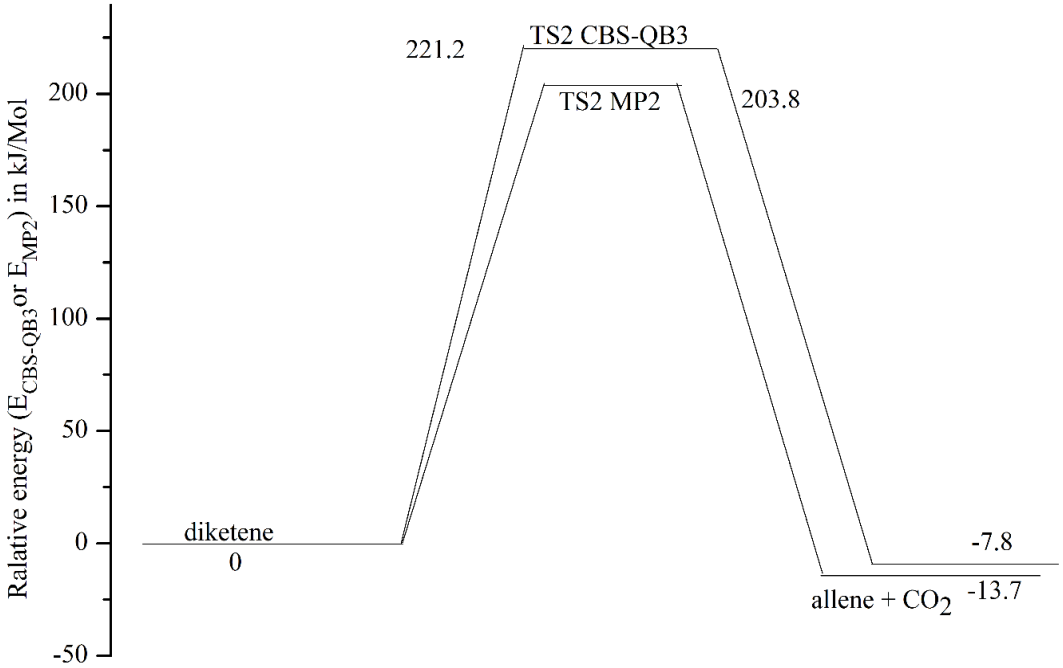

Figure 14: Energy profile diagram for the Pathway 2 (TS2) at 298.15 K with CBS-QB3 and MP2 level of theory. Relative energies are in kJ/mol.

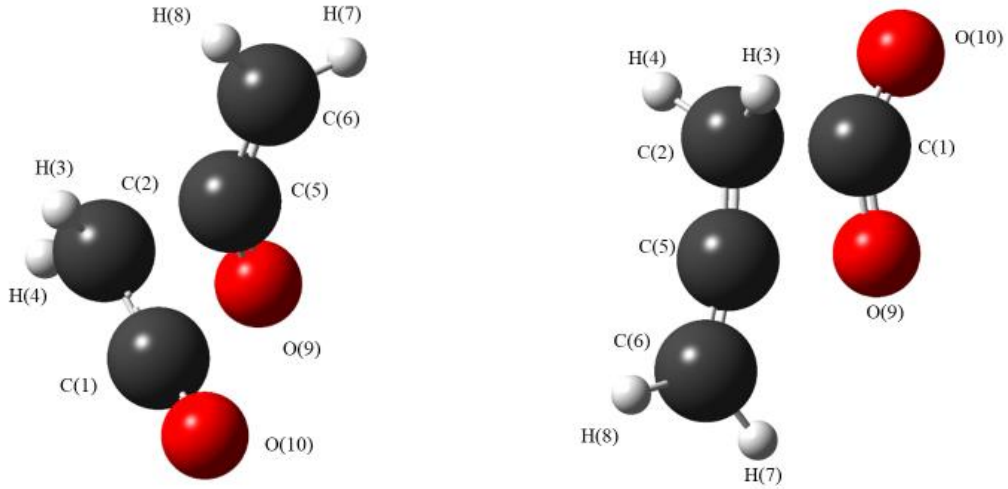

TS1 TS2

Figure 15: Predicted TS structures, optimized at the CBS-QB3 level. TS1 = ketene forming transition state and TS2 = allene and carbon dioxide forming transition state. Calculated coordinates of TS structures are given in Appendix Table A9.2.6.

5.2. Methyleneketene and its preparation from diazotetranoic acid

5.2.1. Quantum chemical calculations

The *ab initio* ground state structure of diazotetranoic acid has C_s symmetry and its decomposition products, methyleneketene, carbon dioxide, carbon sub-oxide and formaldehyde have C_{2v}, $D_{\infty h}$, $D_{\infty h}$ and C_{2v} symmetry respectively. The complete basis set and electron correlation calculations were introduced at the MP2[93] and M06-2X[94] level of theory, using the Pople-type basis sets augmented with diffuse and polarization functions, and Dunning's correlation consistent basis sets.[88] The structural parameters are given in Table 4 and Figure 16 below and can be used to provide initial parameters for the structural refinement of the GED experimental data. Calculated coordinates of each method in Table 4 are given in Appendix Table A9.3.1. to A9.3.5.

Table 4: Optimized structural parameters for diazotetranoic acid, intermediate (4-oxomethylideneoxetan-2-one), methyleneketene, carbon sub-oxide, formaldehyde, carbon dioxide, and nitrogen at different levels of theory and basis set

Parameters	MP2/ 6-31+G*	MP2/ 6-311G	MP2/ 6-311G*	MP2/ 6-311G**	M06-2X/ aug-cc-pVTZ
Diazotetranoic acid					
rC(2/8)=O(7/9)ave	119.1	119.3	118.1	118.1	119.6
rC=O diff	0.7	1.6	0.6	0.6	1.3
rC(1)-O(11)	145.0	149.4	143.9	143.7	142.8
rC(8)-O(11)	136.6	140.3	135.9	136.0	135.8
rC-C av	150.7	151.4	150.8	150.8	148.6
rC-C diff1	2.6	2.3	3.2	3.3	3.3
rC-C diff2	0.2	0.2	2.8	3.0	1.5
rC(1)-H(4/10) fixed	109.3	109.0	109.2	109.2	108.9
rC(3)=N(5)	138.7	136.9	139.5	139.5	138.6
rN(5)-N(6)	118.0	121.3	116.9	116.9	188.0
rC(1)---C(3)	237.3	239.7	236.2	236.2	235.9
∠C(1)-O(11)-C(8)	113.2	113.3	113.0	112.9	112.6
∠C(8)-C(3)-C(2)	109.4	110.3	109.5	109.5	108.7
∠O(9/7)=C-C(3) ave	129.1	128.8	129.2	129.2	128.6
∠O(9/7)=C-C(3) diff	0.5	1.9	1.3	1.4	0.2
∠C(3)-C(2)-C(1)	103.4	105.2	102.7	102.7	104.6
∠C(3)-C(8)-O(11)	106.8	105.3	107.0	107.0	107.8
∠O(11)-C(1)-H fix	109.0	108.4	109.3	109.5	109.6
∠C(3)-N(5)=N(6)	123.7	127.6	123.4	123.3	122.7
∠H(4)-C(1)---C(3)	123.8	123.5	123.7	123.5	123.8
ϕH(4)-C(1)-C(2)=O(7)	61.2	62.3	60.7	60.7	60.9
ϕC(1)-C(2)-C(3)=N(5)	-179.8	-180.0	-180.0	-180.0	-180.0
ϕO(7)-C(2)-C(3)=N(5)	179.9	180.0	180.0	180.0	180.0
ϕO(9)=C(8)-C(3)=N(5)	0.2	0	0	0	0

Intermediate					
rC(18)-O(20)	139.6	138.6	138.8	138.9	137.2
rC(18)=O(19)	120.5	120.0	122.3	119.2	118.2
rC(16)=C(15)	132.4	132.1	132.6	132.0	130.9
rC(15)-C(12)	150.8	150.6	152.3	150.9	150.8
rC(15)-C(18)	147.7	148.0	148.2	148.3	147.9
rC(12)-H(13/14) fixed	109.1	109.0	108.8	109.1	108.7
rC(12)-O(20)	147.9	147.2	154.1	146.4	145.4
rC(18)-O(20)	139.7	139.5	145.7	138.8	137.2
∠C(15)=C=O(17)	179.2	179.1	179.2	179.1	179.4
∠C(16)=C(15)-C(12)	139.0	139.0	136.6	139.0	139.6
∠C(15)-C(12)-H fix	116.7	116.3	116.6	116.1	116.2
∠C(15)-C(12)-O(20)	88.2	88.1	87.4	88.7	88.3
∠C(12)-O(20)-C(18)	91.7	91.3	90.3	92.0	92.6
∠O(20)-C(18)=O(19)	128.4	128.2	128.0	128.4	128.5
∠O(20)-C(18)-C(15)	92.6	92.4	92.2	92.7	92.7
∠C(18)-C(15)-C(12)	87.5	87.5	90.1	86.6	86.4
ϕH(13)-C(12)-C-C(18)	111.8	111.4	111.1	112.5	112.5
ϕH(13)-C(12)-C=C(16)	68.2	68.4	68.9	67.5	67.5
ϕH(14)-C-O-C(18)	117.8	117.4	117.4	117.5	117.5
Methyleneketene #					
rC(21)=O(22)	119.5	119.2	118.1	118.1	116.2
rC(21)=C(23)	128.4	128.3	128.2	128.3	128.7
rC(23=C(24)	132.8	132.6	132.5	132.5	131.4
rC(24)-H(25/26)	109.1	109.1	109.1	109.1	108.7
∠H(25)-C(24)=C(23)	122.1	122.1	122.0	122.0	121.5
Carbon suboxide #					
rC(28/30)=O(27/31)	125.8	120.7	117.1	117.1	115.2
rC(28/30)=C(29)	128.0	128.2	127.9	127.9	127.3

Formaldehyde					
rC(32)=O(33)	122.5	122.2	125.3	121.1	119.6
rC(32)-H(34/35)	110.2	110.1	109.7	110.6	110.3
∠H(34)-C(32)=O(33)	121.7	121.7	121.7	122.2	121.7
Carbon dioxide					
rC(36)=O(37/38)	118.1	116.9	117.0	117.0	115.5
Nitrogen					
rN(39)≡N(40)	113.1	112.6	112.0	112.0	108.6

All bond distances (r) in pm, and bond angles (∠) and dihedral angles (ϕ) are in degree (°)

All MP2 geometries are symmetry constrained to C_{2v} for methyleneketene and $D_{\infty h}$ for cabon suboxide

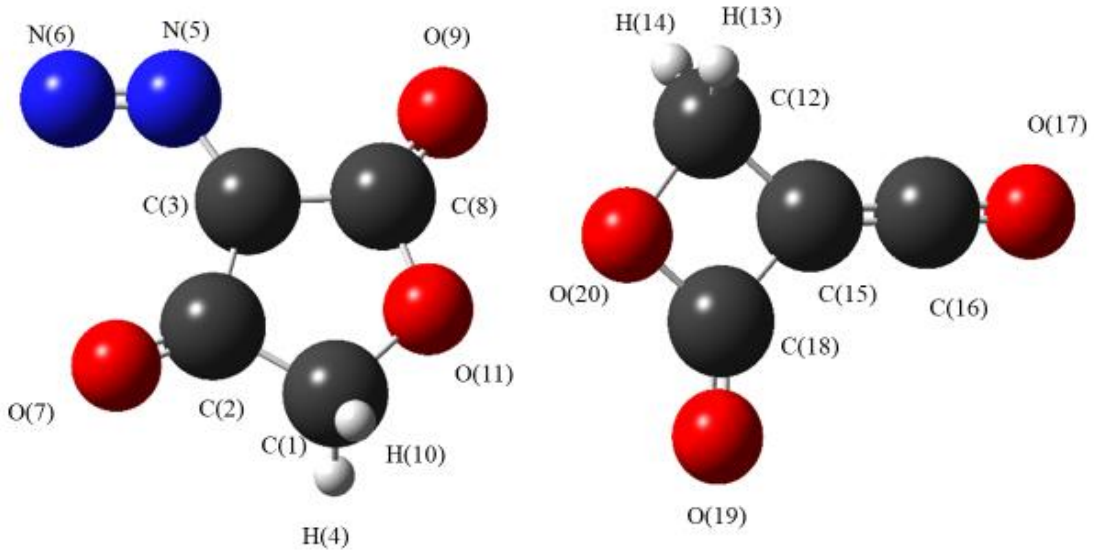

Figure 16 (a): Lowest energy ground-state structures of diazotetranoic acid (left) and the intermediate (right, 3-oxomethylideneoxetan-2-one).

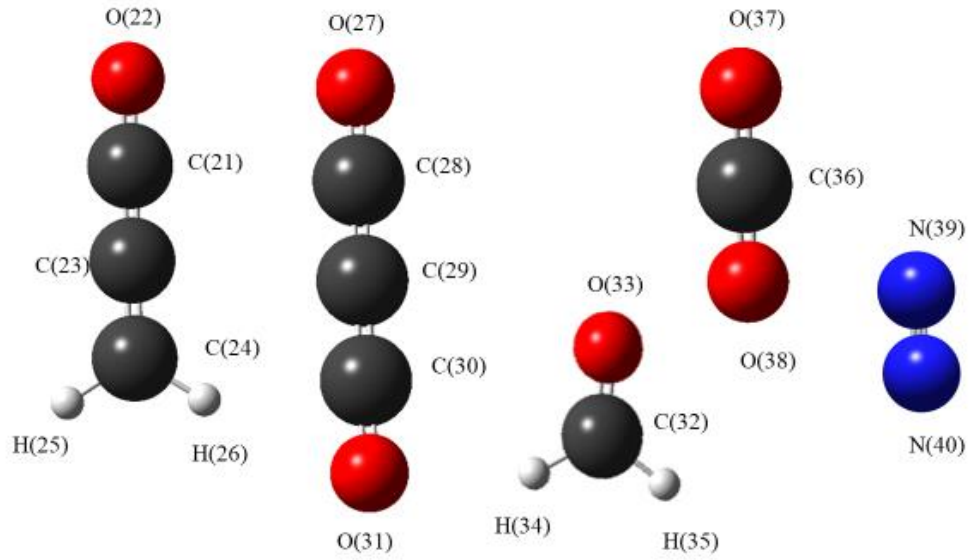

Figure 16 (b): Lowest energy ground-state structures of methyleneketene, carbon sub-oxide, formaldehyde, carbon dioxide, and nitrogen (left to right).

5.2.2. Thermochemical calculations

Two alternative pyrolysis decomposition pathways of diazotetranoic acid via a common intermediate (TS) route (reactions shown in Figure 5, Section 1.3) were studied. Pathway 1 yields methyleneketene and carbon dioxide whilst Pathway 2 yields carbon sub-oxide and formaldehyde. The thermochemical values have been computed at the CCSD(T)/CBS and CBS-QB3 levels of theory. The method based on the extrapolation of the energy to complete basis limit (CBS) using power function extrapolation scheme[102] and the augmented correlation consistent basis sets (aug-cc-pVnZ of Dunning[89] up to n=2, 3 & 4) level was used, thermochemical parameters are shown in Table 5. Formation of the TS and its subsequent decomposition to methyleneketene and carbon dioxide were predicted at 298.15 K to be spontaneous in the forward direction. Pathway 2, the formation of carbon sub-oxide and formaldehyde was predicted to be less energetically feasible than Pathway 1. The calculated energies and thermochemical corrections used to determine the thermochemical parameters are given in Appendix Table A9.3.7.

Table 5: Thermochemical parameters for the decomposition of diazotetranoic acid predicted at 298.15 K at the CCSD(T)/CBS and CBS-QB3 levels of theory.

Property	CCSD(T)/CBS	CBS-QB3
$\Delta G1$	-283.2	-302.2
$\Delta H1$	-237.7	-256.1
$\Delta S1$	153.4	154.4
$\Delta G2$	-59.3	-66.7
$\Delta H2$	-15.9	-22.8
$\Delta S2$	145.5	147.2
$\Delta G3$	-0.8	-8.3
$\Delta H3$	49.4	41.3
$\Delta S3$	168.4	166.6

[Note: 1 is the intermediate (TS) formation reaction, 2 denotes reaction pathway 1 and 3 represents reaction pathway 2, shown in Figure 4; all energies are in kJ/mol except ΔS which is in J/mol].

5.2.3. Kinetic calculations

For the above mentioned two alternative pyrolysis decomposition pathways of diazotetranoic acid via a common intermediate (TS) route the energy profile diagrams (illustrated in Figure 17) and corresponding TS structures (TS1 and TS2, portrayed in Figure 18), were constructed from the calculations at CBS-QB3[81] level. It was predicted that methyleneketene and carbon dioxide formation pathway 1 reaction was kinetically favoured with a lower energy barrier than for formation of carbon sub-oxide and formaldehyde (Pathway 2) by about 30 kJ/mol. The input coordinates of this level were taken from optimized TS structures from the B97D[75]/6-31++G(d, p) level. The TS structures for the compounds along with Pathway 1 and Pathway 2 have been obtained through the synchronous transit-guided quasi-Newton (STQN)[99] method. To ascertain the identity of the relevant transition structures, IRC[77] calculations were undertaken at the B97D[75]/6-31++G(d, p) level.

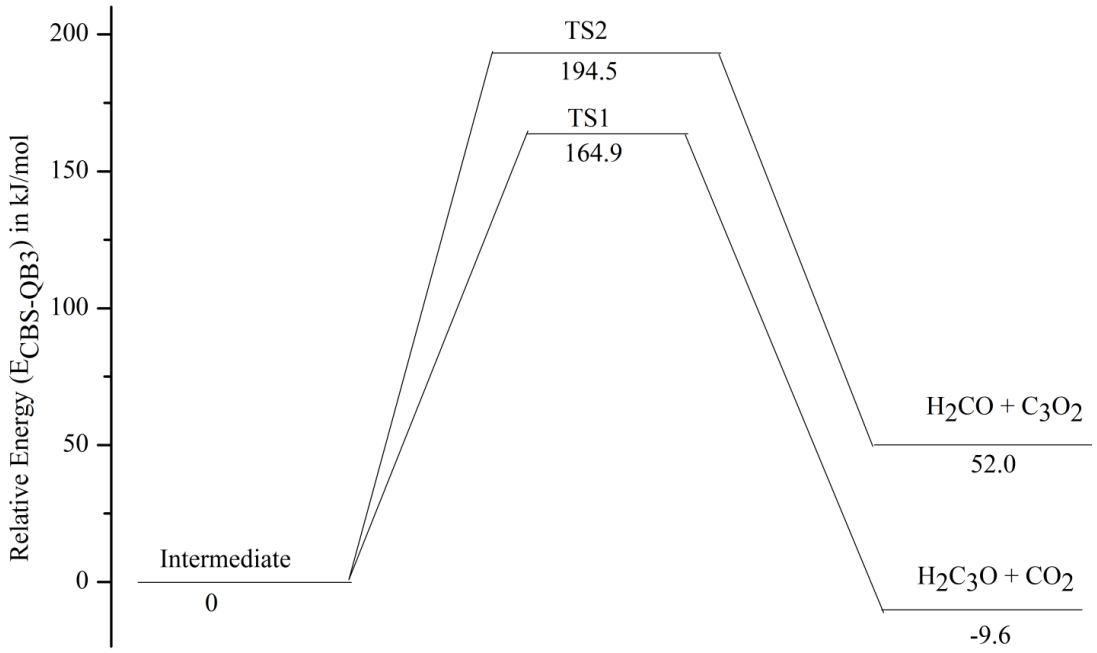

Figure 17: Energy profile for the pyrolysis decomposition pathways of diazotetranoic acid with two pathway reactions at 298.15 K computed at the CBS-QB3 level. Relative energy is in kJ/mol (TS1 leads to methyleneketene and carbon dioxide via Pathway 1 and TS2 leads to carbon sub-oxide and formaldehyde via Pathway 2)

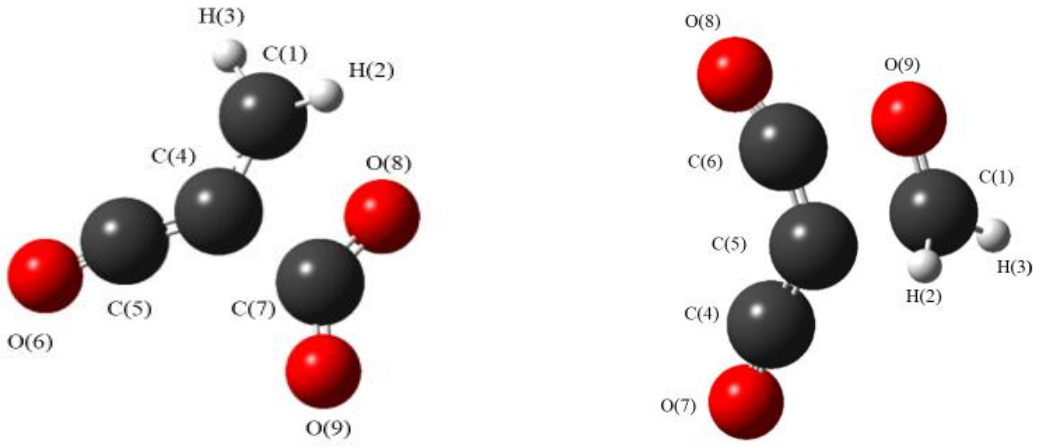

TS1 TS2

Figure 18: Predicted TS structures, optimized at the CBS-QB3 level for the pyrolysis decomposition of diazotetranoic acid, TS1 (left) to form methyleneketene and carbon dioxide intermediate state and TS2

(right) to form carbon sub-oxide and formaldehyde intermediate state. Calculated coordinates of TS structures of this theoretical level are given in Appendix Table A9.3.6.

5.3. Substituted ketenes and their preparation from derivatives of Meldrum's Acid (MA)

5.3.1. Quantum chemical calculations

5.3.1.1. Ketene and its preparation from pyrolysis decomposition of MA

The *ab initio* and DFT ground-state structure of MA has C_s symmetry. The decomposition products acetone, carbon dioxide and ketene with their lowest energy ground state are C_2, $D_{\infty h}$, and C_{2v} symmetry respectively. MA was found to adopt a boat structure. At lower levels the chair configuration was found to return an imaginary frequency in the vibrational analysis indicating that the structure is not real on the potential energy surface. At higher levels such as MP2, the structure failed to optimize. The complete basis set and electron correlation calculations were introduced at the MP2[93] and M06-2X[94] level of theory, using the People-type basis sets augmented with diffuse and polarized functions and Dunnings correlation consistent basis sets.[89] The structural parameters are given in Table 6 and Figure 19 below and can be used in the future to set the initial parameters for refinement of the GED experimental data.

Table 6: Optimized structural parameters for MA, ketene, carbon dioxide and acetone at different levels of theory and basis sets, and calculated coordinates are given in Appendix Table from A9.4.1 to A9.4.5.

Parameters	MP2/ 6-31+G*	MP2/ 6-311G*	MP2/ 6-311+G*	MP2/ 6-311++G**	M06-2X/ aug-cc-pvtz
Meldrum's Acid (MA)					
rC(6/7)=O(9/10)	121.5	120.2	120.3	120.4	119.1
rC(2)–O(4/5)	144.2	143.3	143.6	143.4	142.6
rC(6/7)–O(4/5)	136.7	136.2	136.2	136.2	134.9
rC(1)–C(2)	151.9	151.9	151.9	152.1	152.0
rC(2)–C(3)	150.9	151.0	151.0	151.1	151.2
rC(6/7)–C(8)	151.2	151.4	151.4	151.5	150.9
rC(8)–H(17)	109.8	109.5	109.6	109.6	109.2
rC-H(remaining)	109.2	109.1	109.1	109.2	108.8
∠H(11)–C(1)–C(2)	112.1	112.2	112.4	112.1	111.8
∠H(16)–C–C	109.2	109.0	109.2	109.2	109.3
∠H(11)–C–H(12/13)	108.5	108.3	108.3	108.5	108.6
∠H(16)–C–H(14/15)	109.4	109.3	109.3	109.4	109.4
∠C(1)–C(2)–C(3)	113.2	113.1	113.1	112.9	112.7
∠C(3)–C(1)–O	105.4	105.3	105.4	105.5	106.1
∠C(2)–C(1)–O	110.7	110.5	110.8	110.7	110.4
∠C(2)–O–C(6/7)	119.4	119.0	118.8	118.8	120.3
∠O(4/5)–C=O(9/10)	120.1	120.4	120.3	120.4	120.5
∠C(8)–C–O(4/5)	116.0	115.7	115.8	115.8	115.9
∠C(6/7)–C(8)–H(17)	108.9	108.9	108.9	108.7	108.4
∠H(17)–C(8)–H(18)	106.5	106.3	106.1	106.8	106.9
ϕO(4)–C(2)–C(1)–O(5)	123.9	124.4	124.0	124.0	123.1
ϕC(1)–C(2)–O(4)–C(6)	-78.1	-76.5	-75.4	-75.4	-77.4
ϕC(2)–O–C=O	171.9	170.9	169.7	169.9	170.7
ϕC(2)–O(5)–C(6)–C(8)	9.4	10.8	11.9	11.8	10.7
ϕO(4)–C–C(8)–H(17)	95.0	97.0	97.7	97.2	96.5
ϕC(6)–C(8)–H(17)–H(18)	117.1	116.7	116.8	117.0	117.4

Ketene					
rC(19)=O(21)	118.2	116.9	116.9	116.8	115.5
rC(19)=C(20)	132.3	132.0	132.1	132.2	130.7
rC(20)-H ave	108.1	108.0	108.0	108.0	107.7
∠H-C(20)=C(19)	119.6	119.5	119.5	119.1	119.1
Carbon dioxide					
rC(24)=O(25/26)	118.1	116.9	117.0	117.0	115.5
Acetone					
rC(27)=O(30)	123.2	122.1	122.1	122.0	120.5
rC(27)-C(28/29) fix	151.2	151.5	151.5	151.6	150.9
rC(28/29)-H (Axial)	109.1	109.0	109.0	109.0	108.6
rC(28/29)-H (Edu)	109.6	109.5	109.4	109.4	109.1
∠O(30)=C(27)-C(28/29)	121.6	121.8	121.8	122.0	121.9
∠C(27)-C(28/29)-H ave	110	110.1	110.2	109.9	109.9
∠C(27)-C(28/29)-H diff	0.7	1.0	0.7	1.3	0.3
ϕO(30)=C(27)-C-H (Ax)	-5.9	-6.7	-4.8	-8.4	0

[All bond distances (r) in pm, and bond angles (∠) and dihedral angles (ϕ) are in degree (°)]

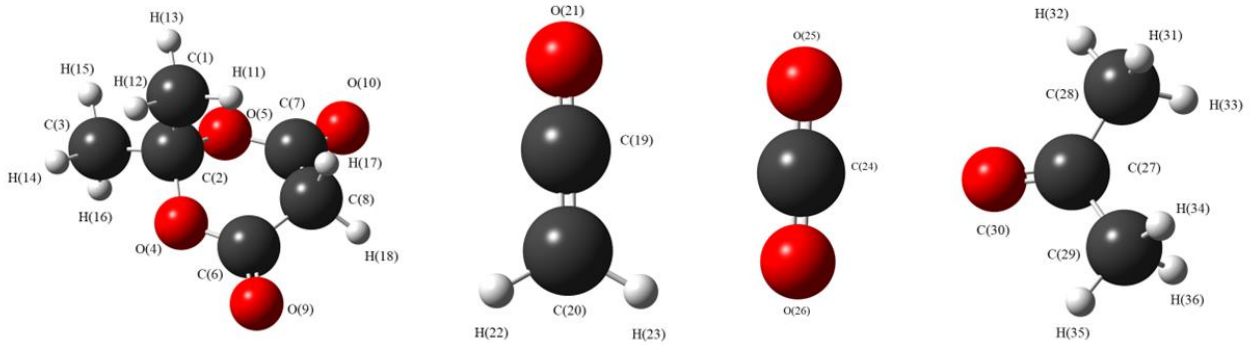

Figure 19: Lowest energy ground state structure of MA, ketene, carbon dioxide and acetone (from left to right).

5.3.1.2. Methyl-ketene and its preparation from pyrolysis decomposition of MMMA

MMMA has C_s symmetry and its thermal decomposition products acetone, carbon dioxide and methyl-ketene were obtained respectively C_2, $D_{\infty h}$, and C_s symmetry with their lowest energy ground state. The computational methods used were MP2[93] and M06-2X[94] level of theory, using the People-type basis sets augmented with diffused and polarized functions and Dunnings correlation consistent basis sets.[89] The structural parameters are shown in Table 7 and Figure 20 below and can be used to provide initial parameters for refinement of the GED experimental data.

Table 7: Optimized structural parameters for MMMA and methyl-ketene at different levels of theory and basis sets. Calculated coordinates are shown in Appendix Tables A9.4.7 to A9.4.11.

Parameters	MP2/ 6-31+G*	MP2/ 6-311G*	MP2/ 6-311+G*	MP2/ 6-311++G**	M06-2X/ aug-cc-pvtz
Mono-methyl-Meldrum's acid (MMMA)					
rC(6/7)=O(9/10)	121.5	120.2	120.4	120.4	119.1
rC(2)–O(4/5)	144.1	143.3	143.5	143.4	142.5
rC(6/7)–O(4/5)	136.8	136.3	136.3	136.3	134.9
rC(1)–C(2)	151.9	152.0	152.0	152.1	151.8
rC(2)–C(3)	151.0	151.2	151.1	151.2	151.0
rC(6/7)–C(8)	152.0	152.1	152.2	152.2	151.7
rC(8)–C(17)	152.5	153.2	152.6	152.7	151.9
rC(17)–H ave	109.1	109.0	109.0	109.0	108.6
rC(1/3)–H ave	109.3	109.1	109.2	109.2	108.8
rC(8)–H(21)	110.1	109.9	110.0	109.9	109.5
rC(2)--C(8)	276.7	274.5	275.0	274.6	275.3
∠H(11)–C(1)–C(2)	112.4	112.5	112.6	112.4	112.3
∠H(16)–C(3)–C(2)	109.6	109.8	109.8	109.5	109.3
∠H(11)–C–H(12/13)	108.5	108.3	108.4	108.6	108.5
∠H(16)–C–H(14/15)	109.4	109.3	109.3	109.4	109.4
∠C(1)–C(2)–C(3)	112.8	112.8	112.7	112.5	112.1
∠C(3)–C(2)–O(4/5)	105.3	105.2	105.2	105.3	105.9
∠C(1)–C(2)–O(4/5)	111.0	110.9	111.1	111.1	110.9

∠C(2)–O(4/5)–C(7/6)	120.0	119.6	119.5	119.4	120.9
∠O(4/5)–C(7/6)=O(9/10)	119.5	119.9	119.7	119.8	120.1
∠C(8)–C(7/6)–O(4/5)	116.3	116.1	116.3	116.2	116.1
∠C(6/7)–C(8)–C(17)	111.9	111.6	111.7	111.6	112.2
∠H(19)–C(17)–C(8)	110.6	110.3	110.5	110.3	110.2
∠H(19)–C(17)–H(18/20)	108.5	108.4	108.4	108.5	108.5
∠H(21)–C(8)–C(17)	108.6	108.5	108.4	108.8	109.8
∠C(1)–C(2)--C(8)	94.7	93.9	93.7	93.4	95.0
ϕO(4)–C(2)–C(1)–O(5)	124.2	124.7	124.4	124.4	123.7
ϕC(1)–C(2)–O(4)–C(6)	-82.1	-80.6	-79.5	-79.2	-81.9
ϕC(2)–O–C=O(9/10)	176.7	176.0	174.6	174.7	176.3
ϕC(2)–O(5)–C(6)–C(8)	3.7	5.1	6.4	6.4	4.3
ϕO(4)–C(7)–C(8)–C(17)	-160.6	-159.1	-158.1	-158.0	-159.9
ϕC(6)–C(8)–C(17)–H(21)	-177.4	-177.4	-177.1	-177.3	-177.3
ϕH(19)–C(17)–C(8)–C(6)	63.0	63.1	63.3	63.2	63.3
Methyl-ketene					
rC(23)=O(24)	118.6	117.2	117.3	117.2	115.9
rC(23)=C(22)	132.3	132.1	132.2	132.2	130.7
rC(22)–C(25)	151.1	151.2	151.3	151.3	150.8
rC(25)–H ave	109.4	109.3	109.3	109.3	109.6
rC(22)-H(29)	108.5	108.4	108.5	108.4	108.0
∠H(29)–C(22)=C(23)	120.3	116.4	116.3	116.1	115.6
∠C(25)–C(22)=C(23)	122.6	122.7	122.6	122.5	123.0
∠C(25)–C(22)–H(29)	120.9	121.0	121.0	121.5	121.4
∠ C(22)–C(25)-H(26)	111.0	111.2	111.2	111.0	111.0
∠H(26)–C–H(27/28)	107.8	107.7	107.7	107.8	110.9
ϕH(29)–C(22)=C(23)=O(24)	-179.6	-179.9	-179.9	-178.9	-180.0
ϕH(26)–C(25)–C(22)=C(23)	-0	-0	-0	-0	-0
ϕC(25)–C(22)=C(23)=O(24)	-0.4	0	0	0	0

[All bond distances (r) in pm, and bond angles (∠) and dihedral angles (ϕ) are in degree (°)]

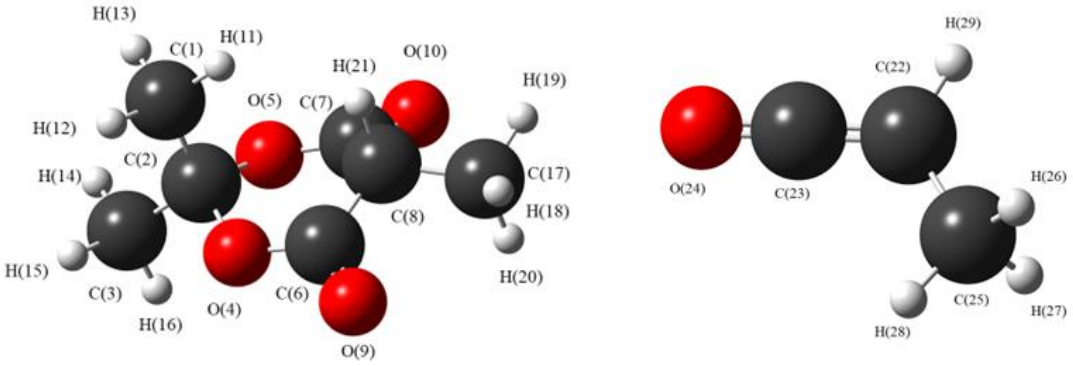

Figure 20: Lowest energy ground state structure of MMMA and methyl-ketene (left to right)

5.3.1.3. Dimethyl-ketene and its preparation from pyrolysis decomposition of DMMA

The *ab initio* and density functional theory (DFT) ground-state structure of DMMA has C_s symmetry and its decomposition products acetone, carbon dioxide and dimethyl-ketene were obtained with C_2, $D_{\infty h}$, and C_{2v} symmetry for their lowest energy ground state. The complete basis set and electron correlation calculation was introduced at the MP2[92] and M06-2X[93] level of theory, using the People-type basis sets augmented with diffused and polarized functions and Dunnings correlation consistent basis sets.[88] The structural parameters are given in Table 8 and Figure 21 below and can be used in setting the initial parameters for structural refinement of the GED experimental data once obtained.

Table 8: Optimized structural parameters for DMMA and Di-methyl-ketene at different levels of theory and basis sets. Calculated coordinates are given in Appendix Tables A9.4.13 to A9.4.17.

Parameters	MP2/ 6-31+G*	MP2/ 6-311G*	MP2/ 6-311+G*	MP2/ 6-311++G**	M06-2X/ aug-cc-pvtz
Dimethyl-Meldrum's acid(DMMA)					
rC(6/7)=O(9/10)	121.8	120.4	120.7	120.6	119.9
rC(2)–O(4/5)	143.8	143.1	143.3	143.2	142.7
rC(6/7)–O(4/5)	136.2	135.8	135.7	135.7	135.6
rC(1)–C(2)	151.3	151.5	151.4	151.6	152.1
rC(2)–C(3)	151.3	151.5	151.4	151.6	151.0
rC(6/7)–C(8)	151.6	151.6	151.7	151.7	152.5
rC(8)–C(17)	154.1	154.0	154.1	154.2	153.1
rC(8)–C(21)	154.1	154.0	154.1	154.2	154.7
rC(2/3)–H ave	109.3	109.2	109.3	109.2	109.5
rC(17/21)–H(18/24)	109.6	109.4	109.5	109.5	109.6
rC(17/21)–H(17/19/22/23)	109.3	109.1	109.2	109.2	109.4
rC(2)--C(8)	294.1	292.2	292.8	292.7	282.7
∠C(1)–C(2)--C(8)	122.9	122.9	123.0	123.1	96.2
∠H(11)–C(1)–C(2)	109.6	109.4	109.7	109.6	110.8
∠H(16)–C(3)–C(2)	109.6	109.4	109.7	109.6	109.4
∠H(11)–C(1)–H(12/13)	109.2	109.0	109.0	109.2	108.5
∠H(16)–C(3)–H(14/15)	109.2	109.7	109.0	109.2	109.5
∠C(3)–C(2)–C(1)	114.3	114.2	114.0	113.8	113.6
∠C(3)–C(2)–O(4/5)	106.9	106.8	106.9	106.9	106.5
∠C(1)–C(2)–O(4/5)	106.9	106.8	106.9	106.9	109.6
∠C(2)–O(4/5)–C(6/7)	125.3	125.2	125.3	117.0	118.0
∠O(4/5)–C(6/7)=O(9/10)	118.5	119.0	118.8	118.9	119.9
∠C(8)–C(7/6)–O(4/5)	119.5	116.9	119.2	119.1	117.6
∠C(6/7)–C(8)–C(17)	107.9	107.8	107.9	107.9	110.5
∠C(6/7)–C(8)–C(21)	107.9	107.8	107.9	107.9	105.5
∠H(19)–C(17)–C(8)	111.3	111.2	111.4	111.3	111.2

∠H(19)–C(17)–H(18/20)	108.7	108.8	108.6	108.7	109.0
∠H(24)–C(21)–C(8)	111.3	111.3	111.4	111.3	111.2
∠H(24)–C(21)–H(22/23)	108.5	108.6	108.8	109.0	108.6
∠C(17)–C(8)–C(21)	109.7	109.6	109.6	109.5	109.7
ϕO(4)–C(2)–C(1)–O(5)	123.8	124.4	124.2	124.3	122.1
ϕC(1)–C(2)–O(4)–C(6)	-118.6	-118.7	-118.8	-118.9	-69.2
ϕC(2)–O(4/5)–C(6/7)=O	180.0	180	180.0	180.0	153.8
ϕC(2)–O(5)–C(6)–C(8)	0	0	0	0	32.1
ϕO(4)–C(6)–C(8)–C(17)	120.8	120.9	120.8	120.9	135.9
ϕC(6)–C(8)–C(7)–C(21)	-120.8	120.9	-120.8	-120.9	-105.6
ϕH(19)–C(17)–C(8)–C(6)	-62.7	-62.9	-62.8	-62.8	-64.1
ϕH(24)–C(21)–C(8)–C(6)	62.7	62.9	61.8	62.8	61.0
Dimethyl-ketene					
rC(26)=O(27)	118.9	117.5	117.6	117.6	116.2
rC(26)=C(25)	132.3	132.1	132.1	132.2	130.7
rC(25)–C(32/28)	151.0	151.1	151.1	151.2	150.7
rC(28/32)–H(29/35)	109.4	109.2	109.2	109.3	108.8
rC(28/32)–H(30/31/33/34)	109.6	109.5	109.5	109.6	109.2
∠C(28/32)–C(25)=C(26)	120.3	120.3	120.3	120.2	120.4
∠C(32)–C(25)–C(28)	119.3	119.3	119.4	119.5	119.2
∠H(35/29)–C(32/28)–C(25)	112.0	112.2	112.2	112.0	112.2
∠H(35/29)–C(32/28)–H(34/31)	107.8	107.9	107.9	108.0	107.7
∠H(33/30)–C(32/28)–H(35/29)	108.0	107.9	107.9	108.0	108.2

[All bond distances (r) in pm, and bond angles (∠) and dihedral angles (ϕ) are in degree (°)]

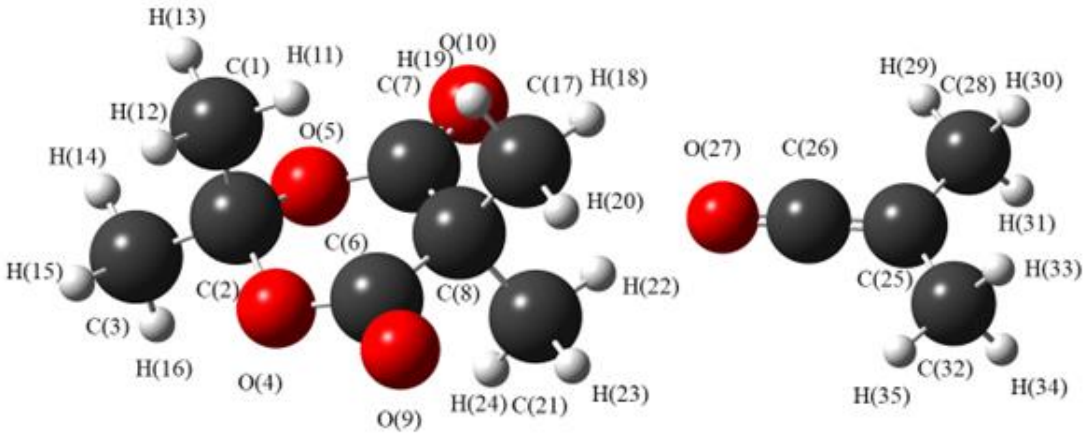

Figure 21: Lowest energy ground state structure of di-methyl-Meldrum acid and di-methyl-ketene (from left to right).

5.3.1.4. Methyleneketene and its preparation from pyrolysis decomposition of MeMA

The ground-state structure of MeMA has C_s symmetry and its thermal decomposition products acetone, carbon dioxide and methyleneketene, optimized with constrained bond distances, with their lowest energy ground state were found to have C_2, $D_{\infty h}$, and C_{2v} symmetry respectively. The computational methods used were MP2[92] and M06-2X[93] level of theory, using the People-type basis sets augmented with diffuse and polarized functions and Dunnings correlation consistent basis sets.[88] The results of structural parameters are given in Table 9 and Figure 22 below and they can be used for setting initial parameters in the refinement of the GED experimental data once obtained.

Table 9: Optimized structural parameters for MeMA and Methyleneketene at different levels of theory and basis sets. Calculated coordinates are given in Appendix Tables A9.4.19 to A9.4.23.

Parameters	MP2/ 6-31+G*	MP2/ 6-311+G*	MP2/ 6-311+G*	MP2/ 6-311++G**	M06-2X/ aug-cc-pVTZ
Methylene-Meldrum's acid (MeMA)					
rC(6/7)=O(9/10)	121.6	120.3	120.6	120.5	119.3
rC(2)–O(4/5)	144.2	143.4	143.6	143.7	142.7
rC(6/7)–O(9/10)	136.8	136.2	136.2	136.2	135.0
rC(8)–C(6/7)	149.3	149.6	149.6	149.6	149.1
rC(2)–C(1)	151.9	151.9	151.9	151.9	151.8
rC(2)–C(3)	150.7	150.9	150.8	150.9	150.7
rC(1/3)–H ave	109.3	109.2	109.2	109.2	108.8
rC(17)–H(18/19)	108.6	108.5	108.5	108.5	108.2
rC(2)--C(8)	271.2	268.8	269.4	269.2	271.5
rC(8)=C(17)	134.4	134.2	134.4	134.3	132.7
∠O(5/4)–C(2)–C(1)	110.4	110.3	110.4	110.4	110.0
∠O(4/5)–C(2)–C(3)	105.6	105.5	105.6	105.6	106.3
∠ C(2)–O(4/5)–C(6/7)	117.9	117.4	117.5	117.4	119.0
∠O(4/5)–C(6/7)=O(9/10)	120.4	120.8	120.7	120.7	120.7
∠O(4/5)–C(6/7)–C(8)	115.1	114.7	114.8	114.8	115.0
∠C(6/7)–C(8)=C(17)	120.2	120.0	120.2	120.2	120.3
∠C(2)--C(8)–C(1)	92.2	91.4	91.4	91.1	93.4
∠C(8)=C(17)–H(18/19)	120.3	120.3	120.3	120.3	120.0
∠C(2/8)–C–H ave	109.8	109.9	109.8	109.7	109.7
ϕO(4/5)–C(2)–C(1)–H(12)	-58.7	-58.3	-58.7	-58.6	-58.8
ϕO(9/10)=C(6/7)–O–C(2)	-164.0	-162.6	-162.7	-162.7	-162.1
ϕO=C(6/7)–C=C(17)	-16	-13.9	-15.7	-15.8	-1.2
Methyleneketene					
rC(21)=O(20)	119.5	118.2	118.2	118.2	116.2
rC(22)=C(21)	128.4	128.2	128.2	128.3	128.7
rC(22)=C(23)	132.8	132.7	132.7	132.6	131.4
rC(23)–H(24/25)	109.1	109.1	109.1	109.1	108.7

∠H(24/25)–C(22)=C(21)	122.1	121.9	121.9	121.9	121.7

All bond distances (r) in pm, and bond angles (∠) and dihedral angles (ϕ) are in degree (°)

All MP2 geometries are symmetry constrained to C_{2v} for methyleneketene and $D_{\infty h}$ for cabon suboxide

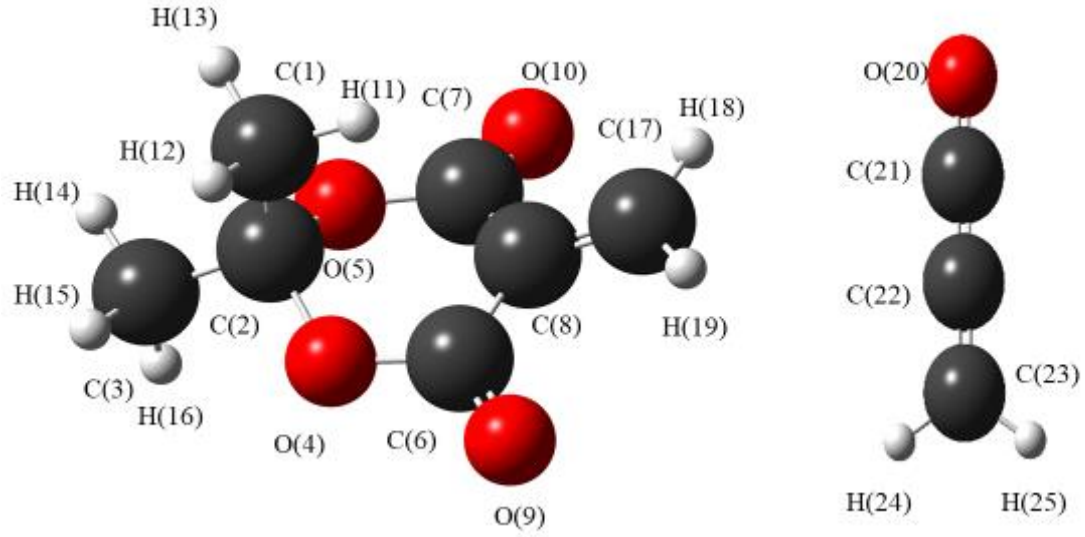

Figure 22: Lowest energy ground state structure of MeMA and methyleneketene (from left to right).

5.3.2. Comparative thermochemistry

The thermochemical values have been calculated at the CBS-QB3[80] levels of theory. The calculated energies and thermochemical corrections at the same level were used to determine the mentioned thermochemical parameters, shown in Table 10. The decomposition reactions of MA, MMMA and DMMA, as shown in Figures 6a and 6b, were predicted at 298.15 K, were found to be spontaneous in the direction of forming substituted ketenes along with carbon dioxide and acetone except MeMA, which was non-feasible at normal temperature. The experimental temperature is higher than the normal temperature so thermal decomposition of MeMA can also be feasible to form methyleneketene, CO_2 and propanone at elevated reaction temperature. MMMA looks more feasible than remaining MA derivatives in terms of more negative value of ΔG_r. The calculated energies and thermochemical parameters are shown in Appendix Table A9.4.25.

Table 10: Comparative thermochemical parameters for the decomposition of MA derivatives predicted at 298.15K at CBS-QB3 levels of theory.

Decomposition	MA	MMMA	DMMA	MeMA
Properties	CBS-QB3	CBS-QB3	CBS-QB3	CBS-QB3
ΔG_r	-36.6	-106.5	-20.1	53.2
ΔH_r	70.4	5.3	90.3	160.4
ΔS_r	358.9	375.2	370.4	359.7

[All energies are in kJ/mol except ΔS which is in J/mol]

5.3.3. Relative kinetic study

The kinetics of decomposition of the MA derivatives, shown in Figures 6a and 6b (Section 1.4), was calculated at CBS-QB3[81] level. The input coordinates for this level were taken from the B97D[75]/6-31++G(d, p). TS structures for the compounds along with their decomposition reactions have been obtained through the synchronous transit-guided quasi-Newton (STQN)[99] method. To ascertain the identity of the relevant transition structures, intrinsic reaction coordinate (IRC)[77] calculations were undertaken at the B97D[75]/6-31++G(d, p) level. This study compares the feasibility of products formation either by a single step mechanism or double step mechanism.

In the single step mechanism, cyclic intermediate state (TS) is formed from reactant molecule and then it decomposes to products as in pericyclic reaction, shown in Figure 23.

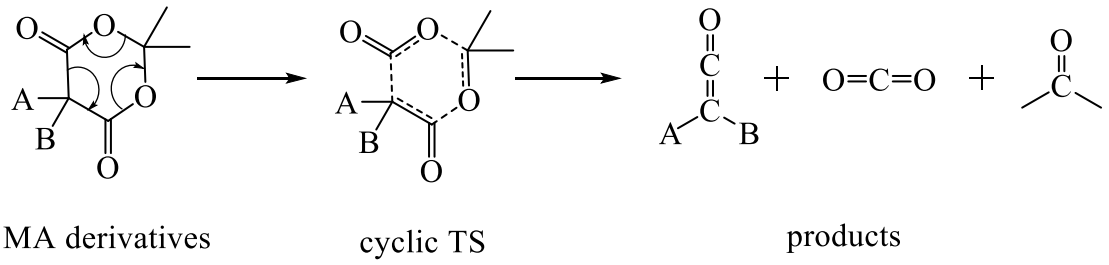

Figure 23: Mechanism of decomposition of MA derivatives with cyclic transition state (cyclic TS).

The second possible mechanism has double steps, firstly the formation of a cyclic intermediate state (TS) and then secondly the formation of TS2 as a result of TS losing acetone to form the required products, shown in Figure 24.

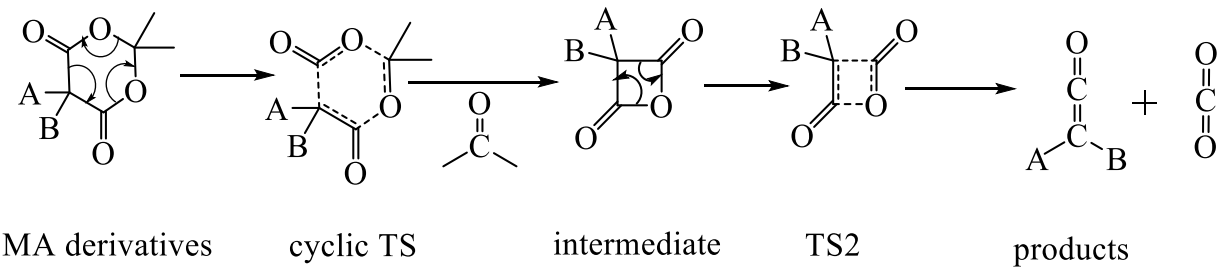

Figure 24: Mechanism of decomposition of MA derivatives with cyclic transition state (cyclic TS) and followed by the second transition state, TS2.

The energy profiles of the decomposition reactions of MA derivatives, as shown in Figures 6a and 6b, were plotted. Relative energies of the reactants, cyclic TS, TS2 and products are shown along with possible structures of the cyclic TS for the single step mechanism and cyclic TS followed by TS2 for double steps mechanism. These are shown in the Figures 25 to 36.

Of the two mechanisms, the one where a cyclic TS formed via a single step mechanism was found to be kinetically more favourable with a lower relative E_a than the alternative double step mechanism at standard temperature, 298.15 K. Comparing the energy required by the MA derivatives to cross the barrier to form products, MA, MMMA, and DMMA have an almost equivalent activation barrier but their E_a values were found to be 40 kJ/mol lower than that of MeMA.

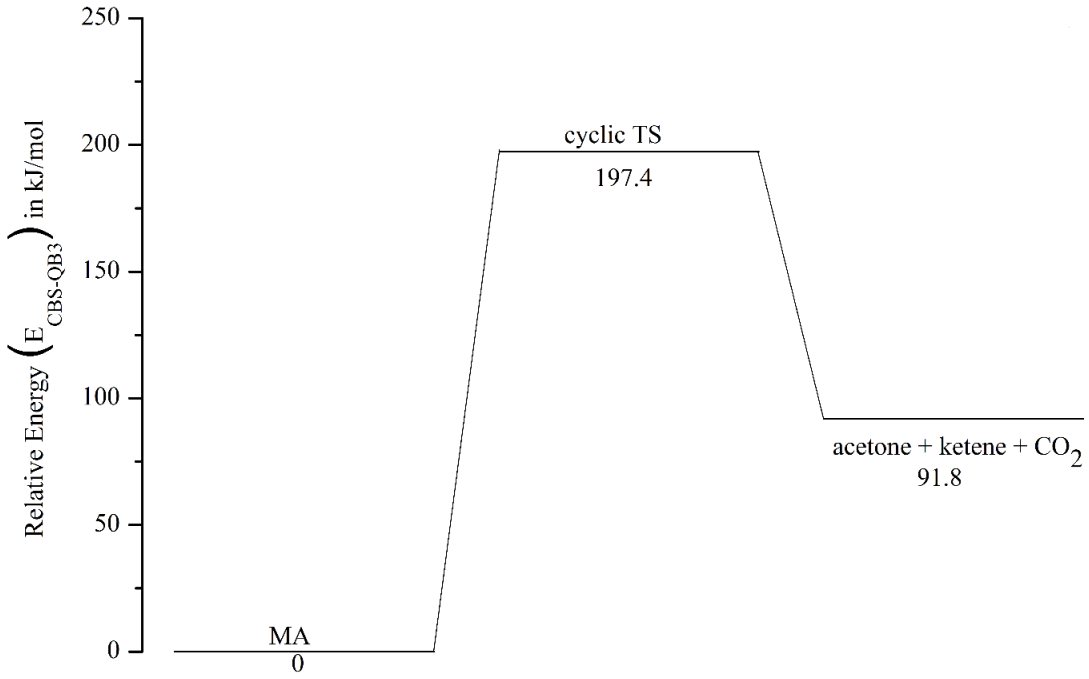

Figure 25: Energy profile diagram for cyclic TS with one step pericyclic mechanism of MA decomposition reaction at 298.15 K computed at the CBS-QB3 level; Relative energy is taken in kJ/mol.

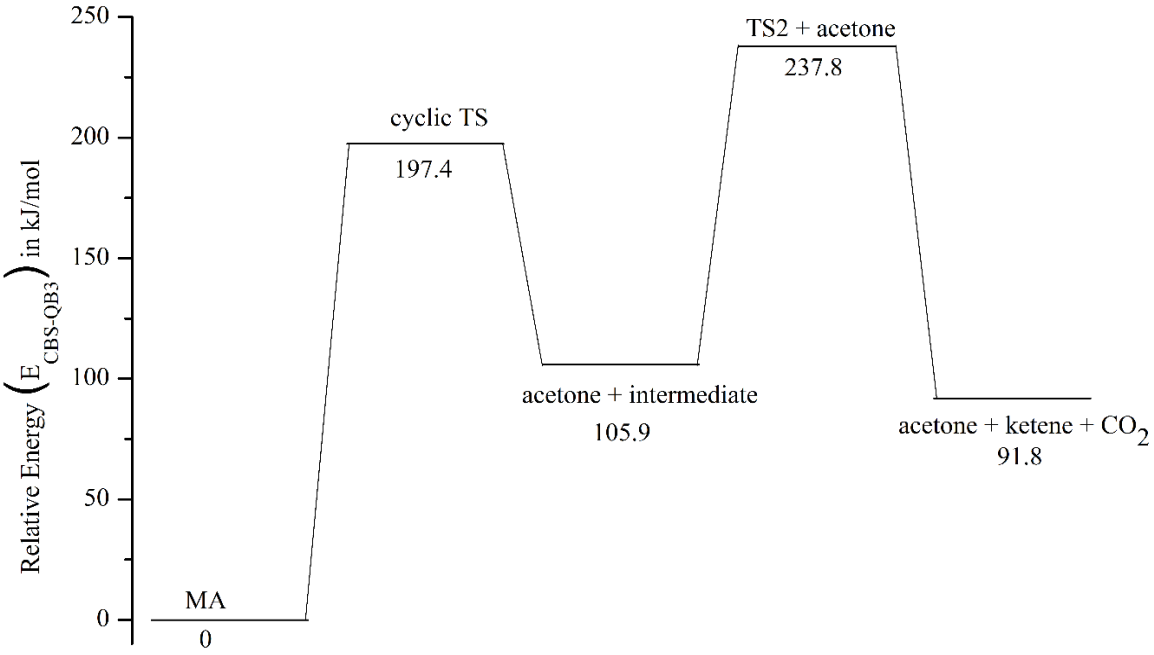

Figure 26: Energy profile diagram of cyclic TS followed by TS2 for two steps mechanism of decomposition of MA reactions at 298.15 K computed at the CBS-QB3 level; Relative energy is taken in kJ/mol.

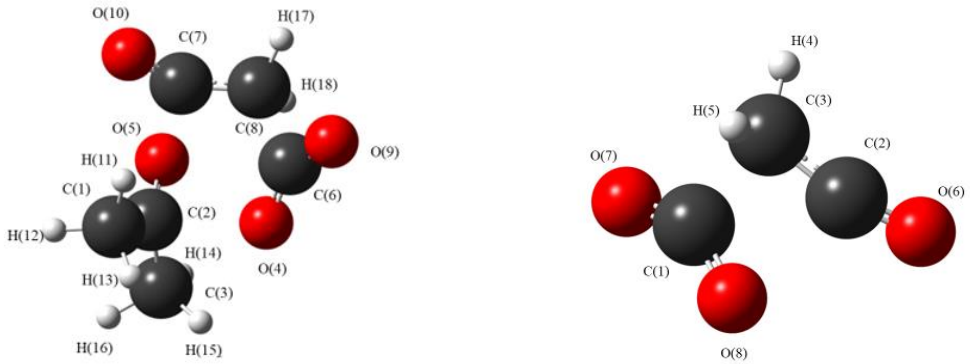

(a) (b)

Figure 27: Predicted cyclic TS (a) and TS2 (b) structures, optimized at CBS-QB3 level for decomposition of MA. Calculated coordinates of this level are given in Appendix Table A9.4.6.

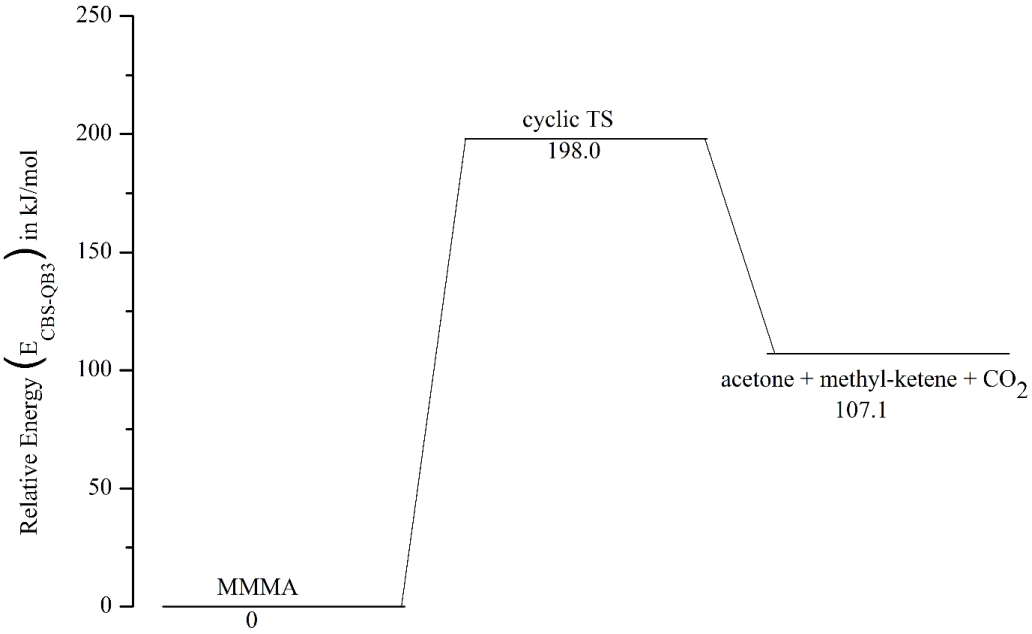

Figure 28: Energy profile for the pyrolysis decomposition MMMA with single cyclic TS forming reaction at 298.15 K computed at the CBS-QB3 level; Relative energy is taken in kJ/mol.

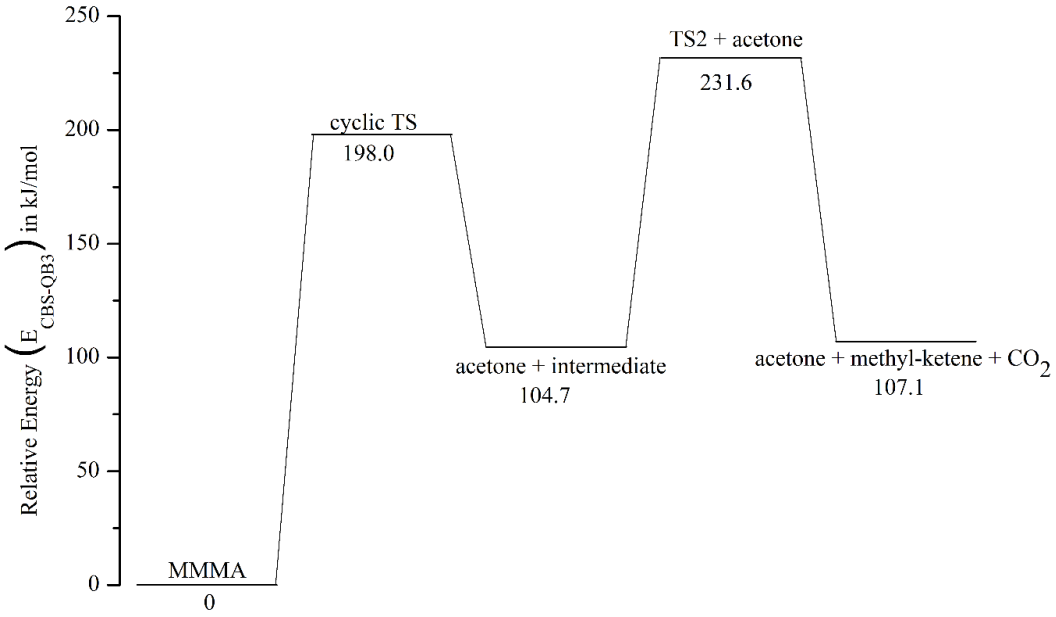

Figure 29: Energy profile for the pyrolysis decomposition MMMA with double steps cyclic TS and TS2 forming reactions at 298.15 K computed at the CBS-QB3 level; Relative energy is taken in kJ/mol.

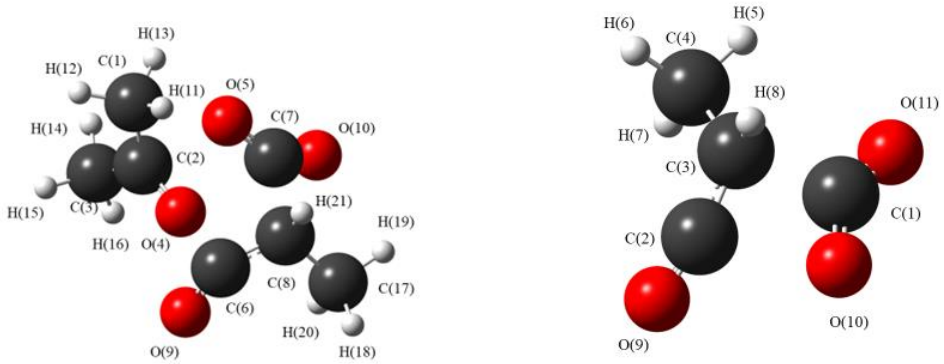

(a) (b)

Figure 30: Possible cyclic TS (a) and TS2 (b) structures, optimized at CBS-QB3 level for decomposition of MMMA. Calculated coordinates at this level are given in Appendix Table A9.4.12.

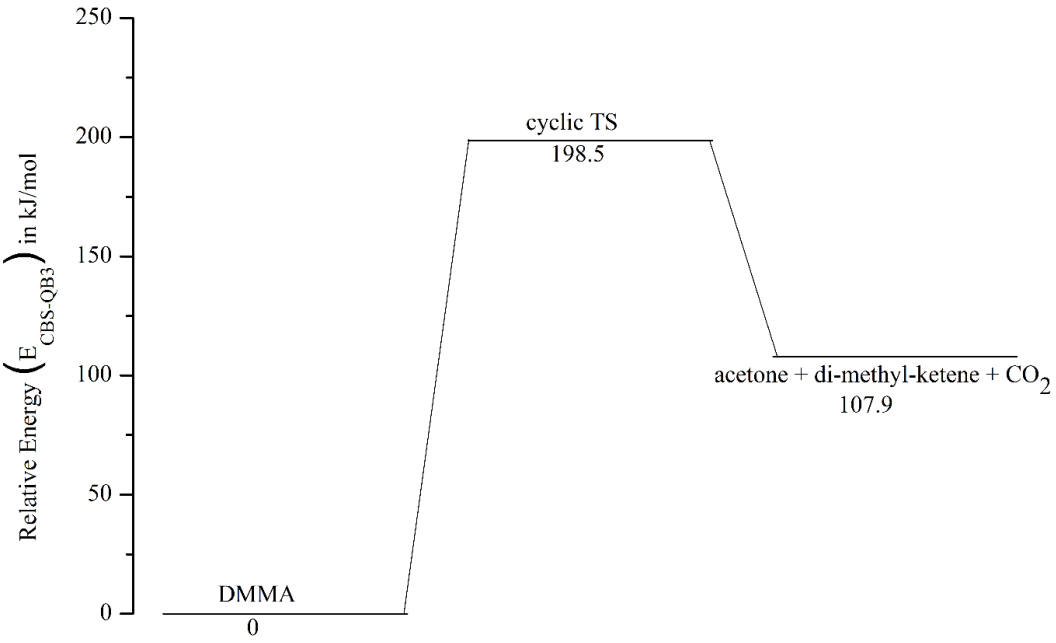

Figure 31: Energy profile for the decomposition DMMA with single cyclic TS forming reaction at 298.15 K computed at the CBS-QB3 level; Relative energy is taken in kJ/mol.

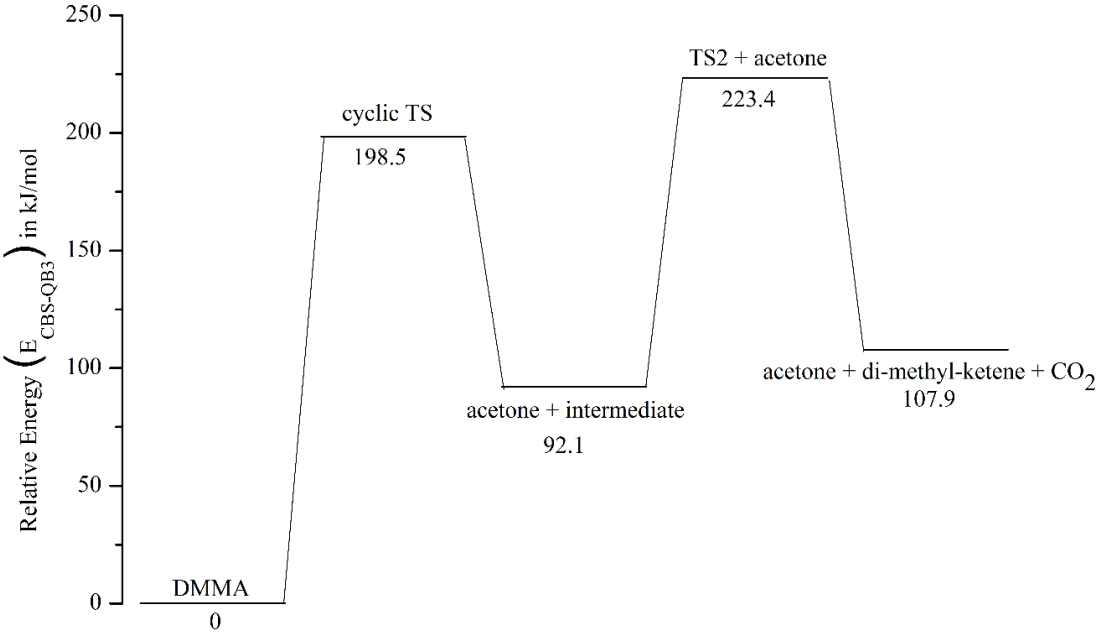

Figure 32: Energy profile for the decomposition DMMA with double steps cyclic TS and TS2 forming reactions at 298.15 K computed at the CBS-QB3 level; Relative energy is taken in kJ/mol.

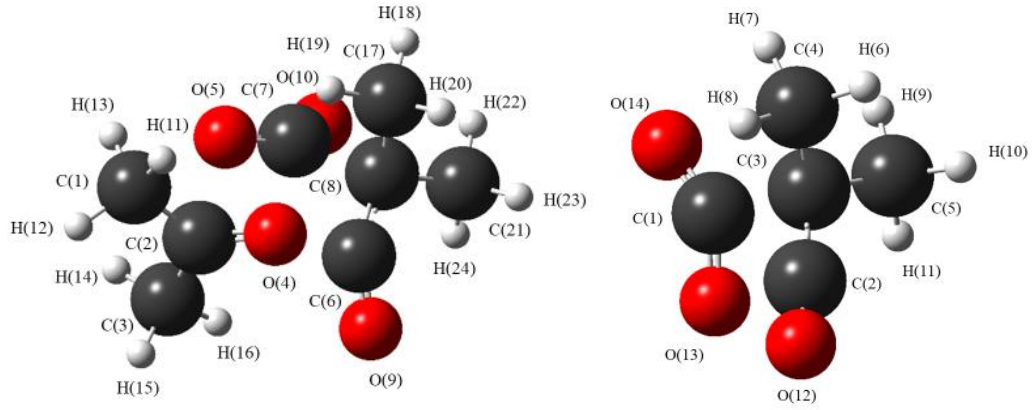

(a) (b)

Figure 33: Possible cyclic TS (a) and TS2 (b) structures, optimized at CBS-QB3 level for decomposition of DMMA. Calculated coordinates at this level are given in Appendix Table A9.4.18.

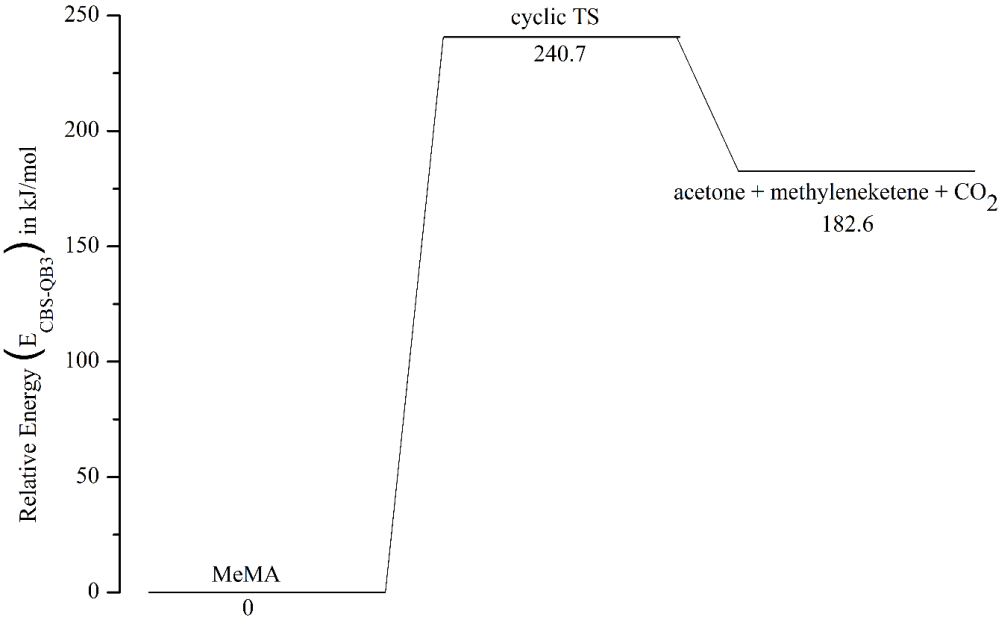

Figure 34: Energy profile for the pyrolysis decomposition MeMA with single step cyclic TS forming reaction at 298.15 K computed at the CBS-QB3 level; Relative energy is taken in kJ/mol.

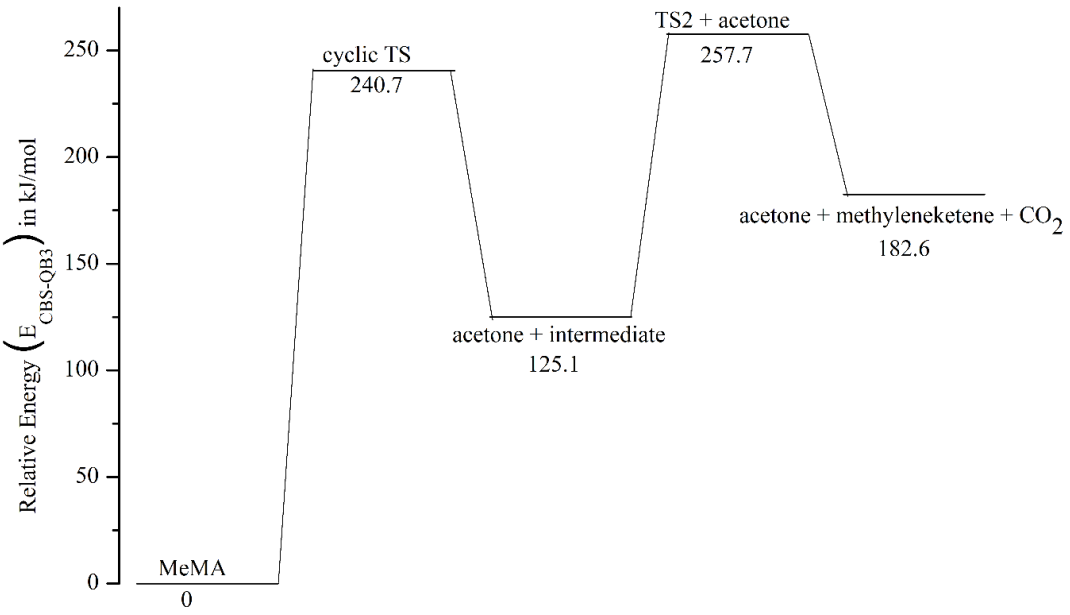

Figure 35: Energy profile for the pyrolysis decomposition MeMA with double steps mechnism with cyclic TS and TS2 forming reactions at 298.15 K computed at the CBS-QB3 level; Relative energy is taken in kJ/mol.

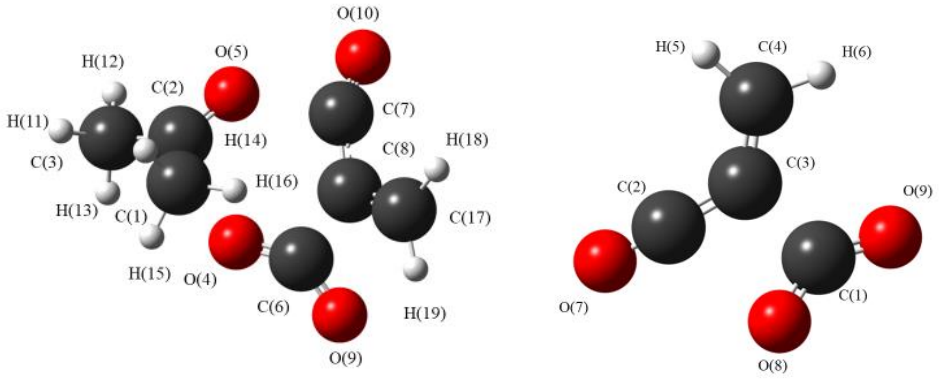

(a) (b)

Figure 36: Predicted cyclic TS (a) and TS2 (b) structures, optimized at CBS-QB3 level of theory for pyrolysis decomposition of MeMA. Calculated coordinates at this level are given in Appendix Table A9.4.24.

6. Discussion

6.1. Ketene and its preparation from diketene

The computed parameters of diketene along with previous computational, GED and X-ray crystallographic study of the structure of diketene are shown below in Table 11. The previous GED structures[9] of diketene differ from computed structure at MP2/6-311++G** level in certain geometrical parameters, such as the bond distances of rC=C, rC–C of ∠C–C=C, and rC–C of ∠C–C=O methoxy by 2.0 pm, 1.4 pm and 0.9 pm respectively and in bond angles at a range of 0.5 pm to 6.5 pm. The problematic differences in the bond angles of diketene were ∠O–C=O, ∠C–C=O, and ∠C=C–C respectively by 6.5°, 5.6° and 3.8°. The most recent X-ray crystal structure[11] of diketene is in very good agreement with the computed structure. This result shows the need for the GED experiments to address the gas-phase structure of diketene.

Table 11: Structural parameters of diketene from *ab initio*, X-ray single crystal diffraction and GED studies

Parameters	MP2/ 6-311++G**	X-ray 1 (C_1)[103, 104]	X-ray 2 (C_1)[10]	X-ray 3 (C_1)[11]	GED (C_s)[9]	CCSD(T)/ ANO1(C_s)[11]
rC=O	118.9	124.0	122.0	119.1	119.0	118.7
rC=C	133.0	135.0	132.0	131.5	131.0	132.5
rC–O methoxy	141.1	139.0	147.0	142.9	141.0	139.7
rC–O carboxy	140.1	140.0	139.0	138.5	141.0	139.7
$rC–C_{ring}$ adjacent to $C=CH_2$	150.7	148.0	154.0	150.3	152.0	150.9
$rC–C_{ring}$ adjacent to C=O	152.9	146.0	151.0	151.6	152.0	153.0
∠C=C–O	126.5	130.0	126.9	126.1	130.0	126.6
∠C=C–C	139.8	136.0	141.6	141.3	136.0	140.1
∠O–C(C)–C	93.6	94.0	91.3	92.6	95.0	93.3
∠C–O–C	90.8	89.0	90.0	90.6	89.0	91.1
∠O–C(O)–C	93.1	94.5	95.8	93.8	95.0	93.0
∠C–C–C	82.5	83.0	83.0	83.0	81.0	82.6
∠O–C=O	127.5	121.0	123.1	126.1	121.0	127.6
∠C–C=O	139.4	145.0	140.9	140.1	145.0	139.3

[All bond distances (r) in pm and bond angles (∠) are in degrees (°)]

Ketene has a good agreement between computed and experimental GED structures except the bond distance of rC=O shown in Table 12.

Table 12: Structural parameters of ketene from *ab initio*, X-ray single crystal diffraction and GED studies

Parameters	MP2/6-311++G**	GED-1[48]	MW[105]	GED-2[17]
rC=C	132.2	130.0	131.4	131.3
rC=O	116.8	116.0	116.1	114.8
rC–H	108.0	107.0	108.3	108.4
∠H–C–H	121.8	117.5	122.4	122.1

[All bond distances (r) in pm and bond angles (∠) are in degree (°)]

In terms of kinetic and thermochemical calculations, the ketene formed via pathway 1 at an elevated temperature was predicted to be spontaneous. The previous kinetic study performed by Chikos[106] extrapolated the Arrhenius plot from his experimental reaction flow system and found the relative activation energy of ketene formation from the pyrolysis of diketene was 209.2 kJ/mol, whilst for the reverse dimerization process it was 129.7 kJ/mol. In this work the calculations at CBS-QB3 level return energies that are lower by 15.5 kJ/mol for decomposition of diketene and 30.9 kJ/mol for dimerization of ketene. This computational finding suggests the decomposition of diketene favours towards ketene forming pathway 1 at the experimental temperature of pyrolysis.

The theoretical RDC was made for the decomposition of the diketene. The starting parameters for r_{h1}-type least-squares refinements were taken from theoretical geometries optimized at the MP2/6-311++G** level for both reactant (diketene) and product (ketenes and alternatively allene and carbondioxide). Parameterized molecular models describing ketene, allene, carbondioxide, and diketene independently were programmed in FORTRAN90 using their optimized coordinates from theory calculation at MP2/6-311++G** level. A theoretical Cartesian force field was obtained at the MP2/6-311++G** level and converted into a force field described by a set of symmetry coordinates using the SHRINK program,[68, 69] which generated both amplitudes of vibration (u_{h1}) and the curvilinear corrections (k_{h1}) for the r_{h1} structure type.[70] The radial distribution curves for diketene, ketene and all species involved in the decomposition reaction with their different % composition have been generated. In the RDC curve, Figure 37a below, it can be seen that there are three groupings of compositions that can be considered distinguishable. 100 % Ketene and 90 % ketene / 10 % diketene are very similar, as a 100 % diketene and 30 % ketene and 70 % diketene. The 60 % ketene / 40 % diketene composition is distinct from the rest.

If all possible species are taken together then RDC curve, as in Figure 37b, the % composition of diketene, ketene, allene and CO_2 sequentially 10%, 70%, 10% and 10% is distinct from other % compositions. This provides a guideline for the future GED refinements. If multiple species are formed due to decomposition of diketene, the theoretical RDC curve is very helpful to determine the experimental proportion of the possible species. The RDCs also show that GED alone is probably not going to be able to determine the composition of the gas samples and that another technique such as MS will be needed to be able to deconvolute the data completely.

(a)

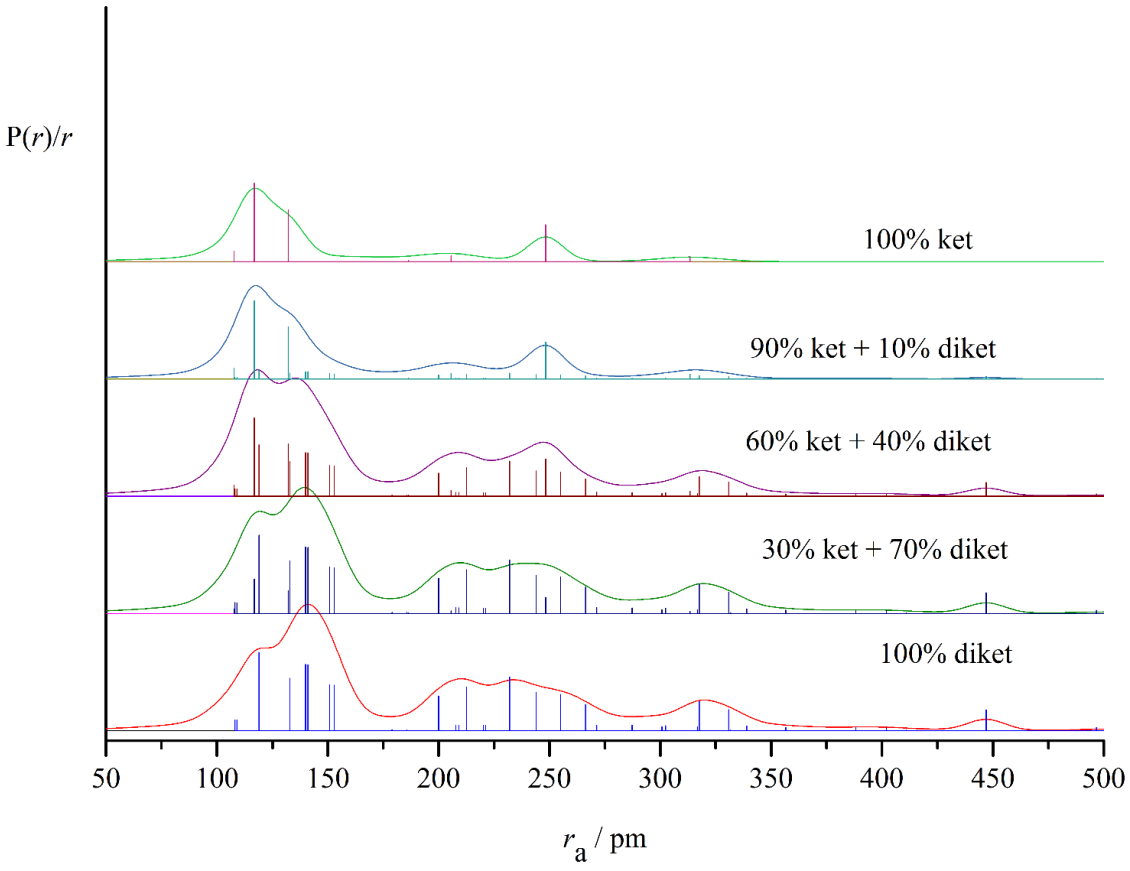

(b)

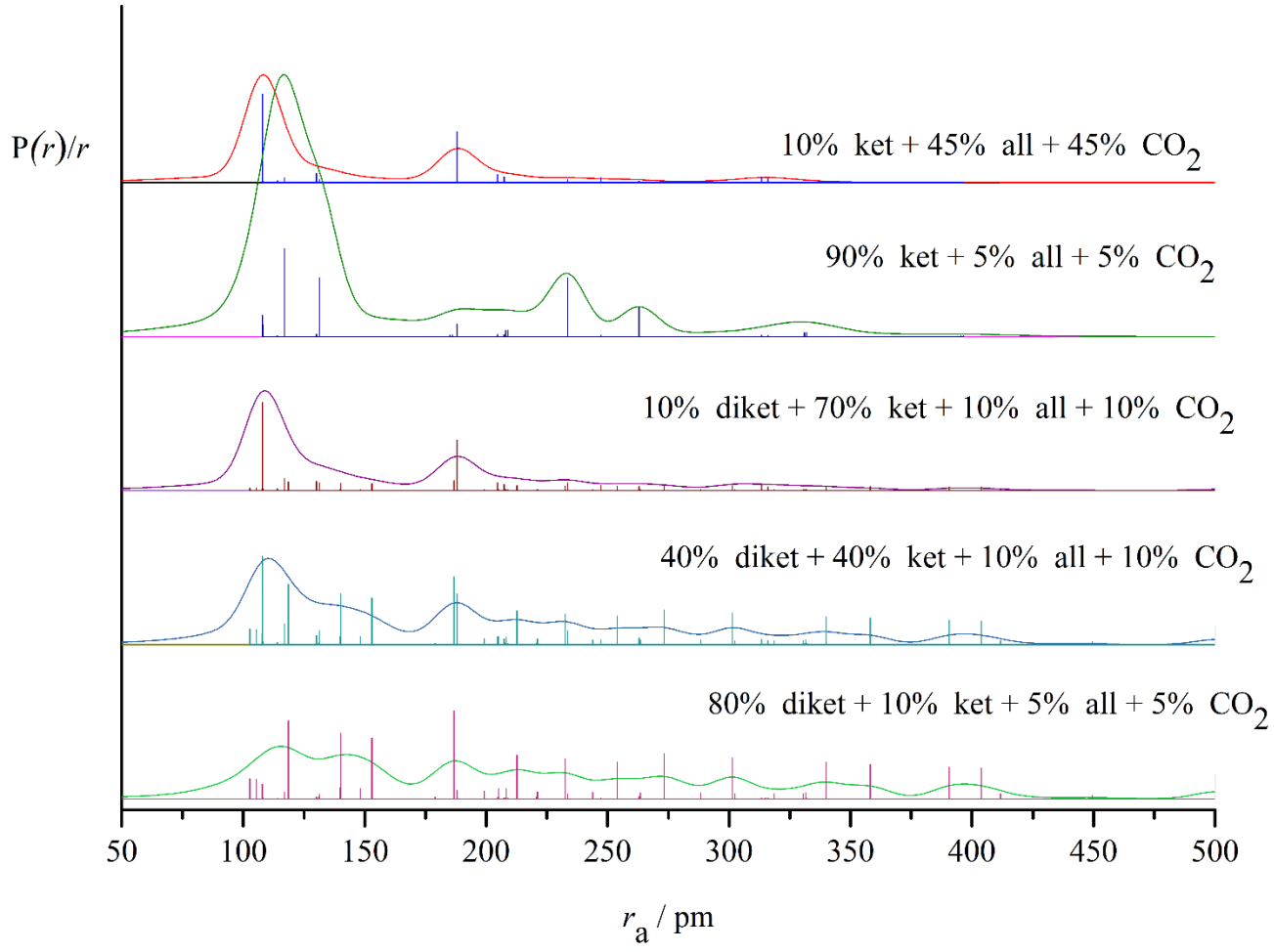

Figure 37: Theoretical RDCs of diketene from data calculated at the MP2/6 311++G** level (a) ketene and diketene and (b) diketene, ketene, allene and CO_2 with their different % composition. [Where diket = diketene, ket = ketene, all = allene and CO_2 = carbon dioxide]

6.2. Methyleneketene and its preparation from diazotetranoic acid

Methyleneketene can be prepared efficiently from high temperature cracking of acrylic anhydride[107] in the gas phase with byproducts and residual starting materials. Also, Masters, Sorensen and Tran[108] generated methyleneketene *in situ* from the reaction of bromopropenoyl chloride and pentacarbonylmanganate with byproducts. Both preparation methods are not suitable for use in the GED experiment due to presence of byproducts and residual materials. Moreover, methyleneketene prepared

from the decomposition of the diazotetranoic acid[22] is spectroscopically identical with methyleneketene prepared from the acrylic acid route.[107]

The pyrolytic route of diazotetranoic acid is best for the GED experiment because the previous experiment[22] with IR spectrum shows the complete breakdown of the parent compounds into methyleneketene and carbon dioxide along with small quantities, less than 10%, of formaldehyde and carbon sub-oxide as the alternative fragmentation. The absorption bands of the minor byproducts were observed but there was no issue in elucidating those of methyleneketene. There was no previous computational study on the parent compound diazotetranoic acid. This work is to the best of our knowledge the first computational investigation for it.

There have only been a few structural studies done on the structure of methyleneketene. The structure is not easily concluded from the computational structural parameters[20] and MW[21] results. Methyleneketene has planar C_{2v} structure at lower level of *ab initio* calculation[20] with bond angle ∠H–C–H 117.1°, which is 4.7° lower than that of ketene bond angle ∠H–C–H. The calculation at HF/6-31+G* level of theory predicted C_s geometry with some similarity in the geometry but a large deviation in bond distance, *r*(C=)C=C, by 3.1 pm and in bond angle, ∠C=C=O, by 7.2° with previous MW experimental results.[21] The previous MW experiment and computation calculation were not clear about the confirmation of the structural parameters of methyleneketene, as shown in Table 23. Following work for this thesis the calculation of methyleneketene from M06-2X/aug-cc-pVTZ (C_s) can be used for possible theoretical parameters to initiate the future GED experimental refinement as the optimized structure using this method is not deformed and verified as a minimum on the potential energy surface by frequency calculation at the same level. The calculation at the MP2 level could not be completed due to structural deformation and also returned an imaginary frequency, but by using a constrained geometry results were able to be obtained and are presented in Table 4.

Table 13: Structural parameters of methyleneketene from *ab initio*, hybrid DFT and MW studies

Parameters	HF/4-31G (C_{2V})[21]	MW (C_s)[22]	HF/6-31+G* (C_1)	M062X- AVTZ (C_s)
rC=O	117.7	117.6	115.5	116.2
r(C=)C=C	126.0	130.1	127.0	128.7
r(H)C=C	130.1	129.9	130.7	131.4
rC-H	107.5	109.9	107.8	108.7
∠H-C-H	115.5	122.1	116.3	116.3
ÐH-C=C	122.3	119.0	121.9	122.2
∠C=C=C	180.0	153.8	154.8	178.8
∠C=C=O	180.0	180.0	172.8	178.9

[All bond distances (r) in pm and bond angles (∠) are in degree (°)]

The theoretical RDC was made for the decomposition of the diazotetranoic acid. The starting parameters for r_{h1}-type least-squares refinements were taken from theoretical geometries optimized at the MP2/6-311G** level for all species involved in the reactions, reactant (diazotetranoic acid) and products (nitrogen, methyleneketene, carbon dioxide, carbon suboxide and formaldehyde). Parameterized molecular models describing the structures of all species were constructed in FORTRAN90 using the optimized coordinates at the MP2/6-311G** level. A theoretical Cartesian force field was obtained at the MP2/6-311G** level and converted into a force field described by a set of symmetry coordinates using the SHRINK program,[68, 69] which generated both amplitudes of vibration (u_{h1}) and the curvilinear corrections (k_{h1}) for the r_{h1} structure type.[70] The radial distribution curves for all species involved in the decomposition reaction with their different % composition have been generated and are shown in the RDC curves, Figure 38. This provides a guideline for the future GED refinements. If multiple species are formed due to decomposition of diazotetranoic acid, the theoretical RDC curve is helpful to determine the experimental proportion of the possible species. The RDCs indicate that deconvoluting these species will be a challenge for GED if there are several products of decomposition.

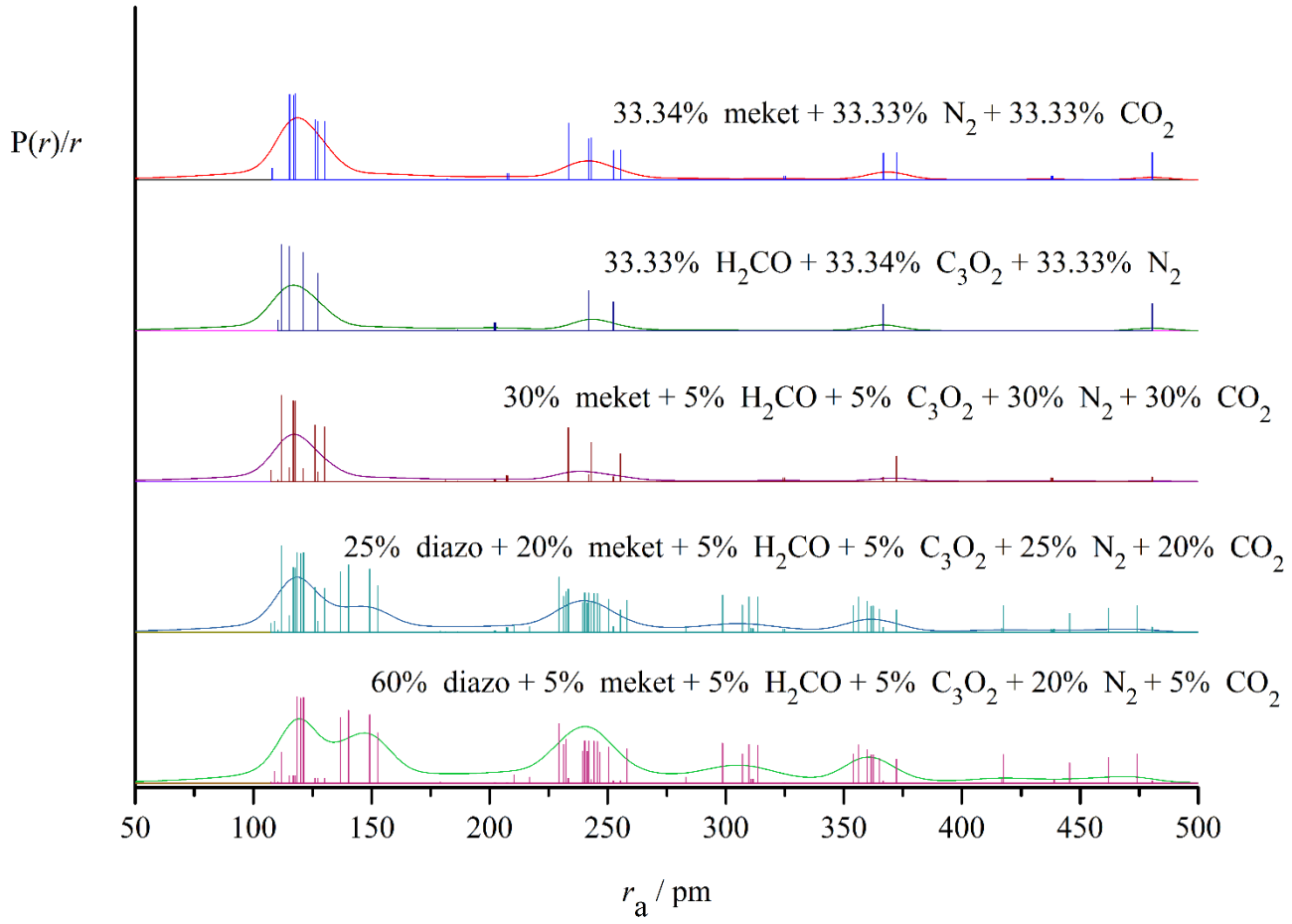

Figure 38: Theoretical RDCs of decomposition reaction of diazotetranoic acid from data calculated at the MP2/6 311G** level with all species involved in the reaction, diazo = diazotetranoic acid, meket = methyleneketene, H_2CO = formaldehyde, C_3O_2 = carbon suboxide, N_2 = nitrogen and CO_2 = carbon dioxide with their different possible % composition.

6.3. Substituted ketenes and their preparation from MA derivatives

The theoretical parameters obtained for the structural elucidation of MA have been found to be good agreement with previous experimental work using X-ray single crystal diffraction and GED. The key parameters are tabulated below. Little deviation was observed in the bond length, rC–C, and bond angle, ∠O(4)–C(2) –O(5), by a range of 0.8 pm and 0.6° respectively.

Table 14: Structural parameters of MA from *ab initio*, hybrid DFT, GED and X-ray single crystal diffraction studies.

Parameters	MP2/ 6-311++G**	M06-2X/ aug-cc-pVTZ	GED 1[17]	GED 2[31]	X-ray[28]
rC(6/7)=O(9/10)	120.4	119.1	119.7	120.1	119.3
rC(2)–O(4/5)	143.4	142.6	144.8	143.4	144.4
rC(6/7)–O(4/5)	136.2	134.9	137.3	136.1	135.2
rC(1)–C(2)	152.1	151.8	151.7	152.8	150.4
rC(2)–C(3)	151.1	150.8	150.7	151.9	150.4
rC(6/7)–C(8)	151.5	150.9	151.1	152.4	149.4
∠C(2)–O–C(6/7)	118.8	120.3	117.6	118.9	120.2
∠O(4/5)–C(6/7)=O(9/10)	120.4	120.5	121.7	120.3	118.9
∠C(8)–C(6/7)–O(4/5)	115.8	115.9	116.8	-	116.3
∠C(1)–C(2)–O(4/5)	112.9	110.4	112.5	113.0	113.7
∠O(4)–C(2)–O(5)	111.4	111.0	111.2	110.8	110.2
∠C(6)–C(8)–O(7)	115.2	114.9	116.1	-	14.8
ϕC(2)–O–C=O(9/10)	169.9	170.7	175.4	170.1	-
ϕC(2)–O(4)–C(6)–C(8)	-11.8	-10.7	-13.7	-12.2	-

[All bond distances (r) in pm, and bond angles (∠) and dihedral angles (ϕ) are in degrees (°)]

From the four component model of the refinement with GED experiment for the decomposition of MA Noble-Eddy[17] concluded 82% decomposition to ketene, carbon dioxide, and acetone. After him, Atkinson[30] constructed a five component model by including the diketene, which is believed to be formed by spontaneous dimerization of ketenes during the pyrolysis decomposition of MA. The five component model returned a lower *R*-factor,[17] presumably due to the increased number of parameters used to fit the data. However, the threshold for what the GED community consider to be an acceptable fit to the experimental data was not achieved, returning an *R*-factor of ~13%. Usually *R*-factors of sub-10% are considered acceptable when considered with other information from the refinement. Parameters to define the structure such as the distance across the ring [rC(2)…C(8)] and the angle across the ring to the methyl group [∠C(1)–C(2)…C(8); (Figure 19, Section 5.2.1.1.)] are not taken into consideration in the previous MA decomposition model.[17,30] Ja'o has shown that using these parameters will reduce the number of

parameters in the model as well as give a more realistic fit to the experimental data.[60] Later work is affected by the relative weighting of each species, which could not be determined in the refinement software of the Masters Research Group. What can be said is that it does not match with the real amount generated during the experiment. There may be chances to form intermediates or other substances which may be resulted from the internal reaction of species during complete and incomplete pyrolysis. One way to remedy this will be to use GED-MS so that the amount of each species generated can be known.

One of the main challenges associated with any GED refinement of the pyrolysis of MA pyrolysis was overlapping peaks in the RDC due to lots of similar bond distances.[17, 31] Where similar distances occur then the peaks in the RDC will be co-located and due to their Gaussian shape the peaks merge and appear as a larger broader peak with several distances sitting under it. The use of computational methods allows these peaks to be deconvoluted and individual inter-nuclear distances to be assigned via the SARACEN[64, 65, 66] method. Therefore even when RDCs look similar with varying proportions of products of pyrolysis present, SARACEN[64, 65, 66] should enable the proportions to be allocated. The introduction of a mass spectrometer should allow the species in the gas flow to be identified and then SARACEN[64, 65, 66] implemented to gain understanding of the proportions of each species at a particular temperature.

When substitutions to MA are made, some parameters among derivatives of MA differed. MeMA, MMMA and DMMA have distorted from the boat conformation of MA to a half-boat or chair or twisted chair confirmation due to the increasing size of substituents on the central ring. The deviation from boat conformation is calculated on the basis of the dihedral angle of the lactone groups relative to the ring,[28] which were believed to bring a planar geometry to the rings of MA derivatives. The calculated dihedral angles of ϕC(2)–O(4/5)–C=O(9/10) at MP2-6-311++G(d p) level were found to decrease by 7° in MeMA, 13.3° in MMMA and 16.9° in DMMA than that of MA (169.9°). The deviation was also observed in the dihedral angle of ϕC(2)–O(5)–C(6)–C(8) by 8.4° in MeMA, 16.7° in MMMA and 21.6° in DMMA than that of MA (11.8°). A small change in the bond length of rC(6/7)–C(8) was observed in MeMA by -1.9 pm, MMMA by 0.7 pm and adjacent rC(8)–C(17) by 2.7 pm and DMMA by 0.9 pm, adjacent rC(8)–C(17) by 1.8 pm and adjacent rC(8)–C(21) by 3.5 pm on comparing with rC(6/7)-C(8) of MA (151.5 pm).

The kinetic study of the single step pyrolysis of MA, MMMA, DMMA and MeMA predicted that it requires an activation energy of at least 197.0 kJ/mol or above to form the various products. The differences between the energy barrier of the cyclic TS for the single step mechanism and formation of TS2 in the double step mechanism vary from about 20 – 40 kJ/mol in the order of MeMA < DMMA <

MMMA < MA. There is also another possibility of formation of intermediates like malonic anhydride[36] or a series of reactions during their partial or complete pyrolysis which is further explained in the next paragraph.

The study of thermal decomposition of diazomeldrum's acid[109] found acetone as the dominant product, formed by a Wolf rearrangement, along with diazoethanone and formylketene with an intricate decomposition mechanism. The main challenge in terms of our understanding is the disconnection in the orbital overlap around the ring due to breaking and forming bonds of mutually orthogonal orbitals. Birney and Wagenseller[110] termed this process, the breakdown of derivatives of MA-like systems, a pseudo-pericyclic reaction mechanism. Further, an experimental mechanistic study on the decomposition of MA derivatives by Fillion and Fishlock[111] suggests the need to remove acetone while trapping the ketene through the Diels-Alder reaction to prevent a reversible retro hetero-Diels-Alder reaction. If MA derivatives, on mild heating, convert to the enolized form, then thermal decomposition of such a retro reaction may result in the formation of carboxyketene intermediates.[112]

The thermochemical investigation predicted that the decomposition reactions of MA, MMMA, and DMMA are spontaneous at standard temperature, 298.15 K. However the experimental temperature is generally higher than room temperature, meaning that the spontaneity will be reinforced. For MeMA the value of ΔG is positive and so the decomposition reaction is predicted to be feasible at elevated reaction temperatures.

The theoretical RDC was constructed for the decomposition of MA derivatives. The starting parameters for r_{h1}-type least-squares refinements were taken from theoretical geometries optimized at the MP2/6-311++G** level for all species involved in the reactions, reactant (MA / MMMA / DMMA / MeMA) and products (ketene / methyl-ketene / di-methyl-ketene / methyleneketene) and common products in all (carbon dioxide and acetone). Parameterized molecular models describing the independent geometries of all species were constructed in FORTRAN90 using the optimized coordinates at MP2/6-311++G**. A theoretical Cartesian force field was obtained at the MP2/3-21+G* level and converted into a force field described by a set of symmetry coordinates using the SHRINK program,[68, 69] which generated both amplitudes of vibration (u_{h1}) and the curvilinear corrections (k_{h1}) for the r_{h1} structure type.[70] The radial distribution curves for all species involved in the decomposition reactions with their different % composition were then generated (Figures 39 to 42). This provides a guideline for the future GED refinements for MA, MMMA, DMMA and MeMA respectively. If multiple species are formed due to

decomposition of MA derivatives, the theoretical RDC curve is helpful to determine the experimental proportion of the possible species.

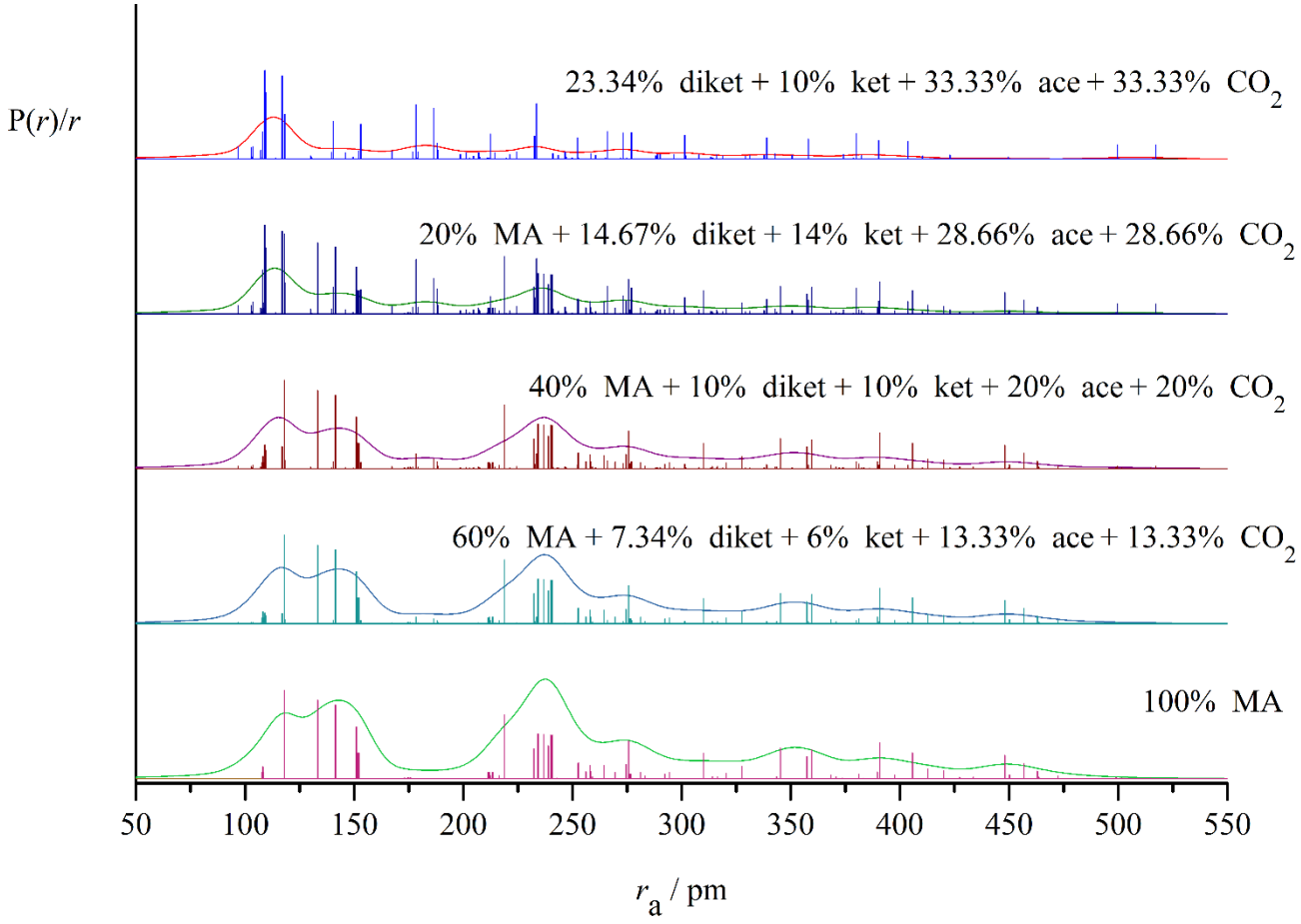

Figure 39: Theoretical RDCs of decomposition reaction of MA from data calculated at the MP2/6 311++G** level with all species involved in the reaction, MA = Meldrum's acid, diket = diketene, ket = ketene, ace = acetone and CO_2 = carbon dioxide with their different possible % composition.

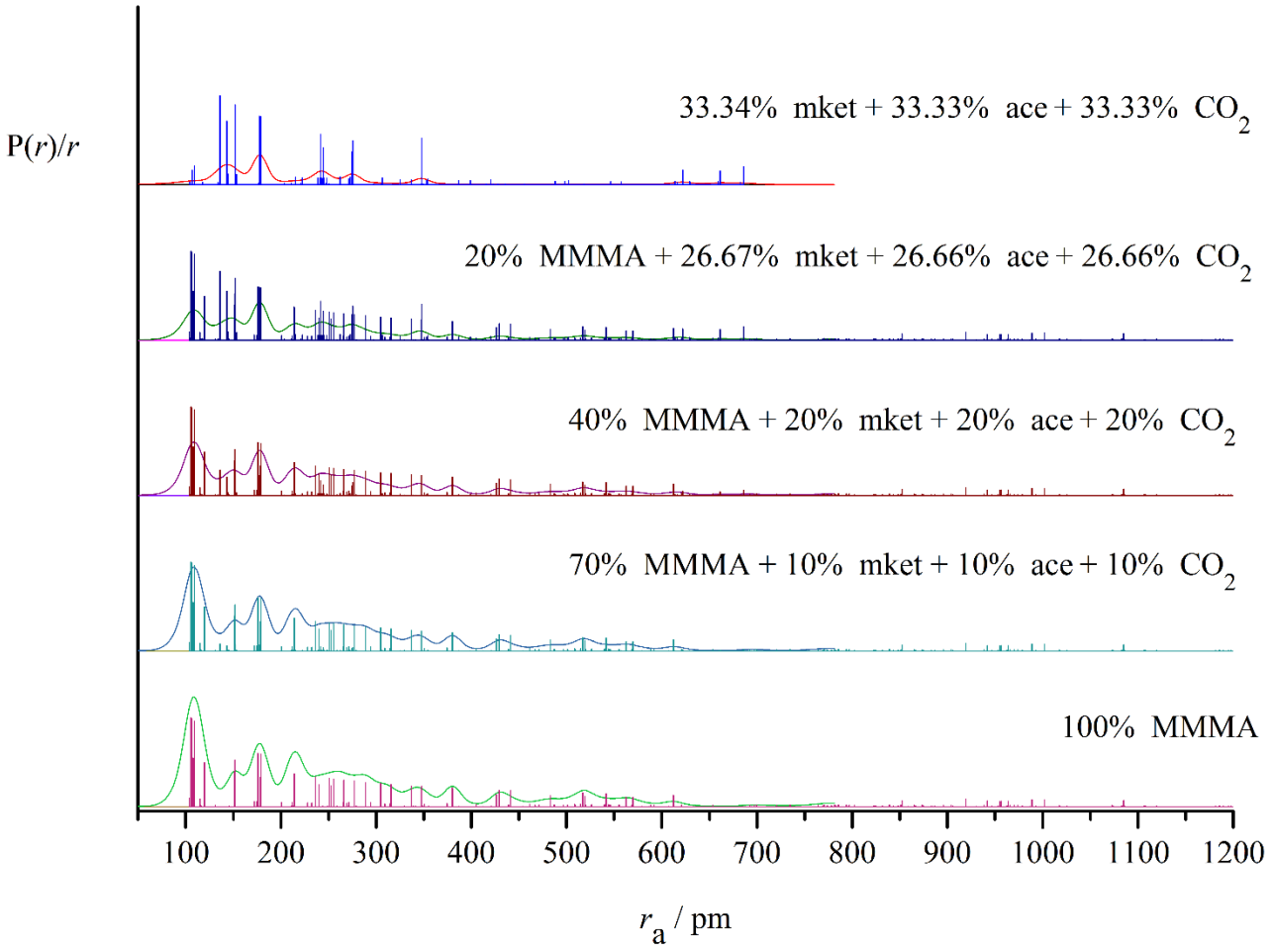

Figure 40: Theoretical RDCs of decomposition reaction of MMMA from data calculated at the MP2/6 311++G** level with all species involved in the reaction, MMMA = mono-methyl-Meldrum's acid, mket = methyl-ketene, ace = acetone and CO_2 = carbon dioxide with their different possible % composition.

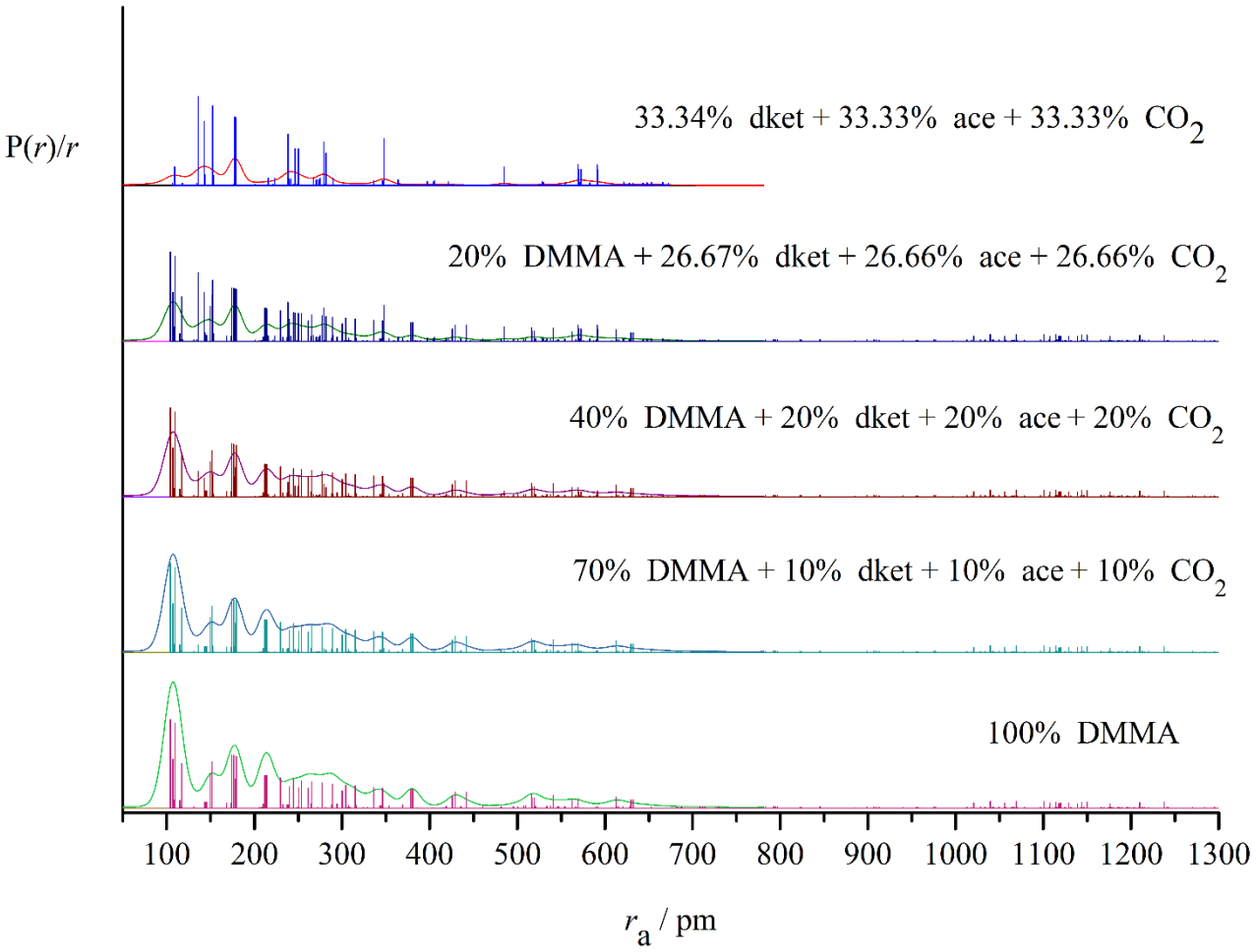

Figure 41: Theoretical RDCs of decomposition reaction of DMMA from data calculated at the MP2/6 311++G** level with all species involved in the reaction, DMMA = di-methyl-Meldrum's acid, dket = di-methyl-ketene, ace = acetone, and CO_2 = carbon dioxide with their different possible % composition.

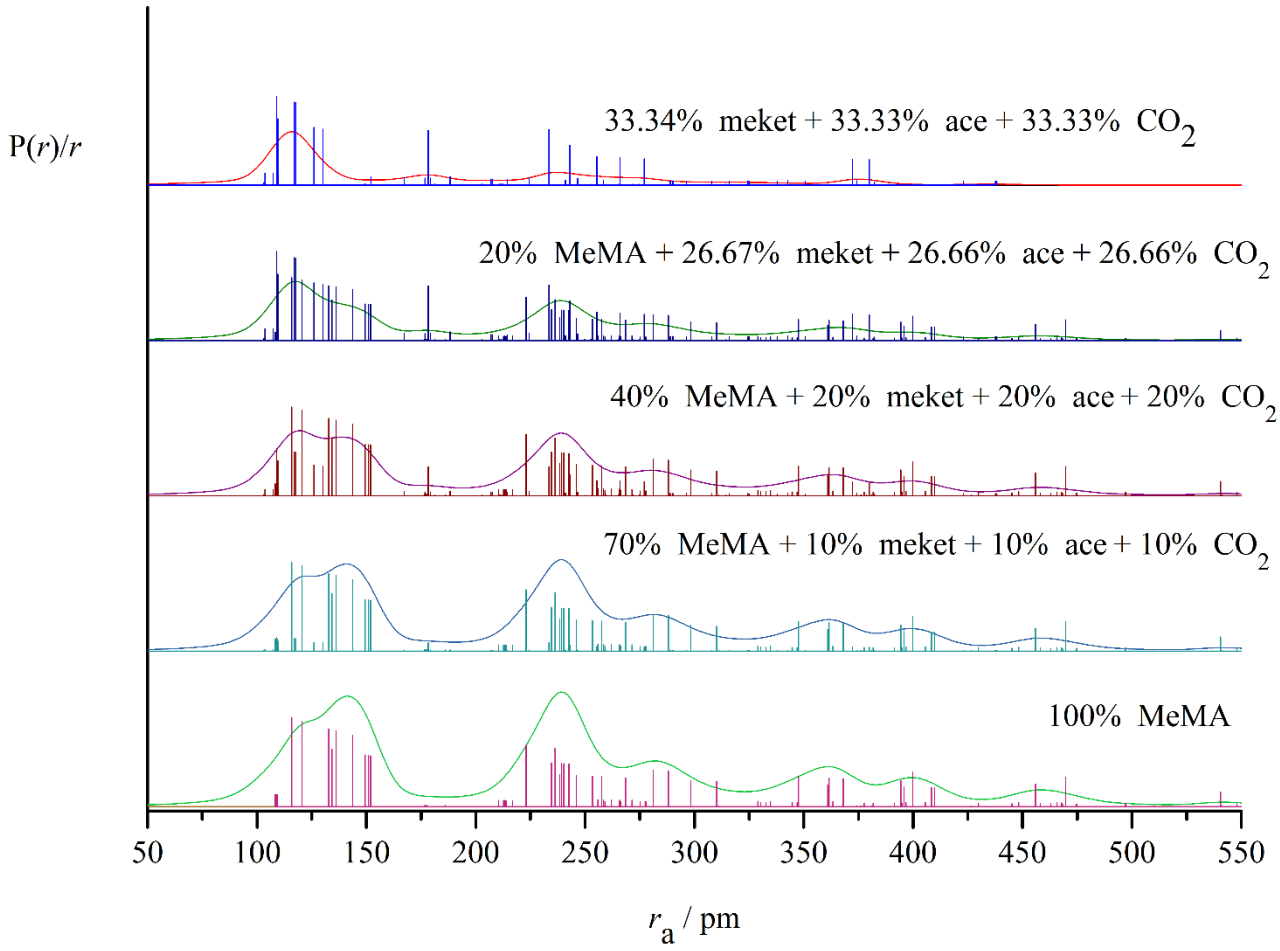

Figure 42: Theoretical RDCs of decomposition reaction of MeMA from data calculated at the MP2/6 311++G** level with all species involved in the reaction, MeMA = methylene-Meldrum's acid, meket = methyleneketene, ace = acetone and CO_2 = carbon dioxide with their different possible % composition.

7. Overall Conclusions

7.1. Ketene and substituted ketenes from decomposition of their precursors

7.1.1. Diketene

The calculated structural parameters of ketene are in good agreement with those reported in the literature for similar compounds. The previous GED study of diketene shows some structural parameters like bond distances and bond angles that deviate from the computed structural parameters. Kinetic and thermodynamic calculations of the decomposition of diketene reveal that ketene formation Pathway 1 is favoured with a lower activation energy barrier. They also show that Pathway 2 (formation of allene and carbon dioxide) is feasible thermodynamically with negative Gibbs free energy at room temperature (289.15 K). Since the reaction temperature of the diketene decomposition occurs at elevated temperatures, the predicted thermochemistry explains the spontaneity of Pathway 1. If the future GED experimental products formation is mixed between pathway 1 and pathway 2 then the fit with varied % composition can be compared to the theoretical curves generated in this work.

7.1.2. Diazotetranoic acid

The computed structural parameters at low level of theory for methyleneketene are in accordance with previous calculations[20] and MW[21] study but at higher level the molecule is distorted and the constrained calculations were made as shown in the results. The thermochemistry and kinetic study of decomposition for diazotetranoic acid shows that the transition state (TS) and Pathway 1 (formation of methyleneketene and carbon dioxide) are both kinetically and thermodynamically feasible compared to Pathway 2 (formation of carbon sub-oxide and formaldehyde).

7.1.3. Meldrum's acid and its derivatives

The molecular structure of MA has been successfully completed by previous researchers[17, 30] in the Masters Research group with computational work used to complement experimental X-ray single crystal diffraction data[27] and GED data. The kinetic and thermodynamic study of the decomposition of MA derivatives to give ketene and substituted ketenes was successfully completed in this thesis. The decomposition of MA, MMMA, DMMA were found to be spontaneous at standard temperature (298.15 K). Thermal decomposition of MeMA was found to not be feasible at standard temperature but the previously established pyrolysis temperature is far higher than 298.15 K. Thus this work agrees with

experimental observation. The energy required for the decomposition of all MA derivatives is in the range of 297 to 260 kJ/mol. Overall the decomposition of MMMA looks to be most feasible from a combined thermodynamic and kinetic viewpoint. The possible decomposition mechanism was studied and compared with the energy values. It was found that for all MA derivatives, the thermal decomposition follows a single step pericyclic reaction mechanism[34, 35] with a cyclic transition state, supported by calculation on the density function theory[74] and synchronous transit-guided quasi-Newton (STQN)[98] methods. The two steps mechanism with the formation of an intermediate, such as malonic anhydride[36] and its derivatives, can also be considered but the second transition state (TS2) was kinetically less preferred than that of single step mechanism. However there is the possibility to form a stable intermediate, such as carboxyketene,[112] which may change the kinetic scheme.

7.2. Additional information and future work

7.2.1. Additional information

The GED experimental work was started and various part of the GED apparatus such as the electron gun have been cleaned, all leak testing and vacuum pressure holding tests have been completed. We were working on the alignment of electron beam and we were waiting for delivery of the quadrupole MS instrument to fit with the apparatus. Due to COVID-19 lockdown, we could not complete the experimental GED work for ketene from pyrolysis decomposition of diketene along with other reactions.

7.2.2. Future work – ketene

Ketene can be prepared experimentally by pyrolysis of acetone using the apparatus outlined in the literature[113] and then spontaneously converted to diketene. The GED experiments will then involve cleanly reconverting diketene back to ketene allowing a proof-of-concept for testing the GED apparatus with the MS.

7.2.3. Future work – methyleneketene

Production of methyleneketene has been investigated using two different precursors with different reaction routes. The first is diazotetranoic acid, itself a very unstable compound. One imaginary frequency was returned from the calculations and further work is needed to analyse this more. However

it should be possible to synthesize methyleneketene according to the literature.[22] The second route is to use MeMA as a starting material,[19, 114] which should be the best alternative for the further GED experimental work.

7.2.4. Future work – substituted ketenes

Previous work studying the decomposition of MA using GED[17, 30] was not satisfactory in terms of the goodness of fit (*R*-value) obtained for the data during the GED refinement process. The study of the relative amounts of each species is also crucial to aid our understanding of the thermal decomposition of complex MA derivatives, which have a lot of potential as precursors to substituted ketenes. The current study of the kinetics of formation of ketenes via decomposition of MA derivatives confirmed that the decomposition products are less stable than the reactant molecules, that the reaction is endothermic and there is a reasonable chance of only partial pyrolysis of the precursors. The thermochemical investigation predicted the decomposition reactions of MA derivatives are spontaneous at normal temperature with negative value of standard Gibbs free energy. The spontaneity of the decomposition of MMMA is favored more towards the decomposed products than other MA derivatives, so MMMA will be good start point for the future GED work.

8. References

(1) Carey, F. A.; Sundberg, R. J. *Advanced Organic Chemistry Part A: Structure and Mechanisms*; Plenum Press: New York N.Y, 1984.

(2) Staudinger, H. Ketene, Eine Neue Korperklasse. *Ber. Dtsch. Chem. Ges.* **1905**, *38* (2), 1735–1739.

(3) Tidwell, T. T. *Ketenes II*, 2nd ed.; John Wiley & Sons, Inc.: Hoboken, New Jersey, U.S.A., 2005. https://doi.org/10.1002/0471767670.

(4) Wilsmore, N. T. M. CLXXXVIII-Ketene. *J. Chem. Soc.* **1907**, *91*, 1938–1941.

(5) Chick, F.; Wilsmore, N. T. M. LXXXIX. - Acetylketen: A Polymeride of Keten. *J. Chem. Soc. Trans.* **1908**, *93* (946), 946–950. https://doi.org/10.1039/CT9089300946.

(6) Clemens, R. J. Diketene. *Chem. Rev.* **1986**, *86*, 241–318.

(7) Chick, F.; Wilsmore, N. T. M. Acetylketen: A Polymeride of Keten. *J. Chem. Soc. Trans.* **1908**, *93*, 946–950. https://doi.org/10.1039/CT9089300946.

(8) Boese, A. B. Diketene: A New Industrial Chemical. *Ind. Eng. Chem.* **1940**, *32* (1), 16–22. https://doi.org/10.1021/ie50361a004.

(9) Bregman, J.; Bauer, S. H. An Electron Diffraction Study of Ketene Dimer, Methylketene Dimer and β-Propiolactone. *J. Am. Chem. Soc.* **1955**, *77* (7), 1955–1965. https://doi.org/10.1021/ja01612a077.

(10) Kay, M. I.; Katz, L. A Refinement of the Crystal Structure of Ketene Dimer. *Acta Crystallogr.* **1958**, *11* (12), 897–898. https://doi.org/10.1107/s0365110x58002565.

(11) Orr, V. L.; Esselman, B. J.; Dorman, P. M.; Amberger, B. K.; Guzei, I. A.; Woods, R. C.; McMahon, R. J. Millimeter-Wave Spectroscopy, X-Ray Crystal Structure, and Quantum Chemical Studies of Diketene: Resolving Ambiguities Concerning the Structure of the Ketene Dimer. *J. Phys. Chem. A* **2016**, *120* (39), 7753–7763. https://doi.org/10.1021/acs.jpca.6b07610.

(12) Bader, A. R.; Gutowsky, H. S.; Williams, G. A.; Yankwich, P. E. The Proton Magnetic Resonance Spectrum and Structure of Diketene. *J. Am. Chem. Soc.* **1956**, *78* (11), 2385–2387. https://doi.org/10.1021/ja01592a011.

(13) Miller, F. A.; Carlson, G. L. Diketene : Infrared Spectrum and Structure. II. *J. Am. Chem. Soc.*

1957, *79* (15), 3995–3997. https://doi.org/10.1021/ja01572a010.

(14) Miller, F. A.; Koch, S. D.; Miller, F. A.; Koch, S. D. Diketene: Infrared Spectrum and Structure. *J. Am. Chem. Soc.* **1948**, *70* (5), 1890–1894. https://doi.org/10.1021/ja01185a068.

(15) Andreades, S.; Carlson, H. D. Ketene. *Org. Synth.* **1965**, *45*, 50–52. https://doi.org/10.15227/orgsyn.031.0077.

(16) Bui, B.; Tsay, T. J.; Lin, M. C.; Melius, C. F. Theoretical and Experimental Studies of the Diketene System: Product Branching Decomposition Rate Constants and Energetics of Isomers. *Int. J. Chem. Kinet.* **2007**, *39*, 580–590. https://doi.org/10.1002/kin.20263.

(17) Noble-eddy, R. Gas-Phase Electron Diffraction Studies of Unstable Molecules. Ph.D. Thesis, University of Edinburgh, UK, 2009.

(18) Atkinson, S. J.; Noble-Eddy, R.; Masters, S. L. Gas-Phase Structures of Ketene and Acetic Acid from Acetic Anhydride Using Very-High-Temperature Gas Electron Diffraction. *J. Phys. Chem. A* **2016**, *120*, 2041−2048. https://doi.org/10.1021/acs.jpca.6b00704.

(19) Williams, J. W.; Hurd, C. D. An Improved Apparatus for the Laboratory Preparation of Ketene and Butadiene. *J. Org. Chem.* **1940**, *5*, 122–125. https://doi.org/10.1021/jo01208a005.

(20) Brown, R. F. C.; Eastwood, F. W.; McMullen, G. L. Evidence for the Pyrolytic Generation of Methyleneketene (Propadienone). *J. Am. Chem. Soc.* **1976**, *98* (23), 7421–7422. https://doi.org/10.1021/ja00439a052.

(21) Radom, L. An Ab Initio Molecular Orbital Study of the Structure and Properties of Propadienone (Methyleneketene). *Aust. J. Chem.* **1978**, *31* (1), 1–9. https://doi.org/10.1071/CH9780001.

(22) Brown, R. D.; Godfrey, P. D.; Champion, R.; McNaughton, D. Microwave Spectrum and Unusual Geometry of Propadienone (Methylene Ketene). *J. Am. Chem. Soc.* **1981**, *103* (19), 5711–5715. https://doi.org/10.1021/ja00409a016.

(23) Chapman, O. L.; Miller, M. D.; Pitzenberger, S. M. Infrared Spectroscopy of Matrix-Isolated Propadienone. *J. Am. Chem. Soc.* **1987**, *109* (22), 6867–6868. https://doi.org/10.1021/ja00256a060.

(24) Meldrum, A. N. LIV. - A β-Lactonic Acid from Acetone and Malonic Acid. *J. Chem. Soc. Trans.* **1908**, *93*, 598. https://doi.org/10.1039/CT9089300598.

(25) Davidson, D.; Bernhard, S. A. The Structure of Meldrum's Supposed β-Lactonic Acid. *J. Am. Chem. Soc.* **1948**, *70* (10), 3426–3428. https://doi.org/10.1021/ja01190a060.

(26) Kiiber, D.; Schuste, P. Semiempirische LCA0--M0--SCF-Rechnungen Zur Koniormation Und Konformativen Beweglichkeit Yon L~3,Dioxan,4,6'dionen. *Monatsh. Chem* **1972**, *103*, 1483--1495.

(27) Abramovitch, R. A.; Rajan, J. B.; Walker, C. E. Proton Magnetic Resonance Spectra of Malonate Esters. *J. Chem. Eng. Data* **1967**, *12*, 594–596.

(28) Pfluger, C. E.; Boyle, P. D. Conformation and Intermolecular Interactions of Meldrum's Acid: An X-Ray Structural Investigation of 2,2-Dimethyl-1,3-Dioxane-4,6-Dione. *J. Chem. Soc. Perkin Trans. 2* **1985**, *II*, 1547–1549. https://doi.org/10.1039/P29850001547.

(29) Lee, I.; Han, I. S.; Kim, C. K.; Lee, H. W. Theoretical Studies on the Structure and Acidity of Meldrum's Acid and Related Compounds. *Bull. Korean Chem. Soc.* **2003**, *24* (8), 1141–1149. https://doi.org/10.5012/bkcs.2003.24.8.1141.

(30) Chopra, D.; Zhurov, V. V.; Zhurova, E. A.; Alan Pinkerton, A. Chemical Bonding and Structure-Reactivity Correlation in Meldrum's Acid: A Combined Experimental and Theoretical Electron Density Study. *J. Org. Chem.* **2009**, *74*, 2389–2395. https://doi.org/10.1021/jo8027054.

(31) Atkinson, S. J. Generation and Structural Characterisation of Transient Gaseous Species, Ph.D. Thesis, University of Canterbury, New Zealand, 2015.

(32) Gaber, A. E. A. M.; McNab, H. Synthetic Applications of the Pyrolysis of Meldrum's Acid Derivatives. *Synthesis (Stuttg).* **2001**, No. 14, 2059–2074. https://doi.org/10.1055/s-2001-18057.

(33) Ivanov, A. S. Meldrum's Acid and Related Compounds in the Synthesis of Natural Products and Analogs. *Chem. Soc. Rev.* **2008**, *37*, 789–811. https://doi.org/10.1039/b716020h.

(34) McNab, H. Meldrum's Acid. *Chemical Society Reviews*. 1978, pp 345–358. https://doi.org/10.1039/CS9780700345.

(35) Dumas, A. M.; Fillion, E. Meldrum's Acids and 5-Alkylidene Meldrum's Acids in Catalytic Carbon-Carbon Bond-Forming Processes. *Acc. Chem. Res.* **2010**, *43* (3), 440–454. https://doi.org/10.1021/ar900229z.

(36) DeClue, M. S.; Baldridge, K. K.; Künzler, D. E.; Kast, P.; Hilvert, D. Isochorismate Pyruvate Lyase: A Pericyclic Reaction Mechanism? *J. Am. Chem. Soc.* **2005**, *127* (43), 15002–15003.

https://doi.org/10.1021/ja055871t.

(37) Perrin, C. L.; Flach, A.; Manalo, M. N. Decomposition of Malonic Anhydrides. *J. Am. Chem. Soc.* **2012**, *134*, 9698–9707. https://doi.org/10.1021/ja301867s.

(38) Gaber, A. E. A. M.; McNab, H. Flash Vacuum Pyrolysis of N-Phenylbenzamide Oxime and Related Compounds. *J. Anal. Appl. Pyrolysis* **2009**, *86* (2), 369–374. https://doi.org/10.1016/j.jaap.2009.09.002.

(39) Patil, H. R. H.; Graham, W. A. G. Hyperconjugative Enhancement of Geminal Coupling Constants. *J. Am. Chem. Soc.* **1965**, *87* (3), 673–674. https://doi.org/10.1021/ja01081a063.

(40) Beeler, A. J.; Orendt, A. M.; Grant, D. M.; Cutts, P. W.; Michl, J.; Zilm, K. W.; Downing, J. W.; Facelli, J. C.; Schindler, M. S.; Kutzelnigg, W. Low-Temperature 13C Magnetic Resonance in Solids. 3. Linear and Pseudolinear Molecules. *J. Am. Chem. Soc.* **1984**, *106* (25), 7672–7676. https://doi.org/10.1021/ja00337a003.

(41) Price, W. C.; Teegan, J. P.; Walsh, A. D. The Absorption Spectrum of Keten in the Far Ultra-Violet. *J. Chem. Soc.* **1951**, 920–926. https://doi.org/10.1039/JR9510000920.

(42) Werstiuk, N. H.; Ma, J.; McAllister, M. A.; Tidwell, T. T.; Zhao, D. C. Conformation Properties of Buta-1,3-Diene-1,4-Diones (Bisketenes): Computational and Photoelectron Spectroscopic Studies. *J. Chem. Soc. Faraday Trans.* **1994**, *90* (22), 3393–3390. https://doi.org/10.1039/FT9949003383.

(43) Surber, B. W. Characterization and Chemistry of Vinylketene Prepared by Flash Vacuum Pyrolysis. Study of the Flash Vacuum Pyrolysis of Hydroaromatic Compounds: 5,8-Diphenyltetralin and the Parent and Substituted 5,6,11,12-Tetrahydrodibenzo[a,e]Cyclooctenes. Ph.D. Thesi, Iowa State University, Ames, Iowa, USA, 1984.

(44) McNab, H. Synthetic Applications of Flash Vacuum Pyrolysis. *Contemp. Org. Synth.* **1996**, *3* (5), 373–396. https://doi.org/10.1039/co9960300373.

(45) Fokin, A. A.; Zhuk, T. S.; Blomeyer, S.; Pérez, C.; Chernish, L. V.; Pashenko, A. E.; Antony, J.; Vishnevskiy, Y. V.; Berger, R. J. F.; Grimme, S.; Logemann, C.; Schnell, M.; Mitzel, N. W.; Schreiner, P. R. Intramolecular London Dispersion Interaction Effects on Gas-Phase and Solid-State Structures of Diamondoid Dimers. *J. Am. Chem. Soc.* **2017**, *139* (46), 16696–16707. https://doi.org/10.1021/jacs.7b07884.

(46) Almenningen, A.; Bastiansen, O.; Fernholt, L.; Cyvin, B. N.; Cyvin, S. J.; Samdal, S. Structure and Barrier of Internal Rotation of Biphenyl Derivatives in the Gaseous State. Part 1. The Molecular Structure and Normal Coordinate Analysis of Normal Biphenyl and Pedeuterated Biphenyl. *J. Mol. Struct.* **1985**, *128* (1–3), 59–76. https://doi.org/10.1016/0022-2860(85)85041-9.

(47) Beach, J. Y.; Stevenson, D. P. The Electron Diffraction Investigation of the Molecular Structures of Ketene and Thiophosphoryl Chloride. *J. Chem. Phys.* **1938**, *6*, 75−80. https://doi.org/10.1063/1.1750206.

(48) Taylor Broun, T.; Livingston, R. L. An Electron Diffraction Investigation of the Molecular Structures of Ketene, Carbonyl Fluoride and Tetrafluoroethylene. *J. Am. Chem. Soc.* **1952**, *74* (23), 6084–6091. https://doi.org/10.1021/ja01143a075.

(49) Rozsondai, B.; Hargittai, I. Electron Diffraction Study of the Molecular Structure of Bis(Trimethylgermyl)Ketene. *J. Mol. Struct.* **1973**, *17*, 53−64. https://doi.org/10.1016/0022-2860(73)85042-2.

(50) Rozsondai, B.; Tremmel, J.; Hargittai, I.; Khabashesku, V. N.; Kagramanov, N. D.; Nefedov, O. M. Molecular Structures of Unstable Dichloroketene and Its Precursor, Trichloroacetyl Chloride, from Electron Diffraction. *J. Am. Chem. Soc.* **1989**, *111* (8), 2845–2849. https://doi.org/10.1021/ja00190a017.

(51) Korn, M.; Mack, H.; Praas, H.; Vdova, C. O. Della. Structure and Conformation of Bis(Trifluoromethylthio)Ketene, (CF3S)2C=C=O. **1995**, *353*, 145–151.

(52) Belova, N. V.; Girichev, G. V.; Kotova, V. E.; Korolkova, K. A.; Trang, N. H. The Molecular Structure of 4-Methylpyridine-N-Oxide: Gas-Phase Electron Diffraction and Quantum Chemical Calculations. *J. Mol. Struct.* **2018**, *1156* (2), 210–215. https://doi.org/10.1016/j.molstruc.2017.11.070.

(53) Broglie, L. de. A Tentative Theory of Light Quanta. *Philos. Mag.* **1924**, *47* (278), 446–458.

(54) Young, T. The Bakerian Lecture: On the Theory of Light and Colours. *Phil. Trans. R. Soc. Lond.* **1802**, *92*, 12–48.

(55) Davisson, C. J.; Germer, L. H. The Scattering of Electrons by a Single Crystal of Nickel. *Nature* **1927**, *119*, 558–560.

(56) Thomson, G. P.; Reid, A. Diffraction of Cathode Rays by a Thin Film. *Nature* **1927**, *119*, 890.

(57) Debye, P.; Bewilogua, L.; Ehrhardt, F. Dispersion of X-Rays by Single Molecules. *Phys. Z.* **1929**, *30*, 84–87.

(58) Mark, H.; Wierl, R. Atomic Form Factor Determination with Electrons. *Phys. Z.* **1930**, *60*, 741–753.

(59) Masters, S. L.; Girichev, G. V.; Shylkov, S. A. The Re-Determination of the Molecular Structure of Antimony(Iii) Oxide Using Very-High-Temperature Gas Electron Diffraction (VHT-GED). *Dalt. Trans.* **2013**, *42* (10), 3581–3586. https://doi.org/10.1039/c2dt32790b.

(60) Ja'o, A. M.; Masters, S. L.; Wann, D. A.; Rankine, C. D.; Nunes, J. P. F.; Guillemin, J. C. Direct Experimental Observation of in Situ Dehydrogenation of an Amine-Borane System Using Gas Electron Diffraction. *J. Phys. Chem. A* **2019**, *123* (32), 7104–7112. https://doi.org/10.1021/acs.jpca.9b05522.

(61) E. A. V. Ebsworth, D. W. H. R. and S. C. *Structural Methods in Inorganic Chemistry*, 2nd ed.; Blackwell Scientific Publishing: Oxford, UK, 1991.

(62) Masters, S. L.; Atkinson, S. J.; Hölbling, M.; Hassler, K. Gas-Phase Molecular Structure of 1,1,1,2-Tetrabromo-2,2-Dimethyldisilane: Theoretical and Experimental Investigation of a Super-Halogenated Disilane and Computational Investigation of the F, Cl and i Analogues. *Struct. Chem.* **2013**, *24* (4), 1201–1206. https://doi.org/10.1007/s11224-012-0152-6.

(63) Hinchley, S. L.; Robertson, H. E.; Borisenko, K. B.; Turner, A. R.; Johnston, B. F.; Rankin, D. W. H.; Ahmadian, M.; Jones, J. N.; Cowley, A. H. The Molecular Structure of Tetra-Terf-Butyldiphosphine: An Extremely Distorted, Sterically Crowded Molecule. *Dalt. Trans.* **2004**, No. 16, 2469−2476. https://doi.org/10.1039/b407908f.

(64) Blake, A. J.; Brain, P. T.; McNab, H.; Miller, J.; Morrison, C. A.; Parsons, S.; Rankin, D. W. H.; Robertson, H. E.; Smart, B. A. Structure Analysis Restrained by Ab Initio Calculations: The Molecular Structure of 2,5-Dichloropyrimidine in Gaseous and Crystalline Phases. *J. Phys. Chem.* **1996**, *100* (30), 12280–12287. https://doi.org/10.1021/jp960084r.

(65) Brain, P. T.; Morrison, C. A.; Parsons, S.; Rankin, D. W. H. Tetraborane(10), B4H10: Structures in Gaseous and Crystalline Phases. *J. Chem. Soc. - Dalt. Trans.* **1996**, No. 24, 4589–4596. https://doi.org/10.1039/dt9960004589.

(66) Mitzel, N. W.; Rankin, D. W. H. SARACEN-Molecular Structures from Theory and Experiment: The Best of Both Worlds. *J. Chem. Soc. Dalt. Trans.* **2003**, *3* (19), 3650–3662. https://doi.org/10.1039/b307022k.

(67) Kafka, G. R.; Masters, S. L.; Rankin, D. W. H. Structure Enhancement Methodology Using Theory and Experiment: Gas-Phase Molecular Structures Using a Dynamic Interaction between Electron Diffraction, Molecular Mechanics, and Ab Initio Data. In *Journal of Physical Chemistry A*; 2007; 111(26), 5913–5920. https://doi.org/10.1021/jp072614x.

(68) Sipachev, V. A. Calculation of Shrinkage Corrections in Harmonic Approximation. *J. Mol. Struct. Theochem* **1985**, *22*, 143−151. https://doi.org/10.1016/0166-1280(85)85062-4.

(69) Sipachev, V. A. Local Centrifugal Distortions Caused by Internal Motions of Molecules. *J. Mol. Struct.* **2001**, *567−568* (2001), 67−72. https://doi.org/10.1016/S0022-2860(01)00534-8.

(70) Wann, D. A.; Less, R. J.; Rataboul, F.; McCaffrey, P. D.; Reilly, A. M.; Robertson, H. E.; Lickiss, P. D.; Rankin, D. W. H. Accurate Gas-Phase Experimental Structures of Octasilsesquioxanes (Si 8O12X8; X = H, Me). *Organometallics* **2008**, *27* (16), 4183–4187. https://doi.org/10.1021/om800357t.

(71) Møller, C.; Plesset, M. S. Note on an Approximation Treatment for Many-Electron Systems. *Phys. Rev.* **1934**, *46* (7), 618–622. https://doi.org/10.1103/PhysRev.46.618.

(72) Hohenberg, P.; Kohn, W. Inhomogeneous Electron Gas. *Phys. Rev.* **1964**, *136* (3B), B864–B871. https://doi.org/10.1103/PhysRev.136.B864.

(73) Zhao, G. L.; Bagayoko, D.; Williams, T. D. Local-Density-Approximation Prediction of Electronic Properties of GaN, Si, C, and RuO2. *Phys. Rev. B - Condens. Matter Mater. Phys.* **1999**, *60* (3), 1563–1572. https://doi.org/10.1103/PhysRevB.60.1563.

(74) Kohn, W.; Sham, L. J. Self-Consistent Equations Including Exchange and Correlation Effects. *Phys. Rev.* **1965**, *140*, A1133. https://doi.org/10.1103/PhysRev.140.A1133.

(75) Grimme, S. Semiempirical GGA-Type Density Functional Constructed with a Long-Range Dispersion Correction. *J. Comput. Chem.* **2006**, *27*, 1787–1799. https://doi.org/10.1002/jcc.20495.

(76) Hehre, W. J.; Ditchfield, R.; Pople, J. A. Self — Consistent Molecular Orbital Methods . XII . Further Extensions of Gaussian — Type Basis Sets for Use in Molecular Orbital Studies of

Organic Molecules Published by the AIP Publishing Articles You May Be Interested in Self - Consistent Molecular Or. *J.Chem. Phys.* **1972**, *56* (5), 2257–2261. https://doi.org/10.1063/1.1677527.

(77) Gonzalez, C.; Schlegel, H. B. Reaction Path Following in Mass-Weighted Internal Coordinates. *J. Phys. Chem.* **1990**, *94* (14), 5523–5527. https://doi.org/10.1021/j100377a021.

(78) Foresman, J. B.; Head-Gordon, M.; Pople, J. A.; Frisch, M. J. Toward a Systematic Molecular Orbital Theory for Excited States. *J. Phys. Chem.* **1992**, *96* (1), 135–149. https://doi.org/10.1021/j100180a030.

(79) Kümmel, H. G. A Biography of the Coupled Cluster Method. In *International Journal of Modern Physics B*; **2003**; 17(28) 5311-5325. https://doi.org/10.1142/S0217979203020442.

(80) Shavitt, I.; Bartlett, R. J. *Many – Body Methods in Chemistry and Physics: MBPT and Coupled-Cluster Theory*; Cambridge University Press: United Kingdom, 2009. https://doi.org/10.1017/CBO9780511596834.

(81) Gaussian 09 User's Reference. Gaussian, I. 1.; Petersson, G. A. Complete Basis Set Models for Chemical Reactivity: From the Helium Atom to Enzyme Kinetics. In *Quantum-Mechanical Prediction of Thermochemical Data*; Springer: Netherlands, 2005; pp 99–130. https://doi.org/10.1007/0-306-47632-0_4.

(82) Parthiban, S.; De Oliveira, G.; Martin, J. M. L. Benchmark Ab Initio Energy Profiles for the Gas-Phase SN2 Reactions Y- + CH3X → CH3Y + X- (X,Y = F,Cl,Br). Validation of Hybrid DFT Methods. *J. Phys. Chem. A* **2001**, *105* (5), 895–904. https://doi.org/10.1021/jp0031000.

(83) Roothaan, C. C. J. New Developments in Molecular Orbital Theory. *Rev. Mod. Phys.* **1951**, *23*, 69. https://doi.org/10.1103/RevModPhys.23.69.

(84) Binkley, J. S.; Pople, J. A.; Hehre, W. J. Self-Consistent Molecular Orbital Methods. 21. Small Split-Valence Basis Sets for First-Row Elements. *J. Am. Chem. Soc.* **1980**, *102* (3), 939–947. https://doi.org/10.1021/ja00523a008.

(85) Gordon, M. S.; Binkley, J. S.; Pople, J. A.; Pietro, W. J.; Hehre, W. J. Self-Consistent Molecular-Orbital Methods. 22. Small Split-Valence Basis Sets for Second-Row Elements. *J. Am. Chem. Soc.* **1982**, *104* (10), 2797–2803. https://doi.org/10.1021/ja00374a017.

(86) Ditchfield, R.; Hehre, W. J.; Pople, J. A. Self-Consistent Molecular-Orbital Methods. IX. An

Extended Gaussian-Type Basis for Molecular-Orbital Studies of Organic Molecules. *J. Chem. Phys.* **1971**, *54*, 720–723. https://doi.org/10.1063/1.1674902.

(87) Hay, P. J. Gaussian Basis Sets for Molecular Calculations. The Representation of 3d Orbitals in Transition-Metal Atoms. *J. Chem. Phys.* **1977**, *66*, 4377–4384. https://doi.org/10.1063/1.433731.

(88) Wachtees, A. J. H. Gaussian Basis Set for Molecular Wavefunctions Containing Third-Row Atoms. *J. Chem. Phys.* **1970**, *52* (3), 1033–1036. https://doi.org/10.1063/1.1673095.

(89) Dunning, T. H. Gaussian Basis Sets for Use in Correlated Molecular Calculations. I. The Atoms Boron through Neon and Hydrogen. *J. Chem. Phys.* **1989**, *90*, 1007–1023. https://doi.org/10.1063/1.456153.

(90) Kendall, R. A.; Dunning, T. H.; Harrison, R. J. Electron Affinities of the First-Row Atoms Revisited. Systematic Basis Sets and Wave Functions. *J. Chem. Phys.* **1992**, *96*, 6796–6806. https://doi.org/10.1063/1.462569.

(91) Frisch, M. J.; Trucks, G. W.; Schlegel, H. B.; Scuseria, G. E.; Robb, M. A.; Cheeseman, J. R.; Scalmani, G.; Barone, V.; Mennucci, B.; Petersson, G. A.; Nakatsuji, H.; Caricato, M.; Li, X.; Hratchian, H. P.; Izmaylov, A. F.; Bloino, J.; Zheng, G.; Sonnenberg, J. L.; Hada, M.; Ehara, M.; Toyota, K.; Fukuda, R.; Hasegawa, J.; Ishida, M.; Nakajima, T.; Honda, Y.; Kitao, O.; Nakai, H.; Vreven, T.; Montgomery Jr., J. A.; Peralta, J. E.; Ogliaro, F.; Bearpark, M.; Heyd, J. J.; Brothers, E.; Kudin, K. N.; Staroverov, V. N.; Kobayashi, R.; Normand, J.; Raghavachari, K.; Rendell, A.; Burant, J. C.; Iyengar, S. S.; Tomasi, J.; Cossi, M.; Rega, N.; Millam, J. M.; Klene, M.; Knox, J. E.; Cross, J. B.; Bakken, V.; Adamo, C.; Jaramillo, J.; Gomperts, R.; Stratmann, R. E.; Yazyev, O.; Austin, A. J.; Cammi, R.; Pomelli, C.; Ochterski, J. W.; Martin, R. L.; Morokuma, K.; Zakrzewski, V. G.; Voth, G. A.; Salvador, P.; Dannenberg, J. J.; Dapprich, S.; Daniels, A. D.; Farkas; Foresman, J. B.; Ortiz, J. V; Cioslowski, J.; Fox, D. J. Gaussian09 Revision D.01, Gaussian Inc. Wallingford CT. *Gaussian 09 Revision C.01*. 2010.

(92) Valiev, M.; Bylaska, E. J.; Govind, N.; Kowalski, K.; Straatsma, T. P.; Van Dam, H. J. J.; Wang, D.; Nieplocha, J.; Apra, E.; Windus, T. L.; De Jong, W. A. NWChem: A Comprehensive and Scalable Open-Source Solution for Large Scale Molecular Simulations. *Comput. Phys. Commun.* **2010**, *181*, 1477−1489. https://doi.org/10.1016/j.cpc.2010.04.018.

(93) Frisch, M. J.; Head-gordon, M.; Pople, J. A. A Direct MP2 Gradient Method. *Chem. Phys. Lett.* **1990**, *166* (3), 275–280.

(94) Zhao, Y.; Truhlar, D. G. The M06 Suite of Density Functionals for Main Group Thermochemistry, Thermochemical Kinetics, Noncovalent Interactions, Excited States, and Transition Elements: Two New Functionals and Systematic Testing of Four M06 Functionals and 12 Other Functionals (T. *Theor. Chem. Acc.* **2008**, *119* (5–6), 525. https://doi.org/10.1007/s00214-007-0401-8.

(95) Krishnan, R.; Binkley, J. S.; Seeger, R.; Pople, J. A. Self-Consistent Molecular Orbital Methods. XX. A Basis Set for Correlated Wave Functions. *J. Chem. Phys.* **1980**, *72* (1), 650–654. https://doi.org/10.1063/1.438955.

(96) Francl, M. M.; Pietro, W. J.; Hehre, W. J.; Binkley, J. S.; Gordon, M. S.; DeFrees, D. J.; Pople, J. A. Self-Consistent Molecular Orbital Methods. XXIII. A Polarization-Type Basis Set for Second-Row Elements. *J. Chem. Phys.* **1982**, *77*, 3654−3665. https://doi.org/10.1063/1.444267.

(97) Frisch, M. J.; Pople, J. A.; Binkley, J. S. Self-Consistent Molecular Orbital Methods 25. Supplementary Functions for Gaussian Basis Sets. *J. Chem. Phys.* **1984**, *80* (7), 3265–3269. https://doi.org/10.1063/1.447079.

(98) Woon, D. E.; Dunning, T. H. Gaussian Basis Sets for Use in Correlated Molecular Calculations. V. Core-Valence Basis Sets for Boron through Neon. *J. Chem. Phys.* **1995**, *103*, 4572–4585. https://doi.org/10.1063/1.470645.

(99) Peng, C.; Bernhard Schlegel, H. Combining Synchronous Transit and Quasi-Newton Methods to Find Transition States. *Isr. J. Chem.* **1993**, *33*, 449−454. https://doi.org/10.1002/ijch.199300051.

(100) Curtiss, L. A.; Raghavachari, K.; Redfern, P. C.; Pople, J. A. Assessment of Gaussian-2 and Density Functional Theories for the Computation of Enthalpies of Formation. *J. Chem. Phys.* **1997**, *106*, 1063−1079. https://doi.org/10.1063/1.473182.

(101) Matus, M. H.; Anderson, K. D.; Camaioni, D. M.; Autrey, S. T.; Dixon, D. A. Reliable Predictions of the Thermochemistry of Boron-Nitrogen Hydrogen Storage Compounds: BxNxHy, x = 2, 3. *J. Phys. Chem. A* **2007**, *111*, 4411–4421. https://doi.org/10.1021/jp070931y.

(102) Helgaker, T.; Klopper, W.; Koch, H.; Noga, J. Basis-Set Convergence of Correlated Calculations on Water. *J. Chem. Phys.* **1997**, *106*, 9639–9646. https://doi.org/10.1063/1.473863.

(103) Katz, L.; Lipscomb, W. N. The Crystal and Molecular Structure of Diketene. *Acta Crystallogr.* **1952**, *5*, 313–118.

(104) Katz, L.; Lipscomb, W. N. The Crystal and Molecular Structure of Diketene. *J. Org. Chem.* **1952**, *17*, 515–517.

(105) Johnson, H. R.; Strandberg, M. W. P. The Microwave Spectrum of Ketene. *J. Chem. Phys.* **1952**, *20*, 687–695. https://doi.org/10.1063/1.1700517.

(106) Chickos, J. S.; Sherwood, D. E.; Jug, K. Mechanism of Thermolysis of Diketene in the Gas Phase. *J. Org. Chem.* **1978**, *43* (6), 1146–1150. https://doi.org/10.1021/jo00400a026.

(107) Blackman, G. L.; Brown, R. D.; Brown, R. F. C.; Eastwood, F. W.; McMullen, G. L.; Robertson, M. L. Methyleneketenes and Methylenecarbenes. x: Precursors for the Generation of Methyleneketene and Deuterated Methyleneketenes for Microwave Spectroscopy. *Aust. J. Chem.* **1978**, *31*, 209–213. https://doi.org/10.1071/CH9780209.

(108) Masters, A. P.; Sorensen, T. S.; Tran, P. M. ChemInform Abstract: A New Procedure for the in Situ Generation of Methylene Ketenes. *Can. J. Chem.* **1987**, *65*, 1499–1502. https://doi.org/10.1002/chin.198751096.

(109) Lang, M.; Holzmeier, F.; Fischer, I.; Hemberger, P. Decomposition of Diazomeldrum's Acid: A Threshold Photoelectron Spectroscopy Study. *J. Phys. Chem. A* **2014**, *118*, 11235–11245. https://doi.org/10.1021/jp509324w.

(110) Birney, D. M.; Wagenseller, P. E. An Ab Initio Study of the Reactivity of Formylketene. Pseudopericyclic Reactions Revisited. *J. Am. Chem. Soc.* **1994**, *116*, 6262–6270. https://doi.org/10.1021/ja00093a028.

(111) Fillion, E.; Fishlock, D. Scandium Triflate-Catalyzed Intramolecular Friedel-Crafts Acylation with Meldrum's Acids: Insight into the Mechanism. *Tetrahedron* **2009**, *65*, 6682–6695. https://doi.org/10.1016/j.tet.2009.05.058.

(112) Sato, M.; Ban, H.; Kaneko, C. An Efficient Method for Generation of α-Oxoketenes: Cycloreversion of Enolized Meldrum's Acid Derivatives. *Tetrahedron Lett.* **1997**, *38*, 6689–6692. https://doi.org/10.1016/S0040-4039(97)01566-9.

(113) Brown, R. F. C.; Eastwood, F. W.; McMullen, G. L. Methyleneketenes and Methylenecarbenes. VIP Evidence for the Pyrolytic Generation of Methyleneketene (Propadienone). *Chem. Informationsd.* **1977**, *30*, 179–193. https://doi.org/10.1002/chin.197718162.

9. Appendix

9.1. Conference contributions

University of Canterbury, Materials @ UC 2020

University of Canterbury, New Zealand, 19 – 20 November 2020

Oral presentation: "*Molecular structure of short-lived species by gas electron diffraction and computational methods."*

University of Canterbury, Annual Postgraduate Research Showcase Symposium

University of Canterbury, New Zealand, 14 December 2020

Oral presentation: "*Molecular Structures of Short-Lived Ketenes by Computational (and Experimental) Methods."*

9.2. Ketene and its pyrolysis preparation from decomposition of diketene

Table A9.2.1. Calculated coordinates at the MP2/6-31+G* level for diketene, ketene, allene and CO_2.

Atom	*x*	*y*	*z*
Diketene			
C	0.05586	1.15104	0.00002
C	1.05035	-0.00506	0.00000
H	0.09712	1.77484	0.89701
H	0.09710	1.77487	-0.89694
C	-0.95805	0.03892	0.00002
C	-2.27332	-0.15114	-0.00003
H	-2.94208	0.70105	-0.00005
H	-2.69351	-1.15016	-0.00004
O	0.03597	-0.97915	0.00004
O	2.23807	-0.18375	-0.00004
Ketene			
C	0.00000	0.00000	0.09967
C	0.00000	0.00000	1.28145
H	0.00000	0.00000	-1.22284
H	0.00000	0.94061	-1.75631
O	0.00000	-0.94061	-1.75631
Allene			
C	-1.31579	0.00000	0.00000
C	1.31579	0.00000	0.00000
H	1.87868	0.92902	0.00150
H	-1.87868	0.00150	-0.92901
H	-1.87868	-0.00150	0.92902
C	0.00000	0.00000	0.00000
H	1.87868	-0.92902	-0.00150
CO_2			
C	0.00000	0.00000	0.00000
O	0.00000	0.00000	1.18087
O	0.00000	0.00000	-1.18087

Table A9.2.2. Calculated coordinates at the MP2/6-311G* level for diketene, ketene, allene and CO_2

Atom	*x*	*y*	*z*
diketene			
C	0.05305	1.15423	0.00000
C	1.04961	-0.00489	0.00000
H	0.08911	1.77555	0.89665
H	0.08911	1.77555	-0.89665
C	-0.94896	0.02990	0.00000
C	-2.26492	-0.15212	-0.00000
H	-2.92871	0.70232	-0.00000
H	-2.68522	-1.15000	-0.00000
O	0.03851	-0.97388	0.00000
O	2.22437	-0.18439	-0.00000
Ketene			
C	0.00000	0.00000	0.10338
C	0.00000	0.00000	1.27214
H	0.00000	0.00000	-1.21676
H	0.00000	0.94003	-1.74842
O	0.00000	-0.94003	-1.74842
Allene			
C	0.00000	0.00000	-1.31312
C	0.00000	0.00000	1.31312
H	0.00000	0.92932	1.87410
H	0.92932	0.00000	-1.87410
H	-0.92932	0.00000	-1.87410
C	0.00000	0.00000	0.00000
H	0.00000	-0.92932	1.87410
CO2			
C	0.00000	0.00000	0.00000
O	0.00000	0.00000	1.16906
O	0.00000	0.00000	-1.16906

Table A9.2.3. Calculated coordinates at the MP2/6-311+G* level for diketene, ketene, allene and CO_2

Atom	*x*	*y*	*z*
diketene			
C	0.05506	1.15461	0.00000
C	1.05008	-0.00512	0.00000
H	0.09337	1.77558	0.89696
H	0.09337	1.77559	-0.89696
C	-0.95148	0.03376	0.00000
C	-2.26746	-0.15358	0.00000
H	-2.93254	0.70035	0.00000
H	-2.68772	-1.1519	0.00000
O	0.03848	-0.97327	0.00000
O	2.22605	-0.18643	0.00000
Ketene			
C	0.00000	0.00000	0.10357
C	0.00000	0.00000	1.27264
H	0.00000	0.00000	-1.21741
H	0.00000	0.94052	-1.74906
O	0.00000	-0.94052	-1.74906
Allene			
C	0.00000	0.00000	1.31430
C	0.00000	0.00000	-1.31430
H	0.00000	0.92976	-1.87476
H	-0.92976	0.00000	1.87476
H	0.92976	0.00000	1.87476
C	0.00000	0.00000	0.00000
H	0.00000	-0.92976	-1.87476
CO2			
C	0.00000	0.00000	0.00000
O	0.00000	0.00000	1.17001
O	0.00000	0.00000	-1.17001

Table A9.2.4. Calculated coordinates at the MP2/6-311++G** level for diketene, ketene, allene and CO_2

Atom	*x*	*y*	*z*
diketene			
C	0.05390	1.15483	0.00000
C	1.05032	-0.00505	0.00000
H	0.09180	1.77258	0.89900
H	0.09180	1.77258	-0.89900
C	-0.95102	0.03187	0.00000
C	-2.26762	-0.15307	0.00000
H	-2.92595	0.70600	0.00000
H	-2.68722	-1.15149	0.00000
O	0.03851	-0.97377	0.00000
O	2.22601	-0.18512	0.00000
Ketene			
C	0.00000	0.00000	0.10357
C	0.00000	0.00000	1.27182
H	0.00000	0.00000	-1.21814
H	0.00000	0.94350	-1.74357
O	0.00000	-0.94350	-1.74357
Allene			
C	0.00000	0.00000	-1.31411
C	0.00000	0.00000	1.31411
H	0.00000	0.93190	1.87109
H	0.93190	0.00000	-1.87109
H	-0.93190	0.00000	-1.87109
C	0.00000	0.00000	0.00000
H	0.00000	-0.93190	1.87109
CO_2			
C	0.00000	0.00000	0.00000
O	0.00000	0.00000	1.17001
O	0.00000	0.00000	-1.17001

Table A9.2.5. Calculated coordinates at the M06-2X/aug-cc-pVTZ level for diketene, ketene, allene and CO_2

Atom	*x*	*y*	*z*
diketene			
C	-0.05427	1.15048	0.00000
C	-1.04383	-0.00673	0.00000
H	-0.08946	1.76686	-0.89436
H	-0.08946	1.76686	0.89436
C	0.94967	0.03033	0.00000
C	2.24895	-0.15632	0.00000
H	2.91181	0.69443	0.00000
H	2.66431	-1.15264	0.00000
O	-0.04221	-0.96037	0.00000
O	-2.20783	-0.18739	0.00000
Ketene			
C	0.00000	0.00000	0.10322
C	0.00000	0.00000	1.25776
H	0.00000	0.00000	-1.20407
H	0.00000	0.94048	-1.72848
O	0.00000	-0.94048	-1.72848
Allene			
C	-1.29924	0.00000	0.00000
C	1.29924	-0.00000	0.00000
H	1.85575	-0.54508	0.75138
H	-1.85577	0.75135	0.54509
H	-1.85577	-0.75135	-0.54506
C	0.00000	0.00000	-0.00002
H	1.85582	0.54507	-0.75132
CO_2			
C	0.00000	0.00000	0.00000
O	0.00000	0.00000	1.15546
O	0.00000	0.00000	-1.15546

Table A9.2.6. Calculated coordinates at the CBS-QB3 level for TS1 (TS for diketene to ketene) and TS2 (TS for diketene to allene and CO_2)

Atom	*x*	*y*	*z*
TS1			
C	-0.22079	-0.94866	0.63236
C	-1.26007	-0.21686	0.03989
H	-0.16975	-0.80517	1.70914
H	-0.25769	-2.00308	0.33937
C	0.92805	0.17693	0.08800
C	1.97002	-0.33742	-0.59071
H	2.07530	-1.39808	-0.75822
H	2.75278	0.32966	-0.92893
O	0.46529	1.27968	0.45579
O	-2.07828	0.19941	-0.62812
TS2			
C	-0.06903	1.21631	0.00001
C	1.04798	-0.20322	0.00000
H	0.10764	1.77719	0.91508
H	0.10764	1.77720	-0.91506
C	-1.14024	0.34132	0.00000
C	-2.28495	-0.26051	-0.00001
H	-3.18046	0.35778	-0.00001
H	-2.38434	-1.33670	-0.00002
O	0.29565	-1.19565	0.00000
O	2.20772	0.05330	0.00000

Table A9.2.7. Energies and corrections for enthalpy (*H*corr.), Gibbs Free Energy (*G*corr.) and Zero Point Energy (ZPEcorr.) at CBS-QB3 and energy at CCSD(T)/CBS and corrections at MP2/cc-pvtz level at different temperatures for all the molecules involved in the calculation of the thermochemical properties of decomposition of diketene. All the energies are in Hartrees.

Energy and corrections both at CBS-QB3 at 278.15 K				
Molecule	Energy	*H*corr.	*G*corr.	ZPEcorr.
Diketene	-304.780795	0.078433	0.043872	0.072326
Ketene	-152.372330	0.036029	0.008647	0.031579
Allene	-116.416553	0.059597	0.032056	0.054858
Carbon dioxide	-188.369467	0.015286	-0.008974	0.011720
Energy at CCSD(T)/CBS and corrections at MP2/cc-pvtz at 278.15 K				
Diketene	-304.930550	0.078806	0.044404	0.072780
Ketene	-152.444407	0.036162	0.008685	0.031657
Allene	-116.492458	0.059902	0.031786	0.055221
Carbon dioxide	-188.442501	0.015128	-0.009163	0.011550
Energy at CCSD(T)/CBS and corrections at MP2/cc-pvtz at 653 K				
Diketene	-304.930550	0.095161	-0.002959	0.072780
Ketene	-152.444407	0.044713	-0.027540	0.031657
Allene	-116.492458	0.070376	-0.005835	0.055221
Carbon dioxide	-188.442501	0.021024	-0.040542	0.011550
Energy at CCSD(T)/CBS and corrections at MP2/cc-pvtz at 823 K				
Diketene	-304.930550	0.105416	-0.029711	0.072780
Ketene	-152.444407	0.049611	-0.046930	0.031657
Allene	-116.492458	0.076875	-0.026440	0.055221
Carbon dioxide	-188.442501	0.024271	-0.056956	0.011550

9.3. Methyleneketene and its pyrolysis preparation from decomposition of diazotetranoic acid

Table A9.3.1: Calculated coordinates at the MP2/6-31+G* level for diazotetranoic acid, intermediate, nitrogen, methyleneketene, CO_2, carbon sub-oxide and formaldehyde

Atom	*x*	*y*	*z*
Diazoteranoic Acid			
C	1.02448	1.57979	0.00025
C	-0.43164	1.12924	-0.00052
C	-0.33352	-0.36574	-0.00022
H	1.24821	2.16462	0.89622
N	-1.34914	-1.31059	-0.00369
N	-2.49716	-1.03735	0.00349
O	-1.39722	1.81881	-0.00087
C	1.11040	-0.77026	0.00040
O	1.58025	-1.86811	0.00021
H	1.24914	2.16451	-0.89555
O	1.84302	0.38284	0.00082
Intermediate			
C	0.60992	-1.47406	-0.00000
C	0.89112	0.57104	-0.00002
C	-0.31385	-0.28250	-0.00013
H	0.62430	-2.08293	-0.90561
H	0.62415	-2.08287	0.90565
O	1.17715	1.74203	0.00000
O	1.74921	-0.53077	0.00006
C	-1.61248	-0.02570	-0.00001
O	-2.76345	0.21788	0.00005
Nitrogen			
N	0.00000	0.00000	0.56533
N	0.00000	0.00000	-0.56533
Methyleneketene			
C	0.00000	0.92457	-2.46422
H	0.00000	0.00000	-0.56273

H	0.00000	0.00000	0.72140
C	0.00000	0.00000	1.91616
C	0.00000	-0.92457	2.46942
O	0.00000	0.00000	-1.89041
Carbon dioxide			
C	0.00000	0.00000	0.00000
O	0.00000	0.00000	1.18087
O	0.00000	0.00000	-1.18087
Carbon sub-oxide			
C	0.00000	0.00000	0.00000
C	0.00000	0.00000	1.27952
C	0.00000	0.00000	-1.27952
O	0.00000	0.00000	2.53792
O	0.00000	0.00000	-2.53792
Formaldehyde			
C	0.00000	0.00000	-0.54000
H	0.00000	0.93813	-1.11901
H	0.00000	-0.93813	-1.11901
O	0.00000	0.00000	0.68475

Table A9.3.2: Calculated coordinates at the MP2/6-311G level for diazotetranoic acid, intermediate, nitrogen, methyleneketene, CO_2, carbon sub-oxide and formaldehyde

Atom	*x*	*y*	*z*
Diazoteranoic Acid			
C	-1.05031	1.60291	0.00003
C	0.40465	1.14140	0.00011
C	0.34094	-0.34870	-0.00005
H	-1.28690	2.17278	-0.89881
N	1.36301	-1.25998	0.00032
N	2.55482	-1.03551	0.00022
O	1.38226	1.83867	-0.00006
C	-1.10953	-0.81644	-0.00017
O	-1.55181	-1.91570	-0.00030
H	-1.28699	2.17272	0.89888
O	-1.87614	0.35802	-0.00006
Intermediate			
C	1.51476	0.56881	0.00000
C	0.14892	-1.06064	0.00000
C	0.00000	0.41369	0.00000
H	1.96301	0.96617	0.90830
H	1.96301	0.96617	-0.90830
O	-0.54304	-2.06967	0.00000
O	1.60285	-0.96992	0.00000
C	-1.05100	1.22218	0.00000
O	-2.01006	1.94001	0.00000
Nitrogen			
N	0.00000	0.00000	0.57489
N	0.00000	0.00000	-0.57489
Methyleneketene			
C	0.00000	0.92182	-2.48507
H	0.00000	0.00000	-0.56864
H	0.00000	0.00000	0.71781

C	0.00000	0.00000	1.93628
C	0.00000	-0.92182	-2.48507
O	0.00000	0.00000	-1.90251
Carbon dioxide			
C	0.00000	0.00000	0.00000
O	0.00000	0.00000	1.20196
O	0.00000	0.00000	-1.20196
Carbon sub-oxide			
C	0.00000	0.00000	0.00000
C	0.00000	0.00000	1.28213
C	0.00000	0.00000	-1.28213
O	0.00000	0.00000	2.48901
O	0.00000	0.00000	-2.48901
Formaldehyde			
C	0.00000	0.00000	-0.55448
H	0.00000	0.93371	-1.13060
H	0.00000	-0.93371	-1.13060
O	0.00000	0.00000	0.69851

Table A9.3.3: Calculated coordinates at the MP2/6-311G* level for diazotetranoic acid, intermediate, nitrogen, methyleneketene, CO_2, carbon sub-oxide and formaldehyde

Atom	*x*	*y*	*z*
Diazoteranoic Acid			
C	1.04807	1.55352	0.00005
C	-0.42163	1.13590	-0.00011
C	-0.33887	-0.35798	-0.00004
H	1.27452	2.13842	0.89382
N	-1.36911	-1.29803	-0.00016
N	-2.50250	-1.00979	-0.00005
O	-1.36665	1.83934	-0.00019
C	1.10055	-0.77922	0.00008
O	1.54759	-1.87564	0.00020
H	1.27472	2.13838	-0.89369
O	1.84698	0.35688	0.00017
Intermediate			
C	-0.60745	-1.46301	0.00001
C	-0.89795	0.56759	0.00000
C	0.32265	-0.27551	-0.00000
H	-0.61151	-2.07256	0.90425
H	-0.61150	-2.07259	-0.90422
O	-1.19084	1.72323	0.00000
O	-1.73974	-0.53407	-0.00001
C	1.61789	-0.02020	0.00000
O	2.75711	0.22233	0.00000
Nitrogen			
N	0.00000	0.00000	0.55989
N	0.00000	0.00000	-0.55989
Methyleneketene			
C	-1.88398	0.00021	0.00001
H	-2.46313	-0.92412	0.00003
H	-2.46220	0.92513	0.00003

C	-0.55853	-0.00047	-0.00002
C	0.72371	-0.00021	-0.00005
O	1.90476	0.00022	0.00003
Carbon dioxide			
C	0.00000	0.00000	0.00000
O	0.00000	0.00000	1.16906
O	0.00000	0.00000	-1.16906
Carbon sub-oxide			
C	0.00000	0.00000	0.00000
C	0.00000	0.00000	1.27900
C	0.00000	0.00000	-1.27900
O	0.00000	0.00000	2.45048
O	0.00000	0.00000	-2.45048
Formaldehyde			
C	0.00000	0.00000	-0.53283
H	0.00000	0.93768	-1.11730
H	0.00000	-0.93768	-1.11730
O	0.00000	0.00000	0.67894

Table A9.3.4: Calculated coordinates at the MP2/6-311G** level for diazotetranoic acid, intermediate, nitrogen, methyleneketene, CO_2, carbon sub-oxide and formaldehyde

Atom	*x*	*y*	*z*
Diazoteranoic Acid			
C	-1.04781	1.55355	0.00004
C	0.42270	1.13488	-0.00018
C	0.33864	-0.35845	-0.00001
H	-1.26795	2.13849	-0.89550
N	1.36835	-1.29913	0.00029
N	2.50170	-1.01102	0.00019
O	1.36788	1.83829	0.00020
C	-1.10082	-0.77849	-0.00020
O	-1.54967	-1.87394	-0.00017
H	-1.26787	2.13829	0.89557
O	-1.84706	0.35882	-0.00014
Intermediate			
C	1.50738	0.48099	0.00000
C	0.14634	-1.05325	0.00000
C	0.00000	0.42250	0.00000
H	1.97234	0.87435	0.90485
H	1.97234	0.87435	-0.90485
O	-0.54478	-2.02435	0.00000
O	1.53216	-0.98254	0.00000
C	-1.02949	1.24905	0.00000
O	-1.94864	1.96383	0.00000
Nitrogen			
N	0.00000	0.00000	0.55990
N	0.00000	0.00000	-0.55990
Methyleneketene			
C	-1.88377	0.00024	0.00002
H	-2.46176	-0.92530	0.00003
H	-2.46075	0.92642	0.00003
C	-0.55878	-0.00051	-0.00002

C	0.72375	-0.00027	-0.00005
O	1.90441	0.00026	0.00003
Carbon dioxide			
C	0.00000	0.00000	0.00000
O	0.00000	0.00000	1.16896
O	0.00000	0.00000	-1.16896
Carbon sub-oxide			
C	0.00000	0.00000	0.00000
C	0.00000	0.00000	1.27900
C	0.00000	0.00000	-1.27900
O	0.00000	0.00000	2.45048
O	0.00000	0.00000	-2.45048
Formaldehyde			
C	0.00000	0.00000	-0.53156
H	0.00000	0.93583	-1.12119
H	0.00000	-0.93583	-1.12119
O	0.00000	0.00000	0.67897

Table A9.3.5: Calculated coordinates at the M06-2X/aug-cc-pVTZ level for diazotetranoic acid, intermediate, nitrogen, methyleneketene, CO_2, carbon sub-oxide and formaldehyde

Atom	*x*	*y*	*z*
Diazoteranoic Acid			
C	0.27839	-1.85317	0.00000
C	1.03974	-0.53756	0.00000
C	0.00000	0.48952	0.00000
H	0.51307	-2.43565	0.88985
N	0.12775	1.86970	0.00000
N	1.18273	2.41597	0.00000
O	2.23367	-0.39640	0.00000
C	-1.31957	-0.17380	0.00000
O	-2.39815	0.32669	0.00000
H	0.51307	-2.43565	-0.88985
O	-1.10937	-1.51510	0.00000
Intermediate			
C	0.60889	-1.45882	0.00000
C	0.60887	0.56589	0.00000
C	-0.32517	-0.27528	0.00000
H	0.61351	-2.06675	-0.90069
H	0.61351	-2.06675	0.90069
O	1.18045	1.71140	0.00000
O	1.72317	-0.52467	0.00000
C	-1.60870	-0.01812	0.00000
O	-2.73141	0.21969	0.00000
Nitrogen			
N	0.00000	0.00000	0.54322
N	0.00000	0.00000	-0.54322
Methyleneketene			
C	-0.56039	-0.23957	-0.00000
C	-1.83338	0.08779	0.00000
H	-2.16513	1.12293	0.00000

H	-2.61363	-0.66713	0.00001
C	0.70393	0.00003	-0.00000
O	1.86472	0.05683	0.00000
Carbon dioxide			
C	0.00000	0.00000	0.00000
O	0.00000	0.00000	1.15546
O	0.00000	0.00000	-1.15546
Carbon sub-oxide			
C	0.00000	0.00000	0.00000
C	0.00000	0.00000	1.27260
C	0.00000	0.00000	-1.27260
O	0.00000	0.00000	2.42478
O	0.00000	0.00000	-2.42478
Formaldehyde			
C	0.00000	0.00000	-0.52548
H	0.00000	0.93857	-1.10529
H	0.00000	-0.93857	-1.10529
O	0.00000	0.00000	0.67043

Table A9.3.6: Calculated coordinates for TS (B97D/6-31++G** level TS for diazotetranoic acid to intermediate and nitrogen), TS1 (at the CBS-QB3 level TS for intermediate to methyleneketene and CO_2), and TS2 (at the CBS-QB3 level TS for intermediate to carbon sub-oxide and formaldehyde)

Atom	*x*	*y*	*z*
TS for diazotetranoic acid to intermediate and nitrogen			
C	-1.94573	-0.91135	-0.14963
C	-0.44645	-1.16879	0.00413
C	-0.09840	0.08897	0.72030
H	-2.55910	-1.51832	0.52875
N	2.43642	0.22990	-0.04656
N	3.52913	0.08604	0.10142
O	0.23586	-2.12539	-0.31263
C	-0.63322	1.18713	0.02149
O	-0.52806	2.26946	-0.46158
H	-2.32606	-0.96087	-1.18052
O	-1.97417	0.49242	0.36047
TS1 for intermediate to methyleneketene and CO_2			
C	0.27238	1.68544	0.18268
C	-1.54010	0.02830	0.00214
C	-0.31205	0.42438	0.29534
H	1.09377	1.95830	0.82539
O	-2.57987	-0.43148	-0.18718
C	1.01825	-0.51401	0.02388
O	1.05851	-1.69674	0.18796
H	-0.16847	2.48633	-0.40823
O	1.82684	0.35456	-0.43095
TS2 for intermediate to carbon sub-oxide and formaldehyde			
C	-0.95585	-1.49613	0.00026
C	1.69289	0.01460	-0.00002
C	0.38758	-0.11160	0.00009
H	-0.68033	-2.03057	0.92239
O	2.84588	-0.08139	-0.00013

C	-0.60942	0.81535	0.00007
O	-1.13368	1.83866	0.00008
H	-0.68017	-2.03184	-0.92109
O	-1.92853	-0.66614	-0.00042

Table A9.3.7: Energies and corrections for enthalpy (*H*corr.), Gibbs Free Energy (*G*corr.) and Zero Point Energy (ZPEcorr.) energy at CBS-QB3 and at CCSD(T)/CBS (corrections at MP2/cc-pvtz level) at 298.15 K for all the molecules involved in the calculation of the thermochemical properties of decomposition of diazotetranoic acid. All energies in Hartrees.

Molecule	Ecbs-qb3	Hcorr.	Gcorr.	ZPEcorr.
DiazotetranoicAcid	-488.023109	0.069865	0.028891	0.061918
N2	-109.396085	0.008881	-0.012857	0.005576
Intermediate	-378.725521	0.061951	0.025152	0.055272
Methyleneketene	-190.359701	0.041620	0.012395	0.036824
CO2	-188.369467	0.015286	-0.009000	0.011720
Carbon sub-oxide	-264.364411	0.027581	-0.003317	0.021972
Formaldehyde	-114.341304	0.030308	0.005495	0.026496

	Eccsdt/cbs	corrections at MP2/cc-pVTZ		
DiazotetranoicAcid	-488.230144	0.073449	0.032033	0.000654
N2	-109.434076	0.008306	-0.013463	0.005001
Intermediate	-378.883723	0.062259	0.025189	0.055506
Methyleneketene	-190.441921	0.041763	0.012464	0.036928
CO2	-188.442501	0.015128	-0.009163	0.011550
Carbon sub-oxide	-264.459084	0.027239	-0.004141	0.021493
Formaldehyde	-114.401548	0.030761	0.005945	0.026950

9.4. Substituted ketenes and their pyrolysis preparation from decomposition of MA derivatives

Table A9.4.1: Calculated coordinates at the MP2/6-31+G* level for MA, ketene, CO_2 and acetone

Atom	*x*	*y*	*z*
MA			
C	1.13956	0.00000	0.02078
C	-0.92258	-1.27379	-0.07928
C	-1.58354	0.00000	0.39742
C	-0.92258	1.27379	0.89622
H	-2.62442	0.00000	0.06626
O	-1.51467	2.32076	-0.24827
O	0.41448	1.19067	-0.34931
O	0.41448	-1.19067	-0.34931
O	-1.51467	-2.32076	-0.24827
H	-1.60501	0.00000	1.49493
C	2.37612	0.00000	-0.84382
H	2.96991	0.89313	-0.63412
H	2.96991	-0.89313	-0.63412
H	2.07906	0.00000	-1.89466
C	1.44805	0.00000	1.50763
H	2.03120	-0.89164	1.75299
H	2.03120	0.89164	1.75299
H	0.54093	0.00000	2.11629
Acetone			
C	0.00000	0.00000	0.17656
O	0.00000	0.00000	1.40825
C	0.00000	1.28731	-0.61634
H	-0.10557	2.13702	0.05983
H	0.93848	1.37815	-1.17528
H	-0.81412	1.28701	-1.34919
C	0.00000	-1.28731	-0.61634
H	-0.93848	-1.37815	-1.17528
H	0.81412	-1.28701	-1.34919

H	0.10557	-2.13702	0.05983
Ketene			
C	0.00000	0.00000	0.09967
C	0.00000	0.00000	1.28145
H	0.00000	0.00000	-1.22284
H	0.00000	0.94061	-1.75631
O	0.00000	-0.94061	-1.75631
CO_2			
C	0.00000	0.00000	0.00000
O	0.00000	0.00000	1.18087
O	0.00000	0.00000	-1.18087

Table A9.4.2: Calculated coordinates at the MP2/6-311G* level for MA, ketene, CO_2 and acetone

Atom	*x*	*y*	*z*
MA			
C	0.27299	1.09110	0.00000
C	-0.15510	-0.90399	1.27902
C	-0.77451	-1.42630	0.00000
C	-0.1551	-0.90399	-1.27902
H	-0.70415	-2.51436	0.00000
O	-0.15510	-1.50836	-2.31754
O	0.45703	0.30960	-1.18698
O	0.45703	0.30960	1.18698
O	-0.15510	-1.50836	2.31754
H	-1.84374	-1.18815	0.00000
C	1.40561	2.08984	0.00000
H	1.34703	2.71516	-0.89209
H	1.34703	2.71516	0.89209
H	2.35365	1.55109	0.00000
C	-1.09780	1.74534	0.00000
H	-1.20112	2.36868	0.89014
H	-1.20112	2.36868	-0.89014
H	-1.90484	1.01176	0.00000
Acetone			
C	0.00000	0.00000	0.18433
O	0.00000	0.00000	1.40197
C	0.00000	1.28783	-0.61620
H	-0.07603	2.13751	0.06131
H	0.92294	1.36782	-1.19869
H	-0.83169	1.30289	-1.32630
C	0.00000	-1.28783	-0.61620
H	-0.92294	-1.36782	-1.19869
H	0.83169	-1.30289	-1.32630
H	0.07603	-2.13751	0.06131

Ketene			
C	0.00000	0.00000	0.10338
C	0.00000	0.00000	1.27214
H	0.00000	0.00000	-1.21676
H	0.00000	0.94003	-1.74842
O	0.00000	-0.94003	-1.74842
CO_2			
C	0.00000	0.00000	0.00000
O	0.00000	0.00000	1.16906
O	0.00000	0.00000	-1.16906

Table A9.4.3: Calculated coordinates at the MP2/6-311+G* level for MA, ketene, CO_2 and acetone

Atom	*x*	*y*	*z*
MA			
C	1.50770	-1.39996	0.00000
C	0.01334	-1.12623	0.00000
C	-0.81930	-2.38583	0.00000
O	-0.37373	-0.41427	1.18567
O	-0.37373	-0.41427	-1.18567
C	-0.08181	0.91258	1.27900
C	-0.08181	0.91258	-1.27900
C	0.38088	1.57805	0.00000
O	-0.22662	1.49515	2.32206
O	-0.22662	1.49515	-2.32206
H	2.09765	-0.48239	0.00000
H	1.76860	-1.97627	0.89005
H	1.76860	-1.97627	-0.89005
H	-0.59673	-2.97490	-0.89131
H	-0.59673	-2.97490	0.89131
H	-1.87640	-2.11740	0.00000
H	1.47608	1.62362	0.00000
H	0.035090	2.61275	0.00000
Acetone			
C	0.00000	0.00000	0.18307
O	0.00000	0.00000	1.40380
C	0.00000	1.28669	-0.61579
H	-0.11884	2.13922	0.05215
H	0.94403	1.38247	-1.16173
H	-0.80145	1.28010	-1.36012
C	0.00000	-1.28669	-0.61579
H	-0.94403	-1.38247	-1.16173
H	0.80145	-1.28010	-1.36012
H	0.118840	-2.13922	0.05215

Ketene			
C	0.00000	0.00000	0.10357
C	0.00000	0.00000	0.10357
H	0.00000	0.00000	-1.21741
H	0.00000	0.94052	-1.74906
O	0.00000	-0.94052	-1.74906
CO_2			
C	0.00000	0.00000	0.00000
O	0.00000	0.00000	1.17001
O	0.00000	0.00000	-1.17001

Table A9.4.4: Calculated coordinates at the MP2/6-311++G** level for MA, ketene, CO_2 and acetone

Atom	*x*	*y*	*z*
MA			
C	1.12948	1.71771	0.00000
C	-0.25785	1.09468	0.00000
C	-1.36489	2.12342	0.00000
O	-0.46253	0.31234	1.18477
O	-0.46253	0.31234	-1.18477
C	0.13881	-0.90602	1.27959
C	-0.13881	-0.90602	-1.27959
C	0.74808	-1.44235	0.00000
O	0.13881	-1.50556	2.32323
O	0.13881	-1.50556	-2.32323
H	1.91860	0.96305	0.00000
H	1.24339	2.33899	0.89152
H	1.24339	2.33899	-0.89152
H	-1.28406	2.74689	-0.89299
H	-1.28406	2.74689	-0.89299
H	-2.32947	1.61267	0.00000
H	1.82007	-1.21510	0.00000
H	0.65692	-2.52936	0.00000
Acetone			
C	0.00000	0.00000	0.18549
O	0.00000	0.00000	1.40512
C	0.00000	1.28591	-0.61718
H	-0.14968	2.13995	0.04372
H	0.96024	1.38806	-1.13433
H	-0.78101	1.25848	-1.38323
C	0.00000	-1.28591	-0.61718
H	-0.96024	-1.38806	-1.13433
H	0.78101	-1.25848	-1.38323
H	0.14968	-2.13995	0.04372

Ketene			
C	0.00000	0.00000	0.10357
C	0.00000	0.00000	1.27182
H	0.00000	0.00000	-1.21814
H	0.00000	0.94350	-1.74357
O	0.00000	-0.94350	-1.74357
CO_2			
C	0.00000	0.00000	0.00000
O	0.00000	0.00000	1.17001
O	0.00000	0.00000	-1.17001

Table A9.4.5: Calculated coordinates at the M06-2X/aug-cc-pVTZ level for MA, ketene, CO_2 and acetone

Atom	*x*	*y*	*z*
MA			
C	0.26700	1.09420	0.00000
C	-0.14709	-0.90671	1.27213
C	-0.75168	-1.44941	0.00000
C	-0.14709	-0.90671	-1.27213
H	-0.66399	-2.53158	0.00000
O	-0.14709	-1.49819	-2.30567
O	0.43841	0.30452	-1.17547
O	0.43841	0.30452	1.17547
O	-0.14709	-1.49819	2.30567
H	-1.81884	-1.21773	0.00000
C	1.39658	2.09398	0.00000
H	1.33154	2.71699	-0.88925
H	1.33154	2.71699	0.88925
H	2.34575	1.56340	0.00000
C	-1.09927	1.75463	0.00000
H	-1.19764	2.37543	0.88806
H	-1.19764	2.37543	-0.88806
H	-1.90258	1.019950	0.00000
Acetone			
C	0.00000	0.00000	0.1864
O	0.00000	0.00000	1.3911
C	0.00000	1.28189	-0.61067
H	-0.00001	2.13746	0.05768
H	0.87722	1.31405	-1.25863
H	-0.87721	1.31404	-1.25864
C	0.00000	-1.28189	-0.61067
H	-0.87722	-1.31405	-1.25863
H	0.87721	-1.31404	-1.25864

H	0.00001	-2.13746	0.05768
Ketene			
C	0.00000	0.00000	0.10322
C	0.00000	0.00000	1.25776
H	0.00000	0.00000	-1.20407
H	0.00000	0.94048	-1.72848
O	0.00000	-0.94048	-1.72848
CO_2			
C	0.00000	0.00000	0.00000
O	0.00000	0.00000	1.15546
O	0.00000	0.00000	-1.15546

Table A9.4.6: Calculated coordinates for cyclic TS (TS for MA to either for formation of ketene, carbon dioxide and acetone or intermediate, malonic anhydride, and acetone) and TS2 (TS for intermediate to ketene and CO_2) at the CBS-QB3 level

Atom	*x*	*y*	*z*
Cyclic TS (MA)			
C	-1.50012	-0.09409	-0.09053
C	0.58032	1.49388	-0.24396
C	1.53819	0.58197	-0.74600
C	1.50852	-0.99023	0.11758
H	1.32594	0.27214	-1.76463
O	-0.90545	0.71758	-0.83885
O	0.36975	-1.43436	0.27916
O	2.64086	-1.3339	0.33249
O	0.39472	2.42023	0.43407
H	2.54475	0.96642	-0.60654
C	-2.34434	-1.14448	-0.74232
H	-1.95744	-2.11842	-0.43446
H	-3.37995	-1.06522	-0.39942
H	-2.29611	-1.05465	-1.82585
C	-1.63699	0.08957	1.39052
H	-2.58525	0.61648	1.55894
H	-1.68780	-0.87821	1.88588
H	-0.83659	0.68536	1.81940
TS2			
C	-1.02599	-0.15342	0.00264
C	1.21423	0.20859	0.03986
C	0.17081	1.11989	0.26031
H	0.27048	2.04857	-0.30411
H	-0.01168	1.28772	1.32034
O	-0.35441	-1.14550	0.35302
O	2.16834	-0.29136	-0.33295
O	-2.11557	0.13853	-0.37421

Malonic anhydride (intermediate)			
C	0.00002	0.00563	1.00892
C	0.00002	0.00563	-1.00892
C	0.00028	1.14791	0.00000
H	-0.89360	1.77238	0.00000
H	0.89413	1.77238	0.00000
O	-0.00034	-0.98081	0.00000
O	0.00002	-0.16583	-2.17548
O	0.00002	-0.16583	2.17548

Table A9.4.7: Calculated coordinates at the MP2/6-31+G* level for MMMA and methylketene

Atom	*x*	*y*	*z*
MMMA			
C	-0.26486	-1.43351	0.00000
C	0.20734	0.59593	1.25622
C	-0.22595	1.33307	0.00000
C	0.20734	0.59593	-1.25622
O	0.55057	1.14386	-2.28483
O	0.20734	-0.77012	-1.18857
O	0.20734	-0.77012	1.18857
O	0.55057	1.14386	2.28483
C	-1.78044	-1.53768	0.00000
H	-2.10046	-2.08423	-0.89121
H	-2.10046	-2.08423	0.89121
H	-2.26504	-0.55939	0.00000
C	0.41493	-2.78195	0.00000
H	0.12278	-3.33984	0.89322
H	0.12278	-3.33984	-0.89322
H	1.49737	-2.63765	0.00000
C	0.24655	2.78326	0.00000
H	-0.12216	3.29103	0.89286
H	1.33817	2.83138	0.00000
H	-0.12216	3.29103	-0.89286
H	-1.32683	1.32153	0.00000
Methylketene			
C	-0.76122	0.13629	0.00002
O	-1.87459	-0.27171	-0.00000
C	0.48444	0.58232	-0.00003
H	0.61384	1.65996	0.00006
C	1.67962	-0.3421	0.00001
H	2.30038	-0.17744	-0.88586
H	2.29969	-0.17842	0.88586
H	1.36577	-1.38952	-0.00071

Table A9.4.8: Calculated coordinates at the MP2/6-311G* level for MMMA and methylketene

Atom	*x*	*y*	*z*
MMMA			
C	-0.02624	1.44589	0.00000
C	0.10192	-0.61164	1.26105
C	-0.43760	-1.26830	0.00000
C	0.10192	-0.61164	-1.26105
O	0.33941	-1.20480	-2.2791
O	0.33840	0.72884	-1.18536
O	0.33840	0.72884	1.18536
O	0.33941	-1.20480	2.2791
C	-1.51011	1.77400	0.00000
H	-1.74837	2.35989	-0.88999
H	-1.74837	2.35989	0.88999
H	-2.13536	0.88122	0.00000
C	0.84567	2.68091	0.00000
H	0.64402	3.27589	0.89222
H	0.64402	3.27589	-0.89222
H	1.89240	2.37509	0.00000
C	-0.19089	-2.77356	0.00000
H	-0.62846	-3.22161	0.89152
H	0.88008	-2.98236	0.00000
H	-0.62846	-3.22161	-0.89152
H	-1.52224	-1.09331	0.00000
Methylketene			
C	-0.76448	0.13492	-0.00000
O	-1.86349	-0.27312	0.00000
C	0.47832	0.58227	-0.00000
H	0.60280	1.65934	0.00001
C	1.67665	-0.33981	0.00000
H	2.29686	-0.17553	-0.88474
H	2.29686	-0.17581	0.88474
H	1.36870	-1.38724	-0.00020

Table A9.4.9: Calculated coordinates at the MP2/6-311+G* level for MMMA and methylketene

Atom	*x*	*y*	*z*
MMMA			
C	-0.03097	-1.44438	0.00000
C	0.10264	0.61227	1.26284
C	-0.42547	1.27686	0.00000
C	0.10264	0.61227	-1.26284
O	0.32610	1.20018	-2.28959
O	0.34461	-0.72643	-1.18390
O	0.34461	-0.72643	1.18390
O	0.32610	1.20018	2.28959
C	-1.51776	-1.75873	0.00000
H	-1.76039	-2.34417	-0.88951
H	-1.76039	-2.34417	0.88951
H	-2.13671	-0.86094	0.00000
C	0.82803	-2.68748	0.00000
H	0.61802	-3.28120	0.89158
H	0.61802	-3.28120	-0.89158
H	1.87944	-2.39704	0.00000
C	-0.16025	2.78003	0.00000
H	-0.59410	3.23366	0.89103
H	0.91326	2.97875	0.00000
H	-0.59410	3.23366	-0.89103
H	-1.51330	1.11603	0.00000
Methylketene			
C	-0.76463	0.13454	0.00000
O	-1.86455	-0.27302	0.00000
C	0.47872	0.58243	0.00000
H	0.60194	1.66019	0.00000
C	1.67754	-0.34006	0.00000
H	2.29741	-0.17496	-0.88474
H	2.29741	-0.17496	0.88474
H	1.36990	-1.38755	-0.00002

Table A9.4.10: Calculated coordinates at the MP2/6-311++G** level for MMMA and methylketene

Atom	*x*	*y*	*z*
MMMA			
C	-0.02685	-1.44194	0.00000
C	0.10429	0.61285	1.26274
C	-0.42868	1.27477	0.00000
C	0.10429	0.61285	-1.26274
O	0.32867	1.20279	-2.28753
O	0.35008	-0.72581	-1.18345
O	0.35008	-0.72581	1.18345
O	0.32867	1.20279	2.28753
C	-1.51550	-1.75363	0.00000
H	-1.75678	-2.33808	-0.89102
H	-1.75678	-2.33808	0.89102
H	-2.12892	-0.85140	0.00000
C	0.82656	-2.69039	0.00000
H	0.61030	-3.28067	0.89295
H	0.61030	-3.28067	-0.89295
H	1.87977	-2.40467	0.00000
C	-0.16521	2.77854	0.00000
H	-0.59955	3.22916	0.89292
H	0.90938	2.97413	0.00000
H	-0.59955	3.22916	-0.89292
H	-1.51449	1.10582	0.00000
Methylketene			
C	0.76393	0.13432	0.00000
O	1.86295	-0.27337	0.00000
C	-0.47942	0.58407	0.00000
H	-0.59669	1.66163	0.00000
C	-1.67660	-0.34044	0.00000
H	-2.29592	-0.17758	0.88668
H	-2.29592	-0.17758	-0.88668
H	-1.36253	-1.38713	-0.00000

Table A9.4.11: Calculated coordinates at the M06-2X/aug-cc-pVTZ level for MMMA and methylketene

Atom	*x*	*y*	*z*
MMMA			
C	-0.25646	-1.42022	0.00000
C	0.20529	0.58979	1.25460
C	-0.21297	1.33283	0.00000
C	0.20529	0.58979	-1.25460
O	0.53139	1.12741	-2.26640
O	0.20529	-0.75726	-1.17386
O	0.20529	-0.75726	1.17386
O	0.53139	1.12741	2.26640
C	-1.77102	-1.52745	0.00000
H	-2.08869	-2.07122	-0.88732
H	-2.08869	-2.07122	0.88732
H	-2.25437	-0.55321	0.00000
C	0.40943	-2.77542	0.00000
H	0.11212	-3.32688	0.88921
H	0.11212	-3.32688	-0.88921
H	1.48890	-3.32688	0.00000
C	0.26619	2.77432	0.00000
H	-0.09436	3.28146	0.89032
H	1.35376	2.80955	0.00000
H	-0.09436	3.28146	-0.89032
H	-1.30789	1.31779	0.00000
Methylketene			
C	0.76113	0.12898	0.00000
O	1.84865	-0.27081	-0.00000
C	-0.46776	0.57439	0.00000
H	-0.57417	1.64969	0.00000
C	-1.67142	-0.33359	0.00000
H	-2.28751	-0.16131	0.88204
H	-2.28751	-0.16131	-0.88204
H	-1.37167	-1.37919	-0.00000

Table A9.4.12: Calculated coordinates for cyclic TS (TS for MMMA to either for formation of methylketene, carbon dioxide and acetone or intermediate, methyl-malonic anhydride, and acetone) and TS2 (TS for intermediate to methyl-ketene and CO_2) at the CBS-QB3 level

Atom	*x*	*y*	*z*
Cyclic TS (MMMA)			
C	1.81168	-0.16731	-0.14619
C	-0.56155	-1.26950	-0.06129
C	-1.38114	-0.24813	-0.60677
C	-0.95094	1.32900	0.18991
H	-1.07563	-0.01705	-1.62487
O	1.00478	-0.87379	-0.79365
O	0.26151	1.55308	0.19379
O	-1.95815	1.89511	0.52760
O	-0.5245	-2.15992	0.68869
C	2.81324	0.62677	-0.92459
H	2.61921	1.68221	-0.71803
H	3.82921	0.39587	-0.59329
H	2.70600	0.43707	-1.99091
C	1.99925	-0.26149	1.33706
H	2.83453	-0.95339	1.50716
H	2.27160	0.71132	1.74248
H	1.12533	-0.64950	1.85158
C	-2.87156	-0.53430	-0.44115
H	-3.11489	-0.74986	0.59991
H	-3.42876	0.35565	-0.72808
H	-3.18967	-1.37833	-1.05912
TS2			
C	1.07158	-0.45219	0.01165
C	-1.17814	-0.32085	0.11358
C	-0.20064	0.62173	0.48212
H	-0.02088	0.57252	1.55693
O	0.56228	-1.57285	0.21484
O	-2.07514	-0.83876	-0.36254

O	2.09963	0.03759	-0.35662
C	-0.31614	2.03089	-0.08110
H	-0.97367	2.67468	0.50599
H	0.69526	2.44514	-0.06783
H	-0.65487	2.02236	-1.11798
Methyl-malonic anhydride (intermediate)			
C	-0.27669	-0.28780	1.00754
C	-0.27669	-0.28780	-1.00754
C	-0.02541	0.83315	0.00000
H	-0.84344	1.55946	0.00000
O	-0.53465	-1.24159	0.00000
O	-0.27669	-0.46411	-2.17485
O	-0.27669	-0.46411	2.17485
C	1.33391	1.52442	0.00000
H	1.43356	2.15410	-0.88595
H	1.43356	2.15410	0.88595
H	2.14992	0.79902	0.00000

Table A9.4.13: Calculated coordinates at the MP2/6-31+G* level for DMMA and dimethylketene

Atom	*x*	*y*	*z*
DMMA			
C	-0.37673	-1.55830	0.00000
C	0.16640	0.39981	1.28545
C	0.30569	1.20302	0.00000
C	0.16640	0.39981	-1.28545
O	0.16640	0.92279	-2.38367
O	0.17690	-0.96655	-1.18741
O	0.17690	-0.96655	1.18741
O	0.16640	0.92279	2.38367
C	-1.88593	-1.38957	0.00000
H	-2.30714	-1.85897	-0.89319
H	-2.30714	-1.85897	0.89319
H	-2.16309	-0.33026	0.00000
C	0.08071	-2.99469	0.00000
H	-0.29605	-3.49967	0.89296
H	-0.29605	-3.49967	-0.89296
H	1.17262	-3.02446	0.00000
C	-0.68298	2.37550	0.00000
H	-1.72201	2.02895	0.00000
H	-0.52096	2.98335	0.89329
H	-0.52096	2.98335	-0.89329
C	1.75520	1.75050	0.00000
H	1.90384	2.36201	0.89406
H	2.48767	0.93611	0.00000
H	1.90384	2.36201	-0.89406
Dimethylketene			
C	0.97911	0.00000	0.00000
O	2.16809	0.00000	0.00000
C	-0.34402	0.00000	0.00000
C	-1.10681	-1.30319	0.00000
H	-1.74913	-1.30319	0.88609

H	-1.74912	-1.37000	-0.88609
H	-0.43851	-2.16928	0.00001
C	-1.10681	1.30319	0.00000
H	-0.43851	2.16928	-0.00001
H	-1.74913	1.36999	-0.88609
H	-1.74912	1.37000	0.88609

Table A9.4.14: Calculated coordinates at the MP2/6-311G* level for DMMA and dimethylketene

Atom	*x*	*y*	*z*
DMMA			
C	-0.40865	-1.52767	0.00000
C	0.16446	0.39068	1.29023
C	0.33716	1.18162	0.00000
C	0.16446	0.39068	-1.29023
O	0.15433	0.91393	-2.37454
O	0.16446	-0.97037	-1.18511
O	0.16446	-0.97037	1.18511
O	0.15433	0.91393	2.37454
C	-1.90855	-1.28785	0.00000
H	-2.35405	-1.73204	-0.89219
H	-2.35405	-1.73204	0.89219
H	-2.13336	-0.21764	0.00000
C	-0.02403	-2.98644	0.00000
H	-0.42122	-3.47295	0.89208
H	-0.42122	-3.47295	-0.89208
H	1.06366	-3.06838	0.00000
C	-0.57581	2.40900	0.00000
H	-1.63170	2.12445	0.00000
H	-0.38230	3.00687	0.89151
H	-0.38230	3.00687	-0.89151
C	1.81807	1.63366	0.00000
H	2.00964	2.23242	0.89262
H	2.49401	0.77395	0.00000
H	2.00964	2.23242	-0.89262
Dimethylketene			
C	-0.98088	0.00000	0.00000
O	-2.15607	0.00000	0.00000
C	0.34018	0.00000	0.00000
C	1.10305	-1.30410	0.00000
H	1.74510	-1.37256	-0.88465

H	1.74510	-1.37256	0.88465
H	0.43790	-2.17049	-0.00000
C	1.10305	1.30410	0.00000
H	0.43790	2.17049	0.00000
H	1.74510	1.37256	0.88465
H	1.74510	1.37256	-0.88465

Table A9.4.15: Calculated coordinates at the MP2/6-311+G* level for DMMA and dimethylketene

Atom	*x*	*y*	*z*
DMMA			
C	-0.40824	-1.53333	0.00000
C	0.17139	0.38834	1.28828
C	0.33503	1.18611	0.00000
C	0.17139	0.38834	-1.28828
O	0.16492	0.90905	-2.37584
O	0.17139	-0.97236	-1.18272
O	0.17139	-0.97236	1.18272
O	0.16492	0.90905	2.37584
C	-1.90848	-1.29293	0.00000
H	-2.35369	-1.73957	-0.89158
H	-2.35369	-1.73957	0.89158
H	-2.13850	-0.22326	0.00000
C	-0.02484	-2.99213	0.00000
H	-0.42476	-3.47895	0.89123
H	-0.42476	-3.47895	-0.89123
H	1.06267	-3.07992	0.00000
C	-0.60036	2.39900	0.00000
H	-1.65265	2.09999	0.00000
H	-0.41505	3.00133	0.89101
H	-0.41505	3.00133	-0.89101
C	1.80732	1.66936	0.00000
H	1.98555	2.27399	0.89202
H	2.50416	0.82579	0.00000
H	1.98555	2.27399	-0.89202
Dimethylketene			
C	0.98080	0.00000	0.00000
O	2.15707	0.00000	0.00000
C	-0.34066	0.00000	0.00000
C	-1.10327	1.30489	0.00000
H	-1.74552	1.37310	-0.88449

H	-1.74552	1.37310	0.88449
H	-0.43799	2.17126	0.00000
C	-1.10327	-1.30489	0.00000
H	-0.43799	-2.17126	0.00000
H	-1.74552	-1.37310	0.88449
H	-1.74552	-1.37310	-0.88449

Table A9.4.16: Calculated coordinates at the MP2/6-311++G** level for DMMA and dimethylketene

Atom	*x*	*y*	*z*
DMMA			
C	-0.39395	-1.53594	0.00000
C	0.17740	0.38615	1.28904
C	0.32098	1.18703	0.00000
C	0.17740	0.38615	-1.28904
O	0.17740	0.90635	-2.37645
O	0.18415	-0.97491	-1.18202
O	0.18415	-0.97491	1.18202
O	0.17740	0.90635	2.37645
C	-1.89624	-1.29738	0.00000
H	-2.33846	-1.74490	-0.89328
H	-2.33846	-1.74490	0.89328
H	-2.12233	-0.22631	0.00000
C	-0.01202	-2.99706	0.00000
H	-0.41524	-3.47967	0.89287
H	-0.41524	-3.47967	-0.89287
H	1.07618	-3.08485	0.00000
C	-0.64670	2.37660	0.00000
H	-1.69089	2.04813	0.00000
H	-0.47428	2.98131	0.89297
H	-0.47428	2.98131	-0.89297
C	1.77930	1.71349	0.00000
H	1.93635	2.32216	0.89405
H	2.49846	0.88797	0.00000
H	1.93635	2.32216	-0.89405
Dimethylketene			
C	-0.98087	0.00000	0.00000
O	-2.15644	0.00000	0.00000
C	0.34110	0.00000	0.00000
C	1.10351	1.30512	0.00000
H	1.74449	1.37231	0.88660

H	1.74449	1.37231	-0.88660
H	0.43502	2.17008	0.00000
C	1.10351	-1.30512	0.00000
H	0.43502	-2.17008	0.00000
H	1.74449	-1.37231	-0.88660
H	1.74449	-1.37231	0.88660

Table A9.4.17: Calculated coordinates at the M06-2X/aug-cc-pVTZ level for DMMA and dimethylketene

Atom	*x*	*y*	*z*
DMMA			
C	-0.34769	-1.55073	0.00000
C	0.17484	0.39318	1.28312
C	0.28221	1.20437	0.00000
C	0.17484	0.39318	-1.28312
O	0.17484	0.90290	-2.36142
O	0.19355	-0.95380	-1.17219
O	0.19355	-0.95380	1.17219
O	0.17484	0.90290	2.36142
C	-1.85730	-1.39344	0.00000
H	-2.27461	-1.86030	-0.88961
H	-2.27461	-1.86030	0.88961
H	-2.13466	-0.33770	0.00000
C	0.10404	-2.98833	0.00000
H	-0.27437	-3.48734	0.88929
H	-0.27437	-3.48734	-0.88929
H	1.19095	-3.02547	0.00000
C	-0.74302	2.33941	0.00000
H	-1.76566	1.96237	0.00000
H	-0.59939	2.94713	0.89038
H	-0.59939	2.94713	-0.89038
C	1.70874	1.79937	0.00000
H	1.83352	2.41010	0.89153
H	2.46495	1.01405	0.00000
H	1.83352	2.41010	-0.89153
Dimethylketene			
C	0.00000	0.00000	0.97457
O	0.00000	0.00000	2.13685
C	0.00000	0.00000	-0.33227
C	0.00000	1.29940	-1.09477

H	0.88191	1.36093	-1.73573
H	-0.88191	1.36093	-1.73573
H	0.00000	2.16358	-0.43421
C	0.00000	-1.29940	-1.09477
H	0.00000	-2.16358	-0.43421
H	-0.88191	-1.36093	-1.73573
H	0.88191	-1.36093	-1.73573

Table A4.18: Calculated coordinates for cyclic TS (TS for DMMA to either for formation of dimethylketene, carbon dioxide and acetone or intermediate, dimethyl-malonic anhydride, and acetone) and TS2 (TS for intermediate to di-methyl-ketene and CO_2) at the CBS-QB3 level

Atom	*x*	*y*	*z*
Cyclic TS			
C	-1.92985	-0.20271	0.08524
C	0.79848	1.30625	-0.43155
C	1.33907	-0.23176	0.37001
C	0.46666	-1.25193	-0.11955
O	0.38805	-2.12775	-0.8839
O	-1.08969	-0.91243	0.68020
O	-0.37830	1.58598	-0.18508
O	1.72163	1.81493	-1.01830
C	-2.12936	-0.20112	-1.39914
H	-2.95388	-0.89581	-1.60695
H	-2.42564	0.79150	-1.73409
H	-1.25499	-0.53538	-1.94925
C	-2.93999	0.52050	0.91962
H	-2.70662	1.58589	0.83730
H	-3.95093	0.36317	0.53637
H	-2.87040	0.21296	1.96153
C	2.76458	-0.55054	-0.10300
H	2.79723	-0.74865	-1.17395
H	3.39114	0.31929	0.08797
H	3.17055	-1.41540	0.43111
C	1.27187	0.09219	1.86931
H	1.96210	0.91433	2.06915
H	0.27690	0.40101	2.17611
H	1.582320	-0.76404	2.47577
TS2			
C	0.99131	-0.69003	-0.11175
C	-1.24079	-0.30866	-0.03788
C	-0.14485	0.57664	0.07838

O	0.41701	-1.70636	0.32837
O	-2.19606	-0.85401	-0.32917
O	2.06104	-0.37901	-0.56520
C	-0.13211	1.67450	-0.98633
H	-0.73195	2.54256	-0.70285
H	0.91509	1.97265	-1.08566
H	-0.46193	1.30938	-1.96026
C	0.10486	1.08735	1.51154
H	0.08779	0.26898	2.23083
H	1.09715	1.54116	1.52504
H	-0.63262	1.84147	1.79701
Dimethyl-malonic anhydride (intermediate)			
C	-1.00698	-0.56013	-0.00028
C	1.00696	-0.56015	-0.00025
C	0.00000	0.59533	-0.00011
O	-0.00001	-1.54871	-0.00030
O	2.17579	-0.73243	0.00004
O	-2.17580	-0.73240	0.00002
C	-0.00001	1.44094	1.27582
H	0.88697	2.07803	1.29742
H	-0.88699	2.07804	1.29739
H	-0.00002	0.82220	2.17573
C	0.00004	1.44198	-1.27524
H	-0.88692	2.07911	-1.29627
H	0.88703	2.07906	-1.29624
H	0.00003	0.82402	-2.17571

Table A9.4.19: Calculated coordinates at the MP2/6-31+G* level for MeMA and methyleneketene

Atom	*x*	*y*	*z*
MeMA			
C	-0.11951	-1.35341	0.00000
C	-0.00041	1.35598	0.00000
C	0.48182	-2.73568	0.00000
H	0.15784	-3.27582	0.89301
H	0.15784	-3.27582	-0.89301
H	1.57087	-2.65391	0.00000
C	-1.63799	-1.34591	0.00000
H	-2.00139	-1.86320	-0.89213
H	-2.00139	-1.86320	0.89213
H	-2.03478	-0.32650	0.00000
C	-0.40643	2.63733	0.00000
H	-0.56781	3.16060	0.93737
H	-0.56781	3.16060	-0.93737
O	0.38675	-0.71046	-1.18791
O	0.38675	-0.71046	1.18791
C	0.25048	0.64650	-1.28947
C	0.25048	0.64650	1.28947
O	0.38675	1.19979	-2.36408
O	0.38675	1.19979	2.36408
Methyleneketene			
C	0.00000	0.92457	-2.46423
H	0.00000	0.00000	-0.56273
H	0.00000	0.00000	0.72140
C	0.00000	0.00000	1.91616
C	0.00000	-0.92457	2.46942
O	0.00000	0.00000	-1.89041

Table A9.4.20: Calculated coordinates at the MP2/6-311G* level for MeMA and methyleneketene

Atom	*x*	*y*	*z*
MeMA			
C	-0.07069	1.34263	0.00000
C	-0.01908	-1.34506	0.00000
C	0.54406	2.72086	0.00000
H	0.23006	3.26489	0.89209
H	0.23006	3.26489	-0.89209
H	1.63045	2.62502	0.00000
C	-1.58988	1.35149	0.00000
H	-1.95076	1.86931	-0.89096
H	-1.95076	1.86931	0.89096
H	-1.99717	0.33768	0.00000
C	-0.43113	-2.62214	0.00000
H	-0.59351	-3.14427	0.93660
H	-0.59351	-3.14427	-0.93660
O	0.42308	0.70294	-1.18502
O	0.42308	0.70294	1.18502
C	0.23681	-0.64212	-1.29525
C	0.23681	-0.64212	1.29525
O	0.33401	-1.19252	-2.36026
O	0.33401	-1.19252	2.36026
Methyleneketene			
C	-1.88398	0.00021	0.00001
H	-2.46313	-0.92412	0.00003
H	-2.46220	0.92513	0.00003
C	-0.55853	-0.00047	-0.00002
C	0.72371	-0.00021	-0.00005
O	1.90476	0.00022	0.00003

Table A9.4.21: Calculated coordinates at the MP2/6-311+G* level for MeMA and methyleneketene

Atom	*x*	*y*	*z*
MeMA			
C	-0.07647	1.35816	0.00000
C	-0.11084	-1.33561	0.00000
C	0.57779	2.71710	0.00000
H	0.27723	3.27083	0.89114
H	0.27723	3.27083	-0.89114
H	1.66191	2.59612	0.00000
C	-1.59454	1.41413	0.00000
H	-1.93823	1.94512	-0.89026
H	-1.93823	1.94512	0.89026
H	-2.03683	0.41468	0.00000
C	-0.59634	-2.58870	0.00000
H	-0.78872	-3.10066	0.93707
H	-0.78872	-3.10066	-0.93707
O	0.40083	0.69888	-1.18308
O	0.40083	0.69888	1.18308
C	0.17213	-0.63899	-1.29372
C	0.17213	-0.63899	1.29372
O	0.25757	-1.19196	-2.36162
O	0.25757	-1.19196	2.36162
Methyleneketene			
H	0.00000	0.92538	-2.46252
C	0.00000	0.00000	-0.55859
C	0.00000	0.00000	0.72385
O	0.00000	0.00000	1.90576
H	0.00000	-0.92538	-2.46252
C	0.00000	0.00000	-1.88544

Table A9.4.22: Calculated coordinates at the MP2/6-311++G** level for MeMA and methyleneketene

Atom	*x*	*y*	*z*
MeMA			
C	-0.07514	1.34066	0.00000
C	-0.02700	-1.34775	0.00000
C	0.52390	2.72647	0.00000
H	0.19791	3.26431	0.89266
H	0.19791	3.26431	-0.89266
H	1.61248	2.64787	0.00000
C	-1.59547	1.33781	0.00000
H	-1.95696	1.85485	-0.89210
H	-1.95696	1.85485	0.89210
H	-1.99442	0.31963	0.00000
C	-0.47667	-2.61332	0.00000
H	-0.65579	-3.12625	0.93905
H	-0.65579	-3.12625	-0.93905
O	0.42646	0.70107	-1.18302
O	0.42646	0.70107	1.18302
C	0.23929	-0.64448	-1.29364
C	0.23929	-0.64448	1.29364
O	0.34699	-1.19499	-2.35962
O	0.34699	-1.19499	2.35962
Methyleneketene			
H	0.00000	0.92652	-2.46141
C	0.00000	0.00000	-0.55884
C	0.00000	0.00000	0.72392
O	0.00000	0.00000	1.90547
H	0.00000	-0.92652	-2.46141
C	0.00000	0.00000	-1.88523

Table A9.4.23: Calculated coordinates at the M06-2X/aug-cc-pVTZ level for MeMA and methyleneketene.

Atom	*x*	*y*	*z*
MeMA			
C	-0.11304	1.34588	0.00000
C	0.19806	-1.35141	0.00000
C	-0.93853	2.60683	0.00000
H	-0.70905	3.18981	0.88911
H	-0.70905	3.18981	-0.88911
H	-1.99455	2.34713	0.00000
C	1.38172	1.60944	0.00000
H	1.64913	2.17752	-0.88849
H	1.64913	2.17752	0.88849
H	1.94475	0.67573	0.00000
C	0.71738	-2.57228	0.00000
H	0.92672	-3.07097	0.9367
H	0.92672	-3.07097	-0.9367
O	-0.48139	0.62582	-1.17511
O	-0.48139	0.62582	1.17511
C	-0.12340	-0.67102	-1.28769
C	-0.12340	-0.67102	1.28769
O	-0.12340	-1.21295	-2.35063
O	-0.12340	-1.21295	2.35063
Methyleneketene			
C	-0.56039	-0.23957	-0.00000
C	-1.83338	0.08779	0.00000
H	-2.16513	1.12293	0.00000
H	-2.61363	-0.66713	0.00001
C	0.70393	0.00003	-0.00000
O	1.86472	0.05683	0.00000

Table A9.4.24: Calculated coordinates for cyclic TS (TS for MeMA to either for formation of methyleneketene, carbon dioxide and acetone or intermediate, methylenemalonic anhydride, and acetone) and TS2 (TS for intermediate to methyleneketene and CO_2) at the CBS-QB3 level.

Atom	*x*	*y*	*z*
Cyclic TS			
C	-1.75861	0.16550	0.25053
C	0.83757	1.44970	-0.22757
C	-2.9308	-0.28900	-0.56932
H	-2.67492	-1.26862	-0.98085
H	-3.82348	-0.40025	0.05239
H	-3.11457	0.41118	-1.38215
C	-1.54553	-0.49535	1.58319
H	-2.29505	-0.08087	2.26973
H	-1.70028	-1.57128	1.51769
H	-0.55777	-0.28114	1.98546
C	2.43507	0.26980	1.01583
H	2.96072	-0.65876	1.21273
H	2.76218	1.17579	1.51534
O	-1.13031	1.17491	-0.10081
O	-0.21988	-1.37013	-0.76903
C	1.40998	0.22257	0.15196
C	0.97670	-1.26803	-0.47893
O	0.89348	2.49190	-0.70188
O	1.94383	-2.00382	-0.49634
TS2			
C	1.02178	-0.49838	-0.01571
C	-1.32422	-0.02127	-0.04566
C	-0.12775	0.67044	-0.05885
O	0.41729	-1.50509	0.40021
O	-2.32005	-0.54599	-0.20853
O	2.14313	-0.16968	-0.31061
C	0.05348	1.97531	0.18245
H	-0.73199	2.65926	0.48256

H	1.06923	2.35020	0.09557
Methylene-malonic anhydride (intermediate)			
C	0.00063	-0.32961	1.01633
C	0.00063	-0.32961	-1.01633
C	-0.00079	0.76478	0.00000
O	0.00199	-1.32229	0.00000
O	0.00063	-0.49270	-2.18572
O	0.00063	-0.49270	2.18572
C	-0.00334	2.08939	0.00000
H	-0.00441	2.64594	-0.93042
H	-0.00441	2.64594	0.93042

Table A9.4.25: Energies and corrections for Enthalpy (*H*corr.), Gibbs free energy (*G*corr.) and Zero Point Energy (ZPEcorr.) energy CBS-QB3 level at 298.15 K for all the molecules involved in the decomposition of MA derivatives for thermochemical calculations. All energies in Hartrees.

Molecule	Ecbs-qb3	*H*corr.	*G*corr.	ZPEcorr.
MA	-533.590859	0.149018	0.104192	0.138637
MMMA	-572.818916	0.178607	0.130587	0.166744
DMMA	-612.045288	0.207794	0.156179	0.194405
MeMA	-571.612821	0.154937	0.108337	0.143776
Ketene	-152.372330	0.036029	0.008650	0.031579
Methyl-ketene	-191.594541	0.066511	0.034083	0.060861
Di-methyl-ketene	-230.820605	0.0962280	0.060757	0.089193
Methyleneketene	-190.359701	0.0416200	0.012395	0.036824
CO2	-188.369467	0.015286	-0.009000	0.011720
Acetone	-192.814100	0.089565	0.055624	0.083232